Minnesota Department of Transportation

RESEARCH SERVICES & LIBRARY

Office of Transportation System Management

Enhancement and Application of the Minnesota Dry Swale Calculator

John S. Gulliver, Principal Investigator
Department of Civil, Environmental and Geo- Engineering
University of Minnesota

April 2016

Research Project
Final Report 2016-15

To request this document in an alternative format call 651-366-4718 or 1-800-657-3774 (Greater Minnesota) or email your request to ADArequest.dot@state.mn.us. Please request at least one week in advance.

Technical Report Documentation Page

1. Report No.	2.	3. Recipients Accession No.
MN/RC 2016-15		

4. Title and Subtitle	5. Report Date
Enhancement and Application of the Minnesota Dry Swale Calculator	April 2016
	6.

7. Author(s)	8. Performing Organization Report No.
Maria Garcia-Serrana, John S. Gulliver, and John L. Nieber	

9. Performing Organization Name and Address	10. Project/Task/Work Unit No.
St. Anthony Falls Laboratory University of Minnesota 2 Third Ave. SE Minneapolis, MN 55414	CTS #2014025
	11. Contract (C) or Grant (G) No. (c) 99008 (wo) 97

12. Sponsoring Organization Name and Address	13. Type of Report and Period Covered
Minnesota Department of Transportation Research Services & Library 395 John Ireland Boulevard, MS 330 St. Paul, Minnesota 55155-1899	Final Report
	14. Sponsoring Agency Code

15. Supplementary Notes
http://www.lrrb.org/pdf/201615.pdf
http://stormwater.safl.umn.edu/resources/roadside-swale-calculator
http://www.dot.state.mn.us/research/TS/2016/RoadsideSwaleCalculator_5_4_16.xlsx

16. Abstract (Limit: 250 words)

Roadside drainage ditches (roadside grassed swales) typically receive runoff directly from the road and water is infiltrated over the side slope of the ditch, similar to a filter strip. Water that runs off the side slopes then has a further opportunity to infiltrate as it flows down the center of the ditch. This research focuses on the volume reduction performance of grassed drainage ditches or swales by infiltration.

A total of 32 tests were performed during three seasons in four different highways maintained by MnDOT in the Twin Cities metro area. The field-measured saturated hydraulic conductivities (K_{sat}) correspond to hydrologic soil group A, even though the soil textures indicated correspondence to hydrologic soils groups A, B and C. This means that the infiltration performance is better than expected for these types of soils. In addition, the trend was to have more infiltration when the saturated hydraulic conductivity was higher and for a greater side slope length, as expected.

A coupled overland flow-infiltration model that accounts for shallow concentrated flow has been developed. The predicted infiltration loss has been compared with the actual infiltration loss determined from the monitored field tests. In this manner, the validity of the model as well as the associated soil hydraulic and surface geometry parameters have been evaluated. Using the coupled infiltration-overland flow model, multiple scenarios with sensitivity analyses have been computed, and the results have been used to generate a simplified calculator to estimate the annual infiltration performance of a grassed roadside drainage ditch.

17. Document Analysis/Descriptors	18. Availability Statement
drainage structures; swales; filters; infiltration; runoff; flow; permeability coefficient	No restrictions. Document available from: National Technical Information Services, Alexandria, Virginia 22312

19. Security Class (this report)	20. Security Class (this page)	21. No. of Pages	22. Price
Unclassified	Unclassified	104	

Enhancement and Application of the Minnesota Dry Swale Calculator

Final Report

Prepared by:

María García-Serrana
John S. Gulliver
Department of Civil, Environmental and Geo- Engineering
University of Minnesota

John L. Nieber
Department of Bioproducts and Biosystems Engineering
University of Minnesota

April 2016

Published by:

Minnesota Department of Transportation
Research Services & Library
395 John Ireland Boulevard, MS 330
St. Paul, Minnesota 55155-1899

Acknowledgments

The following were members of the Technical Advisory Panel for this project:

Bruce Holdhusen (project coordinator), Barbara Loida (technical liaison), David Bauer, David Fairbairn, Michael Findorff, Kristine Giga, Jodi Hreha, Beth Neuendorf, Nicholas Olson, Nicklas Tiedeken and Juanita Voigt.

Table of Contents

List of Figures

List of Tables

Executive Summary

A growing trend in stormwater management is to include techniques that reduce runoff volumes and improve runoff water quality in addition to reducing the peak flow rate. Such techniques are called low impact development (LID) practices or Green Infrastructure (GI) and are typically designed to reduce runoff and to mimic a site's predevelopment hydrology. In most cases, roadside drainage ditches receive road runoff directly and water is infiltrated over the side slope of the ditch, similar to a filter strip (Erickson, et al., 2013). Water that runs off the side slopes then has a further opportunity to infiltrate as it flows down the center of the ditch. Both grassed swales and roadside drainage ditches (all identified as swales herein) act as stormwater treatment practices. This research focuses on the volume reduction performance of roadside swales by infiltration. These vegetated surfaces convey stormwater, infiltrate runoff, and filter and/or settle solids, and they are often placed along roads and other impermeable surfaces.

Infiltration performance of swales is linked to infiltration capacity of the soil, initial soil moisture content, ratio of impervious drainage area-swale area, length and width of the vegetated area, slope, type of flow down the side slope of the swale (spread or concentrated flow), and total depth and intensity of precipitation. The analysis of the results from laboratory and field experiments, together with a coupled infiltration runoff model have provided evidence to determine how these parameters affect the percentage of water infiltrated in the side slope and channel of a drainage ditch or swale.

A total of 32 tests were performed during three seasons in four different highways maintained by MnDOT in the Twin Cities metro area. All of the tests showed that water on the lateral slope of a swale flows in concentrated regions that resemble fingers, not as sheet flow, at the typical intensities for which infiltration practices are designed and utilized to improve surface water quality. A linear relationship between the intensity of precipitation and fraction wetted was observed for the intensities tested. No signs of erosion due to water flow were observed in any of the sites. The field-measured saturated hydraulic conductivities (K_{sat}) corresponded to hydrologic soil group A, even though the soil textures indicated corresponded to hydrologic soils groups A, B and C. Therefore, the infiltration performance is better than the expected for these types of soils. The average percentage of water infiltrated during the two-year storm experiments performed in fall (8 tests) was 84.7% (12.7% standard deviation), this value is higher than the results observed during spring 70% (12.4% standard deviation). During the ten-year storm event tests (8 tests), the average of water infiltrated was 47.1%, with a standard deviation of 24.9%. The average water infiltrated during the one-year events (8 tests) was 68.7%, with a standard deviation of 13.5%. In addition, the trend was to have more infiltration when the saturated hydraulic conductivity was higher and for a greater side slope length, as expected. The vegetation, type of soil and length of the side slope would be important to consider for constructing roadside drainage ditches that will be efficient in stormwater treatment.

A runoff-infiltration model that calculates the amount of water infiltrated along the side slope of a roadside drainage ditch has been coupled with a model of infiltration in the ditch channel. The runoff discharge from the road is added to direct rainfall on the side slope, and the side slope discharge that does not infiltrate is added to the channel. When coupled, a combined one-dimensional runoff-infiltration model for both the side slope and channel of a roadside drainage ditch was obtained. This numerical model can be used to estimate the infiltration performance of

roadside drainage ditches for given rainfall intensities. The Green-Ampt-Mein-Larson assumptions were implemented to calculate infiltration along with a kinematic wave model for overland flow that accounts for short-circuiting of flow. The model has been established in the MATLAB programming language and allows for a wide range of user inputs.

The final objective of this project was to estimate the annual infiltration performance of a grassed roadside drainage ditch. Using the coupled infiltration-overland flow model, multiple scenarios with sensitivity analyses have been computed and the results have been used to generate a simplified calculator to estimate the annual infiltration performance of a grassed roadside drainage ditch. The only inputs of the simplified calculator are: saturated hydraulic conductivity, width of the swale, width of the road, and the location's rainfall volume percentile as a function of rainfall depth. Provided that there is a satisfactory estimation of the saturated hydraulic conductivity in the field and the side slope does not show signs of erosion, the calculator can be used to provide a good estimation of the water captured by the channel and side slope of a roadside swale/drainage ditch.

I. Introduction

A growing trend in stormwater management is to include techniques that reduce runoff volumes and improve runoff water quality in addition to reducing the peak flow rate. Such techniques are called low impact development (LID) practices or Green Infrastructure (GI) and are typically designed to reduce runoff and to mimic a site's predevelopment hydrology. GI or LID practices achieve this by infiltrating, filtering, storing, evaporating, and detaining stormwater runoff close to its source. These practices include bioretention facilities, infiltration basins and trenches, constructed wetlands, sand filters, filter strips, wet and dry swales, among others (Weiss *et al.*, 2010). According to the Minnesota Pollution Control Agency (MPCA, 2013), standards are needed to create consistency in design and performance of stormwater practices.

In most cases, roadside drainage ditches receive road runoff directly and water is infiltrated over the side slope of the ditch (Figure 1), similar to a filter strip (Erickson, *et al.*, 2013). Water that runs off the side slopes then has a further opportunity to infiltrate as it flows down the center of the ditch. Both grassed swales and roadside drainage ditches (all identified as swales herein) act as stormwater treatment practices. This research focuses on the volume reduction performance of roadside swales by infiltration. These vegetated surfaces convey stormwater, infiltrate runoff, and filter and/or settle solids, and are often placed along roads and other impermeable surfaces.

Hypotheses

1. Substantial infiltration takes place in the side slope of the swales.
2. Infiltration rates are typically calculated by assuming that water flows as sheet flow over the side slope of swales. However, for most intensities, water flow occurs in shallow micro-channels and concentrates in depressions rather than flowing as sheet flow. Only a fraction of the soil surface is covered with water.
3. The infiltration-runoff process of a roadside drainage ditch can be modeled with three one-dimensional models (two for the side slopes and one for the channel) running in parallel.
4. A simplified calculator that takes into account only the most significant parameters can be generated based on the results of the coupled one-dimensional models.

Objectives

This research develops and demonstrates the means by which the appropriate pollution prevention credits for swales can be captured. The objectives of this research are:

1. Characterize the spatial pattern of flow for stormwater runoff entering onto the surface of a swale.
2. Study the impact of micro-channels, called rills, in the runoff-infiltration process.
3. Design a coupled infiltration and overland model that facilitates the calculation of stormwater infiltration on the side slopes and the center channel of swales.
4. Perform a sensitivity analysis on the parameters implemented in the model.
5. Verify the coupled infiltration and overland model by comparing predicted reductions in runoff with the actual infiltration loss of several swales.
6. Develop a simplified calculator that quantifies the annual infiltration performance of

drainage ditches or swales in Minnesota.

Figure 1 Side slope of Hwy 47 drainage ditch/swale.

II. Literature Review

1. Infiltration Performance of Swales/Drainage Ditches

Filter strips, grassed swales and drainage ditches reduce runoff volumes and improve water quality by infiltration, filtration and sedimentation. Volume reduction occurs primarily through infiltration into the soil, either as the water flows over the side-slope in a direction perpendicular to the roadway into the swale or down the length of the swale channel parallel to the roadway. Pollutant removal can occur by sedimentation of solid particles onto the soil surface, filtration of solid particles by vegetation, or infiltration of pollutants dissolved in the stormwater into the soil (Abida and Sabourin, 2006). The infiltration capacity of each swale will depend on many variables and each swale should be examined individually (Weiss *et al.*, 2010).

Some guidelines to optimize the performance of swales with respect to stormwater treatment focus on the swale channel (parallel to the road). Ferguson (1998) recommended a swale channel length greater than or equal to 60 m, water velocities less than 0.15 m/s, and a residence time of at least 9 minutes. Yu *et al.* (2001) recommended a swale channel length of 75 m and a bottom slope of no more than 3%. On the other hand, Barrett *et al.* 1998a found that swale channel length is not an important design parameter as long as the road runoff is allowed to flow directly down the side slope into the swale. Under these conditions the side slope acts as a filter strip and infiltration increases with distance from the edge of pavement (CALTRANS, 2003).

Using simulated runoff, Yousef *et al.* (1987) found that swales infiltrated between 9% and 100% of the runoff with significant variability. Multiple studies have monitored natural storm events; for example, Lancaster (2005) monitored infiltration along roadside swales in Washington, and reported 100% infiltration within the first two meters from the edge of pavement in one site (36 precipitation events). At another site, 67% of the events (18 precipitation events) had no observed runoff. Ahearn and Tveten (2008) investigated the performance of four 41 year old, unimproved roadside swales. The results from the monitoring station located at 4 meters from the edge of pavement showed 66% to 94% runoff volume reduction. Fassman and Liao (2009) monitored swales (trapezoidal channel 1 m base width and 0.69 m side slope) located in a bus station and reported 63.7% volume reduction and a median decrease of 73.6% in the peak flow discharge. Additionally, they reported that the runoff volume control is substantial for storms less than 1.3 cm (0.5 in). Furthermore, Lucke *et al.* (2014) reported a mean total flow reduction of 52% in the 30 m swales studied with an average 2 m side slope length.

Hunt *et al.* (2010) investigated the volume reduction capability of a 44.8 m (147 ft) vegetative filter strip over a 16-month period and 23 rainfall events. Total volume reduction over the monitoring period was 85% and the 3 events that produced runoff had total rainfall depths greater than 40 mm (1.6 inches). Knight *et al.* (2013) monitored different vegetative filter strips with level spreader and a swale (side slopes and channel). The swale was trapezoidal, 10.4m long (1% slope), 0.15 m bottom width, and 0.32 m length side slopes (3:1 slope); the infiltration performance reported for the swale was 23%. The strips had 1% slope, sandy loam/clay loam soils, and an estimated 0.1 cm/h hydraulic conductivity. The 8m long by 6m wide average runoff reduction was 36% while the 20 m long by 6 m wide had a 59% average volume reduction.

Davis *et al.* (2012) investigated the hydraulic performance of four grassed roadside swales, with topsoil classified as either loam or sandy loam, over 4.5 years and 52 rainfall events. Based on the results, they concluded that the swales would capture 0.56 cm of rain through initial abstractions

and completely capture runoff when infiltration rates were 1.5 cm/h (0.59 in/h). It was predicted that swales designed similarly would capture 59% of storm events during a typical Maryland year. Furthermore, Stagge *et al.* (2012), based on the observations from Davis *et al.* (2012) concluded that, hydraulically, these swales operate in three phases: completely infiltrating the smallest 40% of storm events, reducing the total runoff volume for an additional 40% of events, and performing simply as flow conveyance with negligible volume attenuation for the largest 20% of events.

Barrett (1998b) indicated that in practice, flow in swales tends to concentrate in small, incised channels that reduce their effectiveness in removing constituents dissolved in highway runoff. Le Bissonnais *et al.* (2004) reported a reduction in the efficiency of grassed strips when the runoff was concentrated in channels and the surface was not completely covered by runoff water. Poletika *et al.* (2009) investigated the effect of drainage area ratio and flow concentration on percentage volume reduction of a vegetative filter strip. The strips with 15:1 and 30:1 drainage area ratio had a mean volume reduction of 41.4 and 33.9%, respectively. The plot with concentrated flow (only 10% of the surface) had a volume reduction of 16.4%.

Finally, Barrett (2008) reviewed the data compiled in the International Stormwater BMP Database, concluding that if the soil has low initial moisture content or high hydraulic conductivity, the infiltration achieved by swales can approach 50% of the runoff volume in semiarid regions. Results from previous research on infiltration performance of swales and filter strips have great variability on percentage of water infiltrated, probably because they have a wide range of inputs and use different methods. They generally vary in location, swale characteristics and type of soil, precipitation intensity and duration, drainage area, and method to input water.

Computational models have also been used to analyze swales; results depend upon soil properties. Ackerman and Stein (2008) used a BMP model with hourly output from a land-use model to evaluate flow-through a swale. They demonstrated that grassed swales reduce mean runoff volume by approximately 52.5%. Hwang and Weng (2015) used ten-year rainfall records as input of the SWMM 5 model to calculate the average runoff coefficients from a catchment in Taiwan. The average runoff coefficients were reduced from 0.95 to 0.80, both without and with a swale system.

Based on previous studies, infiltration performance of swales is linked to infiltration capacity of the soil, initial soil moisture content, ratio of impervious drainage area-swale area, length and width of the vegetated area, slope, type of flow down the side slope of the swale (spread or concentrated flow), and total depth and intensity of precipitation. Consequently, the model proposed in this research takes into account these factors. According to Kachchu Mohamed *et al.* (2013), monitoring the performance of full-scale stormwater treatment devices during real storm events is difficult to do with accuracy. They state that performance monitoring of field installation using simulated rainfall events is a more reliable approach. In this research, the infiltration response of drainage ditches to different rainfall regimes using simulated runoff has been tested with field experiments, and the results have been used to validate the model.

2. Influence of Micro-Topography on Overland Flow and Infiltration (Task 1)

See Appendix A

III. Laboratory Experiments (Task 2)

The current dry swale calculators assume that water flows as sheet flow over the side slope of swales (MIDS calculator, MPCA; Deletic (2011); Akan *et al.* (2014)). However, water, when limited, may flow in shallow micro-channels and concentrates in depressions rather than flowing as sheet flow. The non-uniform distribution of water along a hillslope directly affects infiltration.

At low rates of overland flow, the wetting of a surface will not be uniform, even when the surface is perfectly smooth. A surface that is modulated with micro-topography promotes preferential flow over the surface, such that the fractional wetting of the surface is more important to runoff and infiltration. Surface micro-topography is further modified with erosion and deposition processes until it stabilizes. When water flow is low, rather than flowing over the entire surface, it will concentrate in micro-channels and depressions.

The goal of these experiments was to determine the impact that fractional wetting of the slope surface has on infiltration rates; and whether micro-topographic patterns parallel to the flow enhance runoff generation. A full-scale model of a road shoulder and side slopes was built and used to perform a number of tests with different initial conditions related to the micro-topography of the surface. To relate overland flow processes on hillslopes with micro-topographic conditions, the surface of the side slope was monitored through the use of a surface elevation data acquisition system. The test setup and results will be described below.

1. Method

1.a Experiment Settings and Procedure

A full-scale physical model of a road shoulder and side slopes was built at the St. Anthony Falls Laboratory. A parallel wooden flume representing the cross section of a swale with 1:6 slope was used to perform the laboratory experiments. The flume (Figure 2) consisted of a 2% slope pervious shoulder of 1.83 m (6 ft) and a 5.95 m (19.5 ft) side slope. The shoulder consisted of the same soil as the slope of the swale. The width of the flume was approximately 0.91m (3 ft).

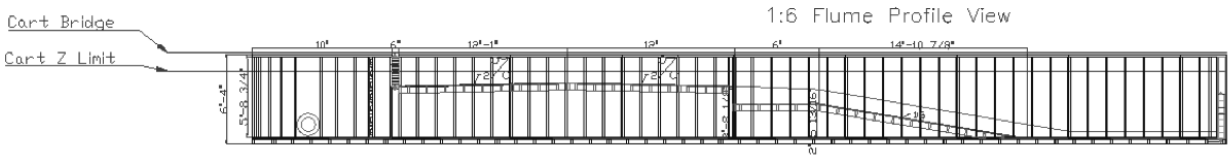

Figure 2 1:6 Flume Profile View.

On the side slope, the soil depth was 0.3m (1 ft). There was a suppressed rectangular weir, horizontal crest that crosses the full channel width, at the transition from the road section to the shoulder. A series of perforated drainpipes were located below the soil layer, 5 in the 1:4 flume and 8 in the 1:6 flume (Figure 3). These drainpipes were covered with a permeable geotextile to keep soil from entering.

Figure 3 Left: Image of the 1:4 Flume with smoothed surface. **Right:** Image of the drain pipes underneath the soil in the flume.

The soil was loamy sand consisting of a mixture of 4% gravel, 88% sand, 6% silt, and 2% clay (Figure 4). It was compacted before each experiment with a 12 lb, 10 in x 10 in tamper. A bulk density value was obtained, following the procedure described by ASTM D2937, 2010. Three bulk density samples were taken, using a cylindrical core sampler and a metal hammer and driver. From those samples, the porosity was calculated to be 40%. The flume was saturated with water 24 hours before each experiment and allowed to drain, so the soil could be considered at field capacity when the experiments began. The initial soil moisture content was approximately 12% in all of the tests.

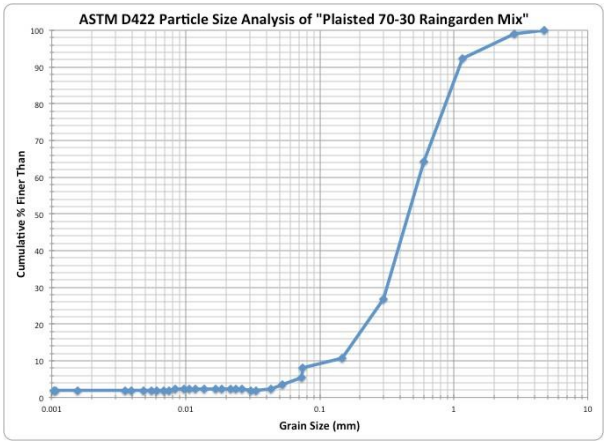

Figure 4 Particle Size Analysis of the laboratory soil (ASTM D422; ASTM D6913). By Mathew Hernick.

Water supply was regulated with a valve and connected to a rectangular constant head tank located

on the road lane closer to the side slope.

A surface elevation data acquisition system with data carriage that provides a three-axis positioning with a tenth of a millimeter precision scanned the soil surface several times during the tests. Next, the data acquisition system software generates a 3D Digital Elevation Model (DEM), which is a representation of the surface of the slope. To document elevations with water on the surface, the water was mixed with titanium dioxide (TiO_2), which allows the laser light to be reflected on the water surface (Legout et al., 2012).

An electronic metering pump was used to add the slurry of water and TiO_2 in a high concentration to the main flow of water (Figure 5). Additionally, titanium dioxide was added to the box where the water was pumped and mixed with a paint mixer. Tests indicated that a 3 g/L concentration of TiO_2 was required for the water surface elevation to be measured by the data acquisition system.

Figure 5 Injection of the mix of titanium dioxide and water. By David Bauer.

A 1.1 in-24hr storm captures 90% of all rainfall events in the Twin Cities area (Figure 6). The appropriate intensity curve to use in this region of the country corresponds to the SCS, Type II storm. For this study, and based on the SCS curve, it was assumed that 90% of the precipitation occurs in one hour (Figure 7) in the middle of the storm event. In light of this, the water applied to the slope was equivalent to a rainfall with constant 2.54 cm/h (1in/h) intensity over a 10m (32.8ft) wide road and 0.91m (3 ft) cross section. Thus, the maximum rainfall intensity of the 1.1 inch storm will be represented by the water applied to the slope.

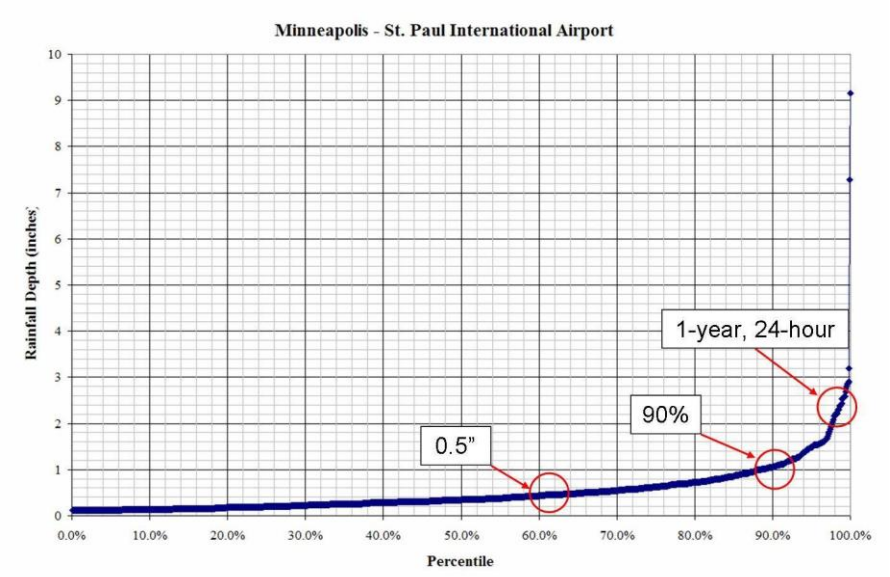

Figure 6 Rainfall frequency in the Minneapolis-St. Paul International Airport Station (Issue Paper "B", Emmons & Olivier Resources (2005)).

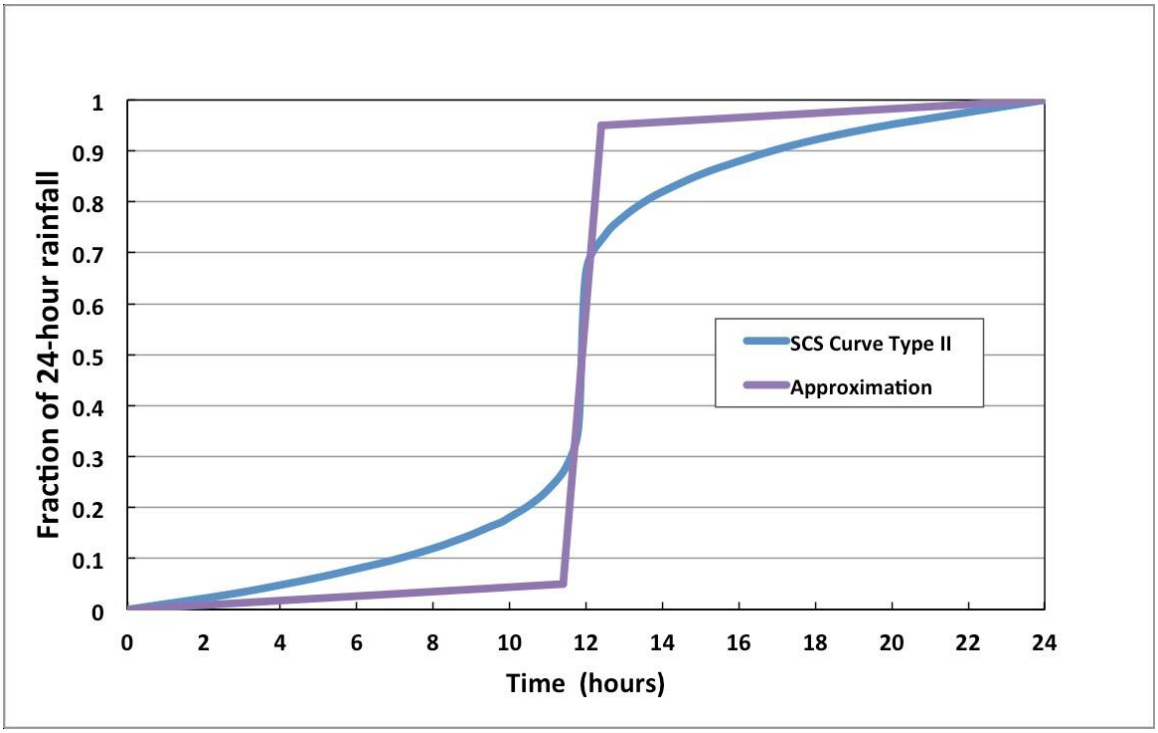

Figure 7 SCS Type II 24-hour rainfall distribution and approximation used in this project (USDA, 1986).

Each experiment lasted for one hour with a 234 liter (61.82gal) application of water. Within each experiment the water inflow was stopped after 15 and then again 40 minutes to scan the surface with the data acquisition system.

The water infiltrated was collected by the drainpipes, transported out the flume by gravity and measured in buckets located underneath the exit of the pipes. The runoff water, or water that was not infiltrated into the side slope of the swale, was collected at the bottom of the flume and discharged into an outflow channel.

Three different micro-topographies were tested over non-vegetated sandy loam soil: a smooth surface, a surface with three parallel rills, and a surface with five parallel rills (Figure 8). For each experiment, the soil was prepared by compaction with a tamper and smoothed with a plastering trowel. For the treatments with rills, longitudinal channels were produced in the compacted soil using a 4.6 cm (1.8 in) diameter steel pipe steel pipe. Each of the scenarios was repeated three times, the total number of tests was nine.

Figure 8 Left: Surface with 5 initial rills. **Right:** Surface with 3 initial rills.

1.b Data Collection

The following data was collected for each experimental run:

- Volume of water infiltrated in each drain pipe over time,
- Total volume of runoff water,
- Micro-topography of the surface, and
- Wetted surface area.

The topographic information collected with the data carriage was processed using MATLAB. The micro-topography of the soil surface was scanned 4 times, at 0, 15, 40 and 60 minutes after the beginning of each experiment.

After 15 and 40 minutes of water flowing down the swale, the water input was stopped and the dry surface was scanned. Then, a mix of TiO_2 and water was added to the inflow with a pump and two more readings of the surface were completed. The wetted surface area was calculated as the points

where there was a difference in elevation between the dry surface reading and the reading with input of water and titanium dioxide. An example can be seen in Figure 9.

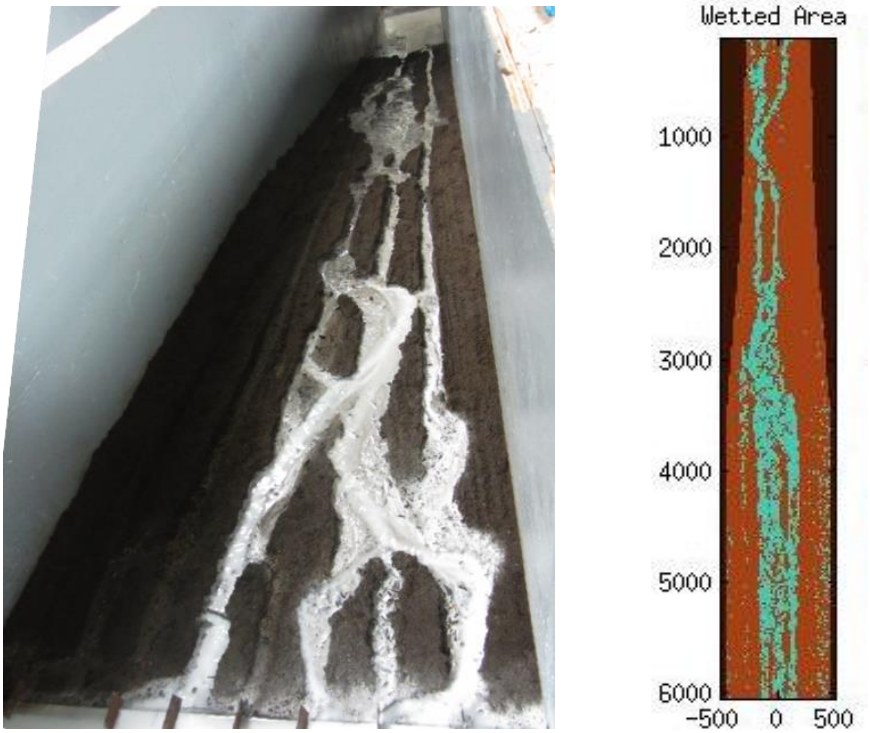

Figure 9 Left: TiO_2 mixed with water flowing over the side slope of the swale surface in the laboratory. **Right:** Computational representation of the wetted areas.

2. Results and Analysis

It is important to note that even in the initially smooth surfaces, erosion in upslope positions and deposition in downslope positions was observed on all the test runs (Figure 10). In grassed roadside drainage ditches, the vegetation would stabilize the soil surface.

Figure 10 Initially smooth surface before and after the laboratory tests.

2.a Infiltration Volume

Figure 11 shows the results of the infiltrated volume for each of the tests. The total input of water was 234 liters (61.82gal).

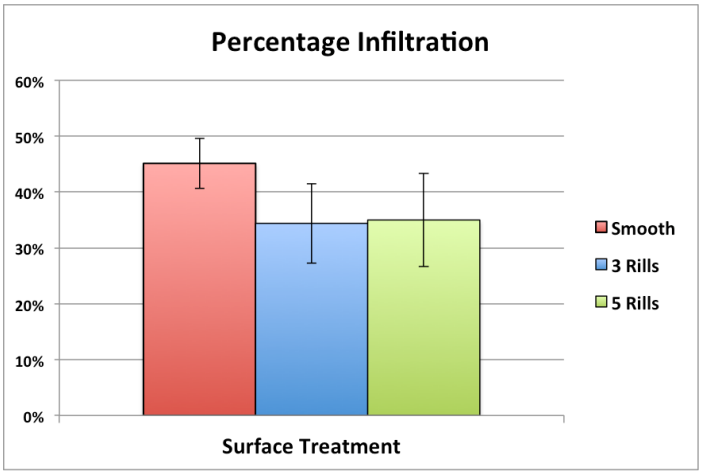

Figure 11 Average percentage of water infiltrated in the different laboratory experiments, the error bars represent the standard deviations.

Although all surfaces experienced erosion, the initially rilled surfaces had less infiltration. The relative difference between an initially smooth surface and both cases with rills was around 30% more water infiltrated. The disparity between the scenarios with 3 and 5 initial rills was insubstantial. The time when runoff first reached the bottom of the slope was affected by the surface treatment. No runoff reached the outlet of the slope for the initially smooth surface until the erosional features developed at 19 min; while for the cases with rills runoff occurred at 2 min.

Table 1 shows the distribution of the water infiltrated in the different underdrains. As the areas associated with each of the eight underdrains were not equal, an area correction factor, inversely

proportional to the drainage area of each drainpipe, was implemented to compare them. The drainage time was around 25 hours in all cases.

Table 1 Example of the percentage infiltrated per underdrain with three tests with three surface treatments: smooth, 3 rills, and 5 rills.

Smooth Case 3	**% Infiltrated per Underdrain (with Area correction)**							
Time (min)	1	2	3	4	5	6	7	8
After 4 hrs	16.2%	8.1%	7.4%	9.6%	18.9%	19.1%	10.4%	10.3%
After 20 hrs	13.8%	6.9%	6.3%	8.1%	16.1%	17.4%	13.1%	18.3%

3Rills Case 3	**% Infiltrated per Underdrain (with Area correction)**							
Time (min)	1	2	3	4	5	6	7	8
After 4 hrs	14.2%	3.3%	3.0%	6.9%	20.6%	13.9%	8.8%	29.4%
After 26 hrs	10.9%	2.5%	2.3%	5.3%	16.0%	11.1%	9.8%	42.0%

5Rills Case 3	**% Infiltrated per Underdrain (with Area correction)**							
Time (min)	1	2	3	4	5	6	7	8
After 4 hrs	11.3%	6.1%	8.3%	17.8%	17.9%	11.2%	4.2%	23.3%
After 30 hrs	8.0%	4.3%	5.9%	12.6%	13.0%	9.1%	8.1%	39.1%

The results from Table 1 show that the distribution of water infiltrated was different for smooth and rilled surfaces. In the smooth scenario water was more evenly distributed, while the rilled surfaces tend to infiltrate more of the water in the last section, possibly because there was less wetted area in the central slope section.

2.b Analysis of Roughness

In order to compare the roughness from different surfaces with one parameter, we used the random roughness factor (RR), which is the standard deviation of surface elevations. The RR reveals the vertical variability in surface elevations (Yang et al., 2013). The slope was divided into 1mm cross sections and the RR was calculated for each of the sections as:

$$RR = \sqrt{\frac{\Sigma(z - z_{mean})^2}{N}} \quad (1)$$

where z is the elevation at a given point, z_{mean} is the mean elevation of a cross section, and N is the number of points in a cross section. Figure 12 summarizes the results of random roughness measurements over time.

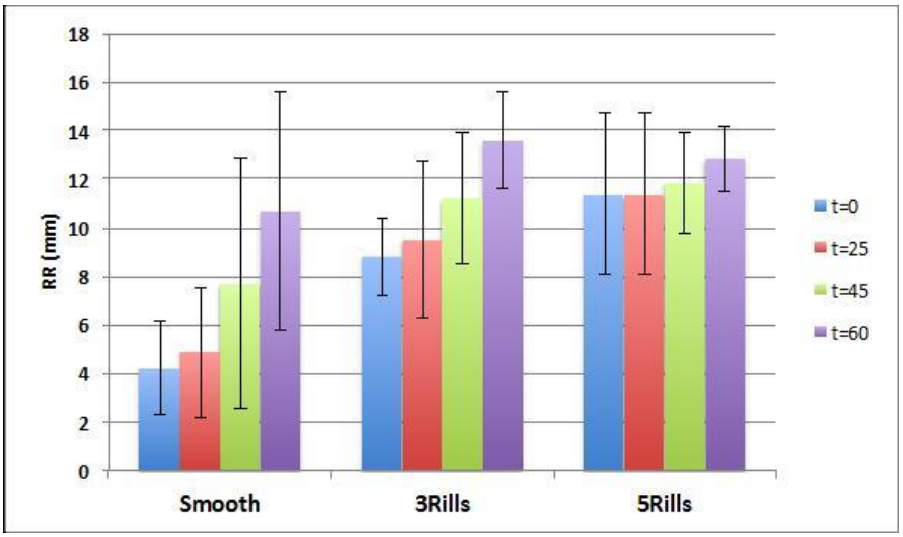

Figure 12 Evolution of the average random roughness over time for the smooth, 3 rills and 5 rills tests. The error bars represent the standard deviations.

The RR measurements changed over time as a consequence of erosion and sediment transport. The final RR of the three and five rill cases approximately 13 mm. The final RR of the smooth cases represented the increase of heterogeneity in surface elevations produced by rills formed by erosion and sedimentation.

The scour volume (Figure 13) was calculated from the digital elevation model (DEM) as the difference in elevation from the initial condition to the final condition after 60 minutes of flow. The initially smooth surface experienced an average of scouring greater than 50 dm^3 and had the greatest variability (st. dev. = 19.6 dm^3) compared to the rilled surfaces (st. dev (3rills) = 11.5 dm^3; st. dev. (5rills) = 4 dm^3). The average deposition volume in the initially smooth surface was 27 dm^3, the remaining scoured material was deposited downstream, outside of the study area.

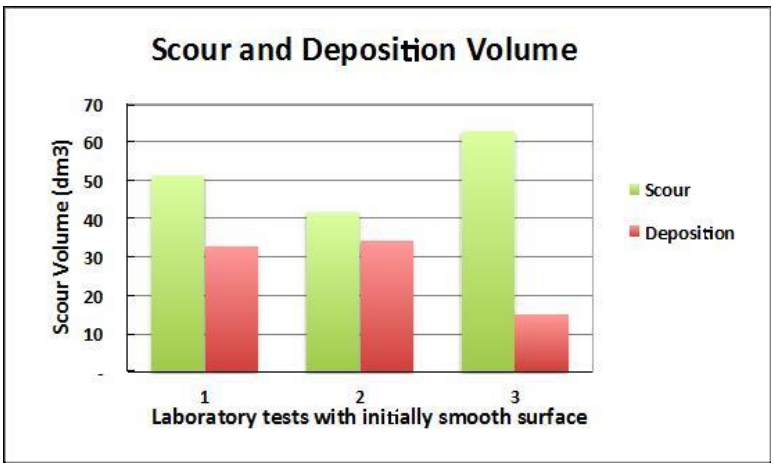

Figure 13 Scour and deposition volume for the three repetitions of the smooth surface tests at time = 60min.

Figure 14 shows the relationship between scour volume and RR for the experiments. The initally smooth surface seems to be well-represented by a linear relationship, which is the only case where all scour was produced by the flow. The 3 rill measurements could also be represented by a linear relationship of greater slope, but the 5 rill measurements are less clear. The total scour volume and percentage of runoff seem to have a linear relationship, having more runoff (less infiltration) for greater scour (Figure 15).

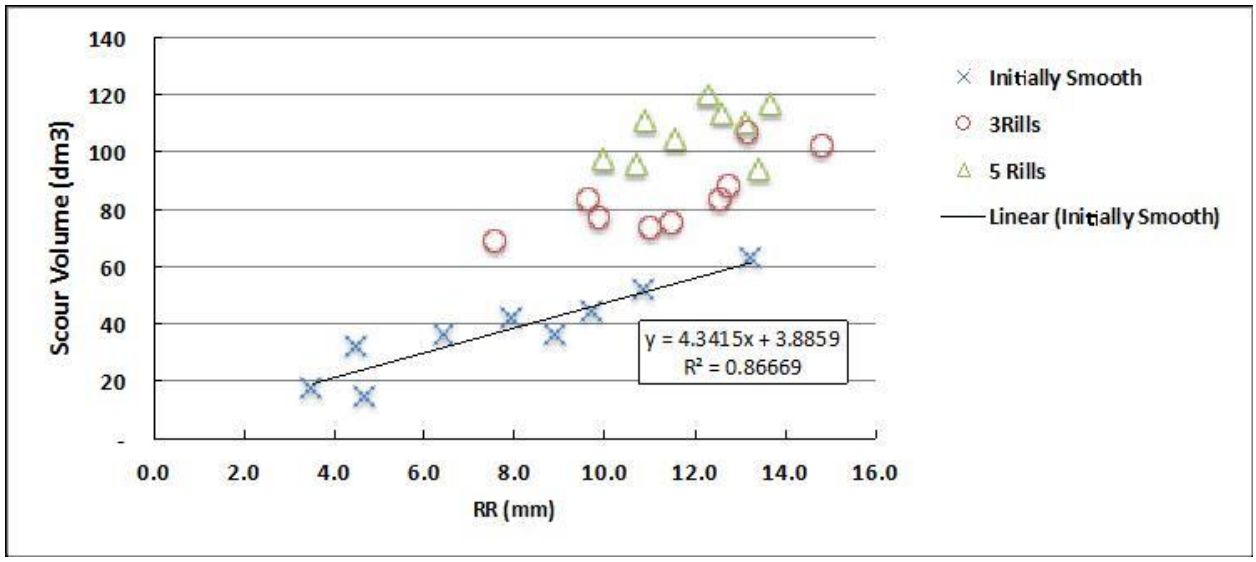

Figure 14 Scour volume (dm^3) versus Random Roughness (mm) for three difference surface treatments. The data corresponds to three repetitions at three different times (20, 40 and 60 minutes).

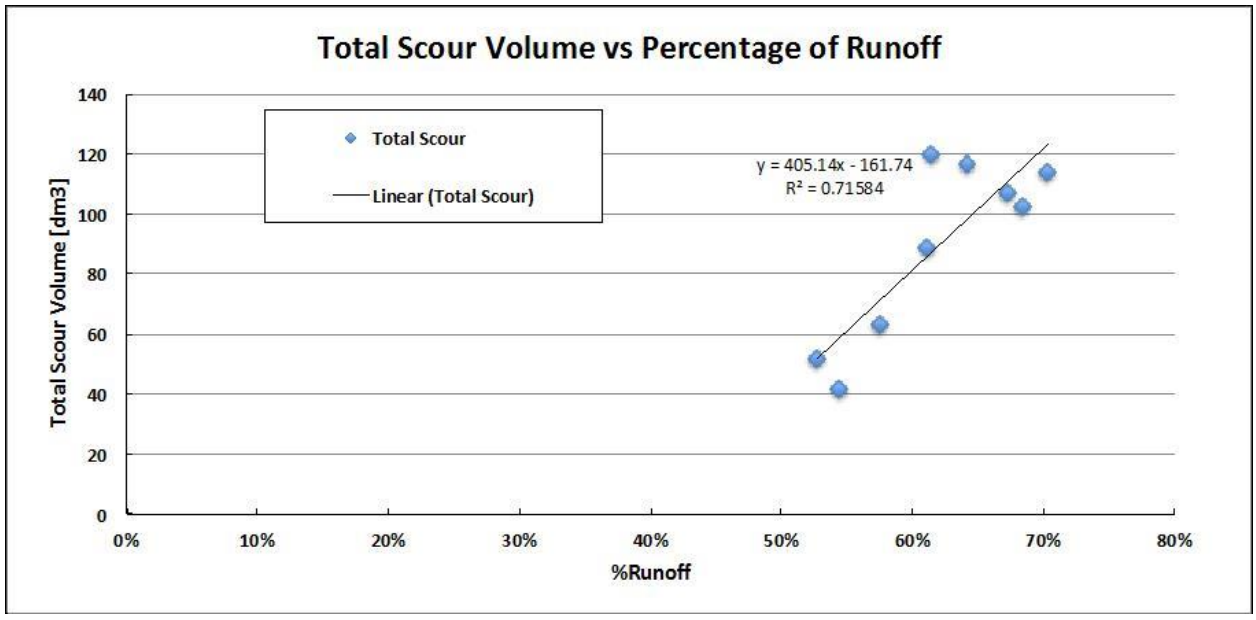

Figure 15 Total scour volume (dm^3) after 1h of flow versus percentage of runoff in all nine tests with different surface treatments.

2.c Wetted Area

Table 2 shows the percentage of wetted area from measurements at two times during the experiments.

Table 2 Percentage of wetted area after 20 minutes and 45 minutes of water flowing down the side slope of the laboratory swale.

Case	Surface	%Water Infiltrated	%Wetted Area after 20min	%Wetted Area after 45min	Average %Wetted Area after 15min	Average %Wetted Area after 45min
1	Smooth	47.3%	23.5%	16.2%	24.6%	18.4%
2		45.6%	29.1%	21.8%		
3		42.5%	21.2%	17.3%		
1	3Rills	38.8%	11.4%	11.8%	14.6%	13.8%
2		32.7%	19.6%	13.0%		
3		31.6%	12.7%	16.5%		
1	5Rills	39.4%	20.9%	21.0%	18.4%	17.3%
2		29.7%	13.8%	12.9%		
3		35.8%	20.6%	17.9%		

In Table 2, it appears the percentage of wetted area tends to decrease with time. Among all the experiments, only a small part of the swale surface received water, and the maximum wetted area was observed to be 29% of the overall slope.

The relationship between the percentage of wetted area and random roughness for initially smooth and rilled surfaces is illustrated in Figure 16. The RR was calculated with the elevation measures taken after 60 min of runoff over the surface. The slope length was divided into seven different sections and both the RR and percentage of wetted area was calculated in each of them. The plot indicates that the percentage of wetted area tends to decrease as RR increases. The difference between initially smooth surfaces and rilled surfaces is a remnant of the initial RR.

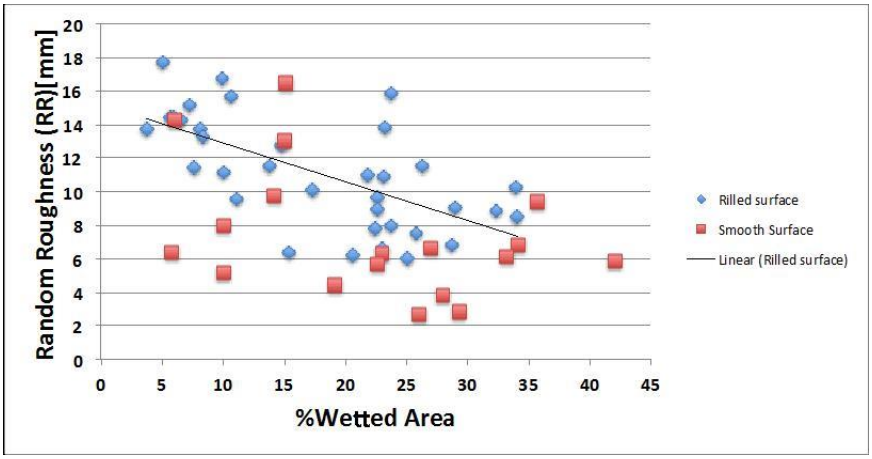

Figure 16 Random Roughness versus percentage of wetted area in each section for initially smooth and rilled surfaces.

The MPD infiltrometer method (Ahmed et al., 2014b) was used to obtain the saturated hydraulic conductivity (K_{sat}) and effective wetting front suction pressure head of the soil. Nineteen measurements were taken in the areas with no eroded channels. The saturated hydraulic conductivities obtained with this technique had a geometric mean of 12.8 cm/h (5.1 in/h) and a standard deviation of 5.5 cm/h (2.2 in/h), and the effective wetting front suction head of 0.56 cm (0.22 in). This mean K_{sat} value is higher than those Ahmed *et al.* (2014b) obtained in the field from swales located in the Twin Cities area. For example, the geometric mean of the K_{sat} calculated for the side slope of Highway 51 was 3.6 cm/h (1.4 in/h), and for Highway 13 was 4.3 cm/h (1.7 in/h). However, a swale in Madison, WI had a K_{sat} of 16 cm/h (6.3 in/h).

Figure 17 represents the relationship between water infiltrated and percentage of wetted area in each cell for a 1.1 in-24hr storm. Assuming that the given best fit line can be extrapolated to a higher percentage of wetted area, all the water added would be infiltrated (12.5% x 8 cells= 100%) if each cell had 86% of its area wetted. If we assume uniform sheet flow rather than fractional flow, the percentage of wetted area would be 100%, the volume infiltrated in each cell would be 14.5% of the total volume, and so the entire volume would be infiltrated before the end of the seventh cell (14.5 x 7 cells = 102%).

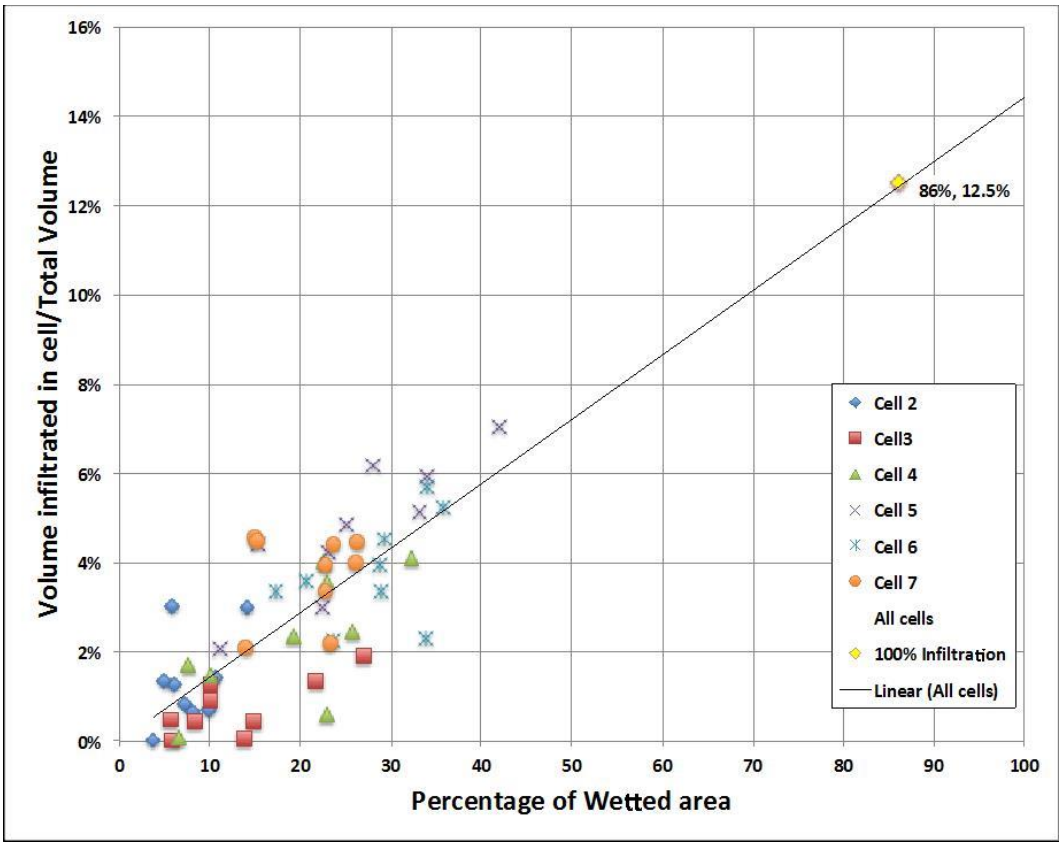

Figure 17 Volume infiltrated in each cell over the total volume of input water versus the percentage of wetted area of each cell. There were a total number of 8 cells. The first and last cells are not included because of the excessive erosion occurred on those cells.

3. Summary

The goal of this task of flume analysis was to analyze the effect of fractional coverage of water on infiltration rates. All the tests showed that water on the lateral slope of a swale flows as a concentrated flow, not as sheet flow, at the typical intensities for which infiltration practices are designed and utilized to improve surface water quality. The slope analyzed represents the worst-case scenario for erosion of a drainage ditch: without vegetation or surface protection of any kind. A more common field condition is the one where the surface is stabilized with vegetation.

The random roughness factor changes with time as a consequence of erosion and sediment transport. The final RR of the three and five rill cases was similar; this could be a sign of reaching a stable surface. The final RR of the smooth cases represented the increase of heterogeneity in surface elevations produced by rills. The volume of water infiltrated in an initially smooth surface is roughly 10% greater than a rilled surface. Although all surfaces experienced erosion, the initially rilled surfaces had less infiltration. This is also indicated by the time required for runoff to occur, an average of 19 min for smooth surfaces (when erosional features have developed) and 2 min for the cases with rills.

The laboratory experiments demonstrate that there is a relationship between the percentage of wetted area and the amount of volume infiltrated. The trend is to have more infiltration when there is more wetted area. The percentage of wetted area in each of the cells for all of the tests ranged

from 4% to 42% of total area. The reason the percentage of wetted area was low even for initially smooth surfaces was the development of rills during the experiment.

IV. Flow Pattern of Runoff in Field Experiments (Task 3)

Field experiments have been conducted to investigate the effective contact surface for infiltration modeling. Four highways in the Minneapolis-St. Paul metropolitan area with grassed roadside swales 30 to 50 years old and different soil types (loam, loamy sand, sandy loam, and sandy clay loam) were selected for a series of field studies. Results have been used to both analyze infiltration performance of grassed roadside swales and to calibrate a coupled infiltration and overland model that allows the calculation of stormwater infiltration efficiency of roadside drainage ditches.

1. Method

1.a Experiment Settings and Procedure

The four highways selected for this study were analyzed previously in the MnDOT project: "Assessing and Improving Pollution Prevention by Swales" by Ahmed *et al.* (2014a). In the aforementioned project, after collecting a soil sample from fifteen swales in the Twin Cities area, soil textural analysis was performed and the swales were divided into soil types. For each soil texture class, one swale was selected for infiltration measurement and the number of swales was narrowed down to five on which infiltration measurements were taken. Due to safety concerns, Hwy 212, located at the median of the highway, was not included. The four highways studied in this Task were: Hwy 13 (Hwy 13 and Oakland Beach Ave. SE, Savage, MN), Hwy 47 (University Ave. NE and 83rd Ave. NE, Fridley MN), Hwy 55 (Snelling Ave. and County Rd. E, Arden Hills, MN), and Hwy 77 (Cedar Ave. and E 74th St. North of Hwy 494, Bloomington, MN).

The soil types studied (loam, loamy sand, sandy loam, and sandy clay loam) represent approximately 53% of the soils found in road embankments in the State of Minnesota (Figure 18). The soil types belonged to hydrologic soil groups A, B, and C (NRCS, 1986). Soil samples were taken in the specific locations selected for this study and the soil textures were in agreement with the previous MnDOT project (Ahmed et al., 2014a). Two locations were tested in each highway.

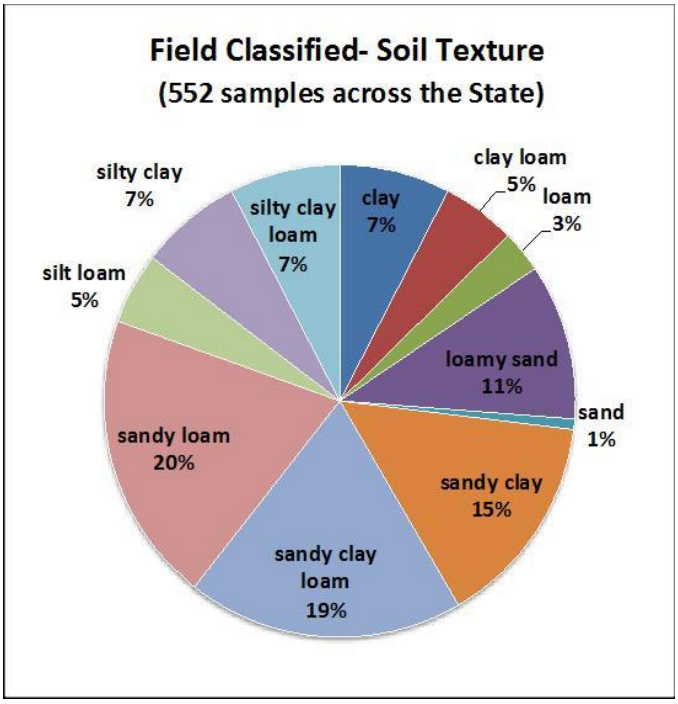

Figure 18 Field classified soil texture from 552 samples of road embankment soil across Minnesota. Data obtained from the MnDOT project: "Minnesota Steel Culvert Pipe Service-Life Map" by Marr, J. and Heitkamp, B. (June 2015).

The Green Ampt (1911) parameters (saturated hydraulic conductivity (Ksat) and wetting-front suction (ψ)) were previously estimated at these highways using a MPD infiltrometer (Ahmed et al., 2014b). At the end of all the field tests, these two parameters have been estimated again in the specific ditch sections studied in this project.

For the field tests, the grass was mowed with a lawn mower and shears were used to finish cutting the surface vegetation to approximately 1cm (0.39 in) in height. The grass clippings were collected with the lawn mower and the remaining were cleared with a bamboo rake. Figures 19 and 20 show an example of the initial and final surface of the drainage ditch after cutting the vegetation. The roots of the vegetation were not modified, leaving the existing soil matrix and soil macroporosity in the original state.

Figure 19 Initial condition of Hwy 77 grassed drainage ditch during the spring experiments.

Figure 20 Grassed drainage ditch at Hwy 77 after cutting the surface vegetation.

Surface roughness data was collected using a pin meter operated on a fixed frame (Figures 21 and 22). Cross-sectional pin meter measurements were taken with a camera, collecting the relief every 10.16 cm (4 in) along the whole length of the swale side slope.

Figure 21 Pin meter located on fixed frame.

Figure 22 Pin meter measuring the relief of a cross section on Hwy 13.

Three different application rates were used, equivalent to a rainfall of 2.79 cm/h (1.1 in/hr), 2.79 cm/30min (1.1 in/30min), and 2.79 cm/15min (1.1 in/15min) intensity over a 10 m (32.8 ft) wide road and shoulder. The 1.1in-60min, 1.1in-30min and 1.1in-15min storms are approximately 1-year, 2-year and 10-year events in the Twin Cities (NOAA Atlas 14).

The equivalent runoff water from each of these events was applied to a strip width of 0.91 m (3 ft) at the top of the slope along the edge of the road. The water was pumped with a hose from a 113.56 L (30 gal) container with a submersible pump. The flow was adjusted with a valve, volumetrically calibrated before every experiment. The hose pumped the water to a plastic box with a rectangular weir (Figure 23). To enable visualization of the flow patterns, the water was mixed with kaolin,

using a paint mixer, to achieve a 13 g/l (0.1 lb/gal) uniform concentration. The total volume of water for every experiment was 255.4 L (67.47 gal).

Figure 23 Input water system: mixing container (blue) with a calibrated submersible pump in it, and plastic box with a rectangular weir to input the water into the side slope of the ditch.

The water patterns were recorded by installing a camera with a mounting pole set in the channel of the drainage ditch. The camera was programmed to take one picture every five seconds. A 1x1m (3.28 x 3.28 ft) mesh frame was installed on the swale to facilitate corrections of angle distortions in the pictures taken.

Figure 24 shows the original and projected images of the water pattern flowing down a swale side slope.

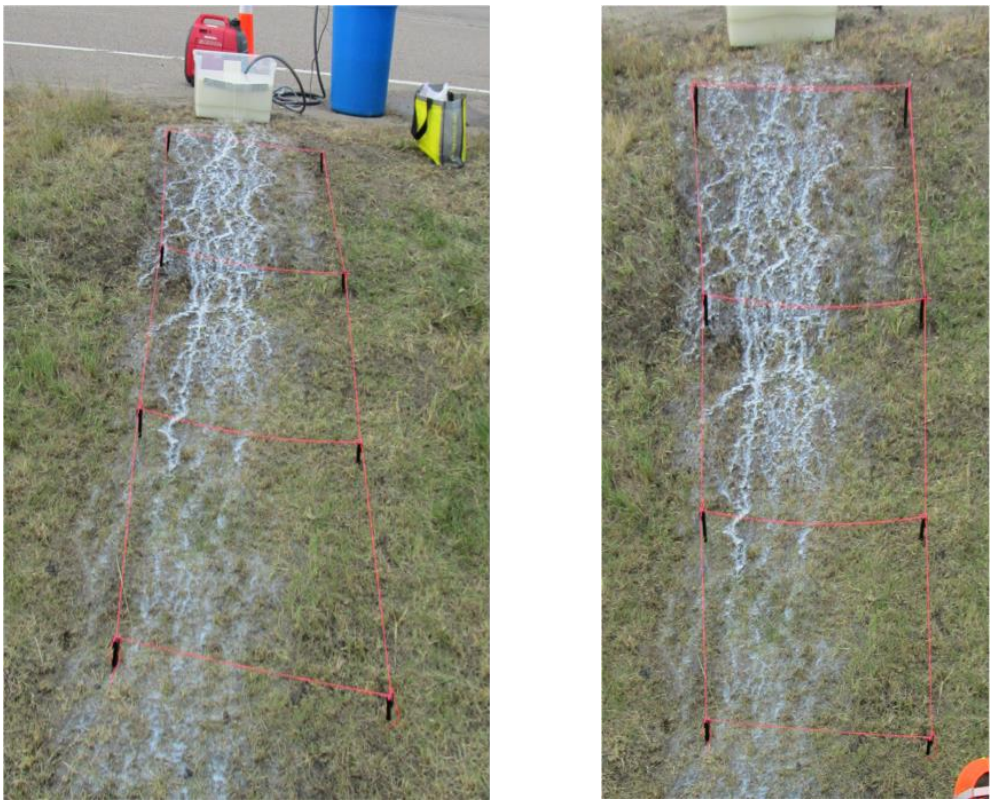

Figure 24 Left: Original and projected **Right:** Images of the water pattern flowing down the drainage ditch during a simulated a 1.1in-30min storm.

The water not infiltrated by the side slope of the swale was collected from a trench dug at the bottom of the side slope connected to a receiving bucket. The total volume of water that was not infiltrated (runoff) was recorded using measuring buckets, as well as the runoff rate when the system reached steady state, that is when the volume collected over 30 seconds intervals was constant.

1.b Data Collection

The following data were collected:

- Micro-topography of the surface,
- Total volume of runoff water (water not infiltrated in the swale),
- Intensity of runoff water,
- Wetted surface area over time,
- Soil texture and bulk density,
- Initial soil moisture content, and
- Saturated hydraulic conductivity and effective wetting front suction.

For each highway, eight soil cores between the soil surface and 12.7 cm (5in) were collected, using a cylinder core sampler to examine bulk density and porosity (ASTM D2937-10). Two of those samples were used to investigate soil texture; the soil samples were processed using the wet sieving analysis (ASTM D6913) and hydrometer analysis (ASTM D422) to determine % clay, % silt and

% sand in each sample. Before each test, three soil samples were collected to determine initial soil moisture content (ASTM D2216).

The MPD infiltrometer method (Ahmed *et al.*, 2014b) was used to estimate the saturated hydraulic conductivity (K_{sat}) and effective wetting front suction (ψ) (Figure 25).

Figure 25 MPD Infiltrometer measurements at Hwy 51.

The topographic contour collected with the pin meter and the camera was analyzed using GIMP, GNU Image Manipulation Program (free and open-source raster graphics editor).

To evaluate the wetted area, images were processed following a five step procedure using the software ImageJ, an image processing and analysis software. First, based on the frame positioned in the field, the image was orthogonally projected (Figure 26), using the ImageJ plugin Projective_Mapping by M. Schlüter with a bilinear approximation. Second, the picture was transformed into an 8-bit grey scale. Afterwards, a study area was selected and cropped based on the spread of the water along the slope. Then, a Fuzzy Contrast Enhancement (Figure 26 center) plugin (Alestra and Battiatto, 2008) was used to differentiate the wetted from the dry area. Finally, a thresholding method that binarises 8-bit images was implemented to select the wetted area. The preferred technique was the "Intermodes" method (Prewitt et al., 1966), which assumes a bimodal histogram (Figure 26 right).

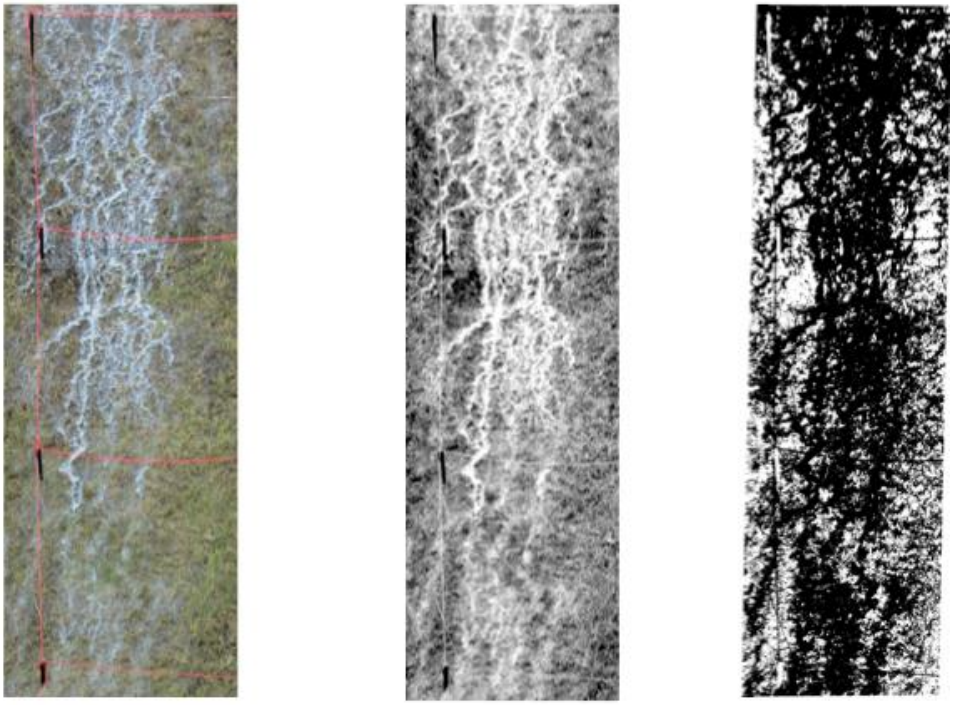

Figure 26 Processing of the picture taken in the field. **Left:** Projected image. **Center:** Projection with Fuzzy Contrast Enhancement applied. **Right:** Final selection of wetted area (in black).

Analysis of the Design Parameters in the Field tests:

The field tests were designed to investigate the parameters that are believed to be the most significant in the process. The field tests are a partial simulation of what would happen in reality. The differences between side slope infiltration on a real storm event and the field tests are the following:

- The rainfall over the side slope was not considered in the field tests. The pre-wetting of the soil due to rainfall overestimates the infiltration capacity of drainage ditches side slopes.
- The shoulder was assumed to the impervious, but in reality a volume of water is infiltrated in the shoulder.
- The water retained on the surface of the road is not accounted for.
- The interception of the rainfall by vegetation is not taken into account.
- The vegetation mulch was swept to clear the grass clippings. This natural organic matter layer of decaying plants would absorb some fraction of the direct precipitation and road discharge.
- It is assumed that the rainfall over the road directly flows to the side slope, without a lag time. The time of concentration is assumed to be zero.
- It was assumed that the road discharge was a uniform sheet flow at the location it entered the side slope.

To test the impact of not considering rainfall over the side slope, a simulation has been performed to compare runoff and infiltration 1) including only the road runoff and 2) including both rainfall and road runoff. Hwy 13 spring tests data has been used as inputs for side slope and soil characteristics. The rainfall intensity was 1.1 in – 60 min (1-year event). The amount of water infiltrated into the fractionally wetted area (both before the road runoff gets to the slope and after it gets there) increases only a small amount (about 2 percent) over the amount that infiltrates when there is no rainfall applied. Essentially, when rainfall falls onto the areas that is wetted by the encroaching road runoff, that added water becomes runoff because the surface is already ponded. Thus, the increase in runoff at the bottom of the swale is primarily the rainfall that falls onto the surface wetted by the road runoff.

2. Results and Analysis

The analysis of the field work is based on a total of 32 tests performed during Fall 2014, Spring 2015, and Summer 2015 on highways: 51, 77, 47, and 13 in the Twin Cities Metropolitan area. Table 3 indicates the tests performed in each highway.

Table 3 Summary of the field tests performed and intensities used. The duration of the 1-year, 2-year and 10-year storms was 60, 30 and 15 minutes, respectively.

	Season	# tests	Event Intensity
Hwy 51	Fall	2	2-year storm
	Spring	6	1-year, 2-year and 10-year storm
Hwy 77	Fall	2	2-year storm
	Spring	6	1-year, 2-year and 10-year storm
Hwy 47	Fall	2	2-year storm
	Spring and Summer	6	1-year, 2-year and 10-year storm
Hwy 13	Fall	2	2-year storm
	Summer	6	1-year, 2-year and 10-year storm
	Total	32	

2.a Characteristics of the Swales

Table 4 provides information about the sections of the swales examined during the field experiments. Using the percentages of clay, silt and sand in a textural triangle (USDA, 2014) the soil texture class was determined. Rows with two soil textures (Hwy 51, 47, and13) indicate that the highway contains all corresponding textural classes of soil. The slope and length were measured in each site. The saturated hydraulic conductivity was estimated in the test strips once all the tests were completed. The representative saturated hydraulic conductivity for infiltration given in Table 4 is computed by taking 0.68 times the geometric mean plus 0.32 times the arithmetic mean of 20 estimates of K_{sat} performed on the strips tested (Weiss and Gulliver, 2015).

The soil textures correspond to hydrologic soils groups A, B and C; however, the saturated hydraulic conductivities (K_{sat}) estimated correspond to hydrologic soil group (HSG) A (Minnesota Stormwater Manual Version 2, MPCA). Therefore, the infiltration performance of these soils is better than the expected for these types of soil. It is particularly interesting that Hwy 13, with a loam/sandy clay loam soil texture type, corresponds to a HSG A soil. In the field, it was observed that the clay was not distributed homogeneously as a layer, instead it was heterogeneously spread in lumps. The K_{sat} values are given for a given temperature (20ºC) because viscosity changes with temperature and K_{sat} is inversely proportional to viscosity. Despite the initial compaction during the construction, the porosity of consolidated drainage ditches soil was high due to the macropores generated by vegetation roots, activity of macrofauna (e.g. earthworms), and construction practices. For example, the 2000 MnDOT Standard Specifications for Construction specified that if hardpan layers or compacted soil layers were exposed below the normal planting depth, additional deep ripping or other measures to ensure proper root development and drainage were required. In addition, re-aeration and loosening of the affected planting soil was required; the loosening had to be 500 mm (18 inches) wide adjacent to the spade-moved soil and 300 mm (12 inches) deep. The 2016 MnDOT Standards specify to use a spading machine to deep cultivate the planting hole and bed areas by loosening the soil to at least 300 mm (12 in) deep and a compaction level of no more than 1,400 kPa (200 psi) to this depth.

Table 4 Characteristics of the swales studied based on soil cores samples, estimations of saturated hydraulic conductivity (at 20ºC), and length and slope of the sections used in the experiments. Hydrologic Soil Group based on Ksat from Minnesota Stormwater Manual Version 2, MPCA. *Coefficient of variation in parenthesis

	Soil Texture	HSG (based on soil texture)	Ksat (cm/h) (at 20°C) (estimated in the field)	HSG (based on Ksat)	Bulk Density (gm/cm3)	Porosity (%)	Average Initial Soil Moisture Content (Fall) (%)	Average Initial Soil Moisture Content (Spring) (%)	Slope	Av. Length studied (cm)
Hwy 51	loam/sandy loam	A / B	3.54 (1.44)*	A	1.12	0.56	0.15	0.30	5:1	406
Hwy 77	loamy sand	A	5.74 (0.94)*	A	1.18	0.56	0.15	0.20	5:1	407
Hwy 47	loamy sand/sandy loam	A	3.47 (1.29)*	A	1.21	0.54	0.12	0.27	5:1	779
Hwy 13	loam/sandy clay loam	B / C	4.14 (1.87)*	A	1.11	0.58	0.13	0.29	4:1	422

Soil texture, bulk density and porosity were based on soil cores obtained during Fall 2014. K_{sat} estimations were done in Summer 2015. The initial soil moisture content data is based on soil samples taken before each of the Fall 2014 and Spring 2015 tests.

2.b Infiltration Volume

The total input of water was 255.4 L (67.47 gal) for all tests. The flow during the 1-year, 2-year, and 10-year storm events lasted 60, 30, and 15 minutes, respectively. Table 5 shows the results of the different experiments done in highways 51, 77, 47, and 13 during fall 2014, and spring and summer 2015, with percentage of volume infiltrated, start time of runoff (flow not infiltrated entering the channel) and approximate runoff rate (at the bottom of the side slope) after steady state in runoff was approached for the different cases studied. The sequence of the tests is important to understand the percentage infiltration obtained. The first tests were performed in Fall 2014 (2-year storm). After winter, three tests were performed during spring and summer 2015: 1) 2-year storm 2) 1-year storm 3) 10-year storm.

Table 5 Results of the field experiments at the four highways selected during the three different seasons using three different intensities of rainfall.

	Season	Event Intensity	Site	Runoff start time (min)	Rate runoff (steady state) (L/min)	%Infiltrated
Hwy 51	Fall	2-year storm	Site 1	17	2.75	86.5%
			Site 2	9	3.1	74.1%
	Spring	2-year storm	Site 1	11.6	5.5	61.4%
			Site 2	12	4.2	72.4%
		1-year storm	Site 1	8.8	3.1	59.2%
			Site 2	5.6	3	62.1%
		10-year storm	Site 1	1.7	16.25	32.2%
			Site 2	1.4	16.5	32.7%
Hwy 77	Fall	2-year storm	Site 1	6.3	3.75	64.8%
			Site 2	15	4.2	76.6%
	Spring	2-year storm	Site 1	9	4.85	61.8%
			Site 2	8.8	4.75	65.9%
		1-year storm	Site 1	17.6	2.5	68.9%
			Site 2	28.8	2.5	72.9%
		10-year storm	Site 1	2	16.25	20.6%
			Site 2	3.3	15	37.5%
Hwy 47	Fall	2-year storm	Site 1	-	-	100%
			Site 2	27.6	0.04	99.96%
	Spring	2-year storm	Site 1	25	1	98.0%
			Site 2	9.8	4.4	72.7%
	Summer	1-year storm	Site 1	-	-	-
			Site 2	14.8	2.5	65.0%
	Summer	10-year storm	Site 1	10	2.8	95.0%
			Site 2	5.9	8	74.9%
Hwy 13	Fall	2-year storm	Site 1	18.5	2.5	88.4%
			Site 2	18.25	2.6	87.0%
	Summer	2-year storm	Site 1	10.9	4.5	68.4%
			Site 2	9.2	6.9	59.1%
	Summer	1-year storm	Site 1	11.8	2.82	60.7%
			Site 2	13	2.8	60.7%
	Summer	10-year storm	Site 1	1.5	13	41.8%
			Site 2	1.6	13.2	42.2%

During spring 2015, before the 1-year storm test, the roadside drainage ditch of Hwy 51 was impacted by the allocation of fiber optic cable across the ditch and the nearby construction of the County Road E bridge (Figure 27). The surface of the drainage ditch had vegetation losses and compaction due to truck and excavation operation. The length studied changed in Site 1 from 398 cm to 278 cm and in Site 2 from 413cm to 330cm. At highway 47, gopher holes (Figure 28) were observed and the infiltration rates in these sites were especially high, with almost 100% infiltration for all intensities on site 1.

Figure 27 Condition of Hwy 51 after before the 1-year storm test. Truck transit and excavation operations altered the surface of the swale.

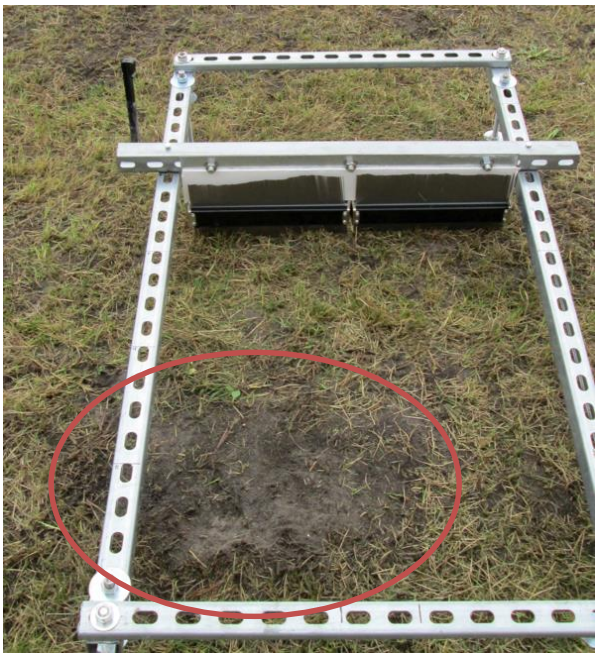

Figure 28 Evidence of a gopher hole in Hwy 47.

Figure 29 displays the average infiltration percentage for the different intensities. The average percentage of water infiltrated during the 2-year storm experiments performed in fall (8 tests) was 84.7% (12.7% standard deviation), this value is higher than the results observed during spring 70% (12.4% standard deviation). During the 10-year event (8 tests) the average of water infiltrated was 47.1%, with a standard deviation of 24.9%. The average water infiltrated during the 1-year events was 68.7%, with a standard deviation of 13.5%. The infiltration data collected from the 2-year storm experiments performed in spring was similar to the 1-year storm events. These results imply that there was a reduction in the saturated hydraulic conductivity in the consecutive tests; the first tests having a higher K_{sat} than the rest. This situation was previously observed in filter strip field tests by Deletic and Fletcher (2006). The kaolinite particles suspended in the water could have precipitated and clogged several pores. The following tests would have started with an initially sealed surface, where the infiltration rates were lower than for the first experiment.

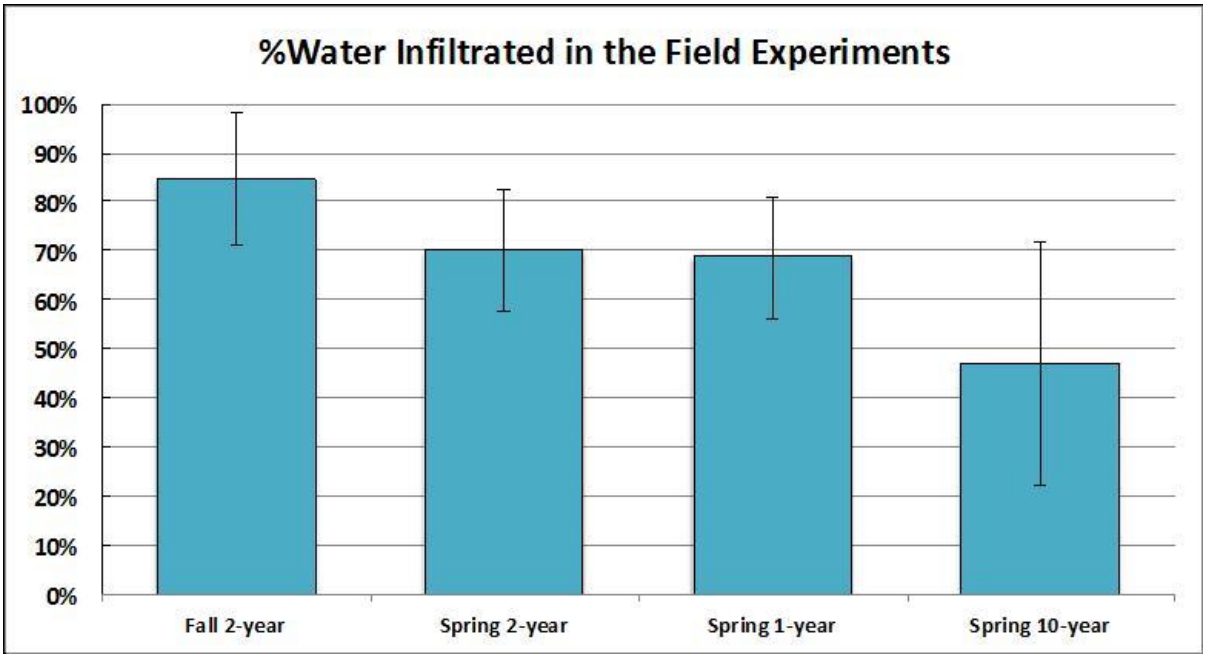

Figure 29 Average percentage of water infiltrated in the field experiments. Two sites were tested for each of the four highways. Three intensities were applied: 1, 2, and 10-year storms, the tests are shown in chronological order. The error bars represent the standard deviations.

2.c Roughness Analysis

The surface of the drainage ditches studied neither showed signs of previous erosion nor experienced erosion during the experiments. The measurements taken with the pin meter were translated into a random roughness factor (RR) (Allmaras *et al.* 1966), which is the standard deviation of surface elevations. The RR reveals the vertical variability in surface elevations (Yang et al., 2013). The average RR (perpendicular to the flow) for all the swales was 4 mm (0.157 in) with a standard deviation of 1mm (0.04in). The average RR (parallel to the flow), corrected for slope, was 5 mm (0.197 in), with a standard deviation of 3 mm (0.118 in). In summary, the soil surface was relatively smooth with no prominent topographical features.

One item of interest for Section V is the depression storage on the slope that will be used in predictions of infiltration. Onstad (1984) developed a relation, given in Equation 1, that relates maximum depression storage (*MDS*) with RR and slope (S). Because Onstad's equation was developed for a maximum slope of 12%, a slope correction was applied to estimate *MDS* for slopes of 20% and 25%. Álvarez-Mozos *et al.* (2011) developed a series of equations to estimate maximum depression storage based on the slope. Using Onstad solutions with Álvarez-Mozos *et al.* exponential reduction of *MDS* due to the slope, the depression storage for the side slope was estimated to be less than a millimeter for all field sites.

$$MDS = 0.112\ RR + 0.031\ RR^2 - 0.012\ RR \times S \qquad (1)$$

2.d Wetted Area

The wetted area appeared to be related to the rainfall intensity. The more intensity, the more area covered by water (Figure 30).

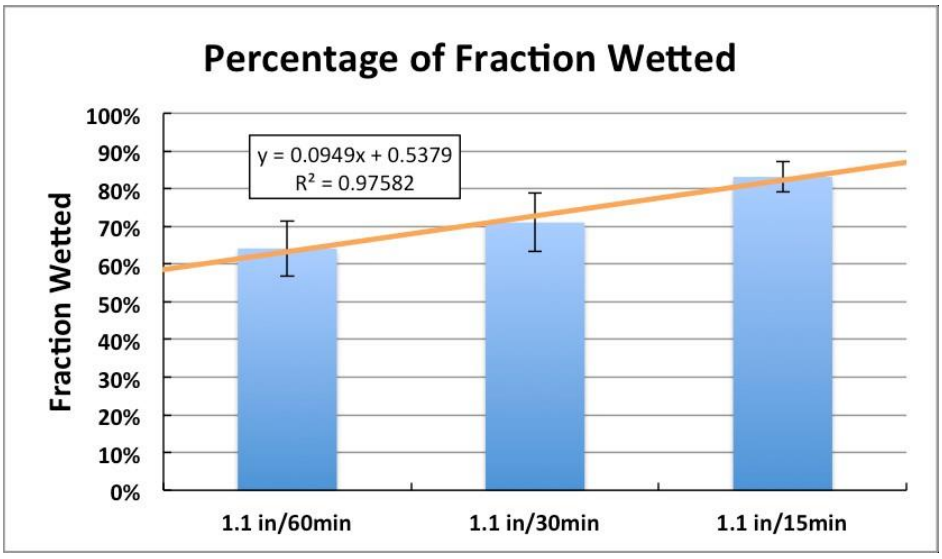

Figure 30 Percentage of fraction of the side slope wetted during the field experiments for three different intensities. The error bars represent the standard deviation and the line is the linear trend.

Figure 31 represents the relationship between water infiltrated and percentage of wetted area for a 1.1 in-30min storm (2-year event). The tests represented include all four highways studied.

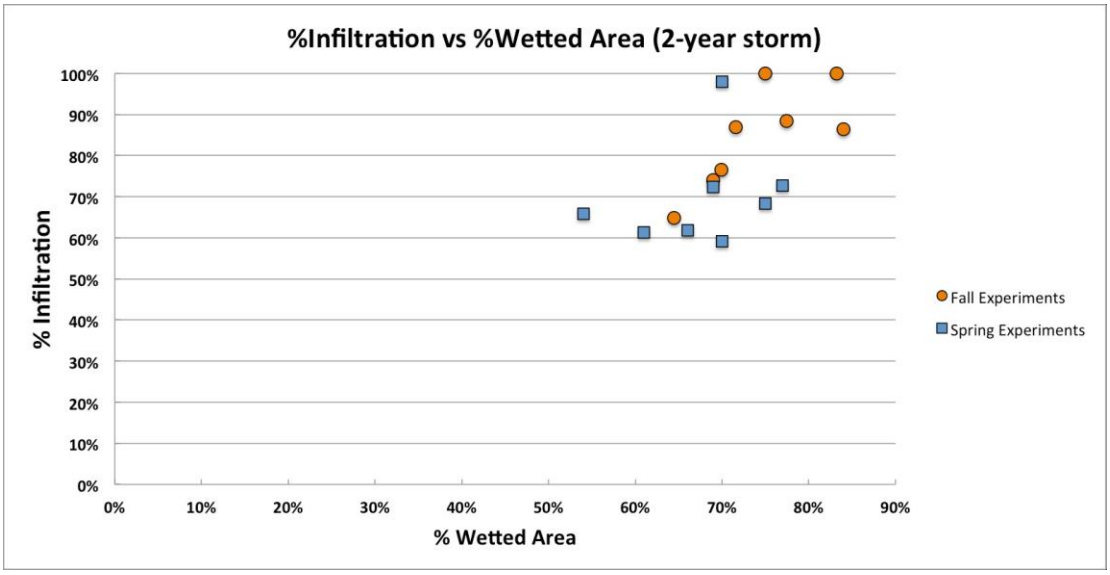

Figure 31 Dimensionless percentage water infiltrated versus percentage wetted area in the 8 field experiments performed during Fall 2014 and 8 during Spring 2015 under a 1.1 in-30min storm (2-year event).

The soil during the spring experiments had higher initial soil moisture content, which often resulted in a larger overall spread in the flow (higher total area) and lower percent wetted area (wetted area over total area). The fall experiments indicated a more linear relationship between percentage of wetted area and infiltration than the spring tests. The variability of other inputs such as soil moisture content and wetting soil suction, also have an effect on the infiltration percentage.

In addition to the 1.1 in-30min storms, two further intensities (1.1in-60min and 1.1in-15min storm) were tested during spring 2015. Figure 32 shows the relationship between water infiltrated and percentage of wetted area for all three intensities in the four highways and the laboratory experiments.

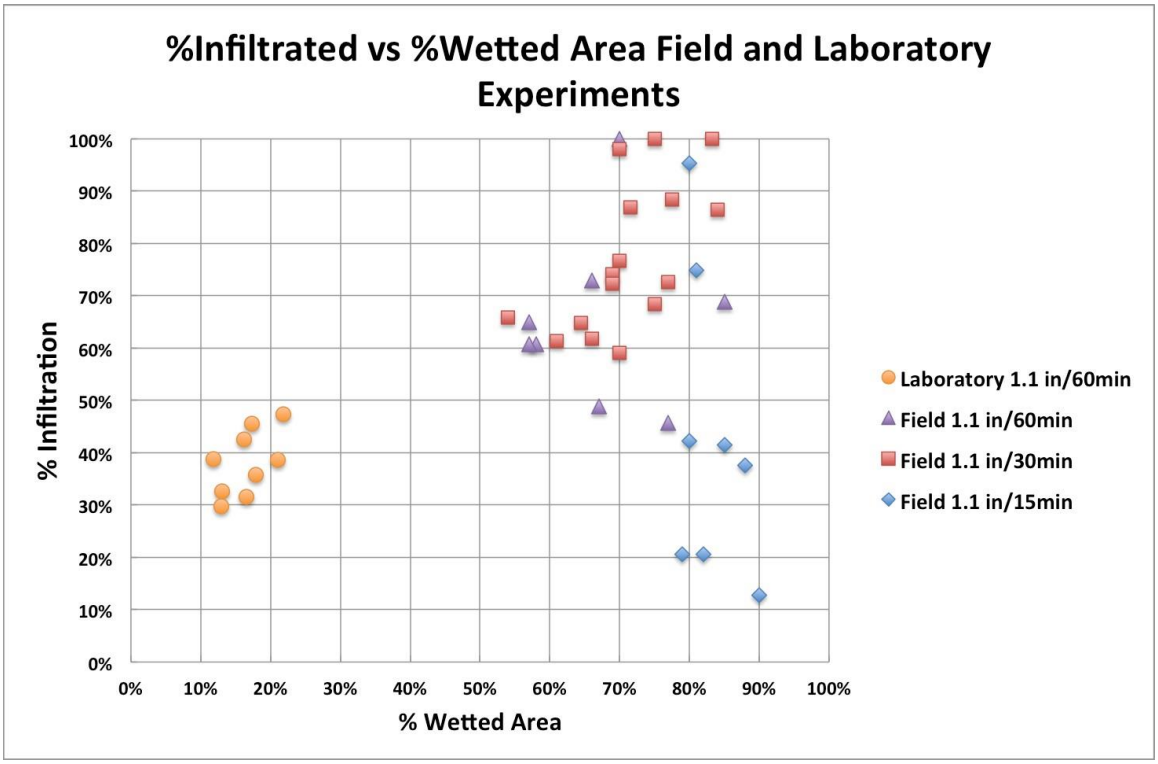

Figure 32 Dimensionless percentage water infiltrated versus percentage wetted area in the 9 laboratory experiments and the 24 field experiments performed during Spring 2015 under a 1.1in-60min, 1.1in-30min and 1.1 in-15min storm (1, 2, and 10-year events).

In the laboratory experiments, the wetted area is lower than in the field experiments due to the erosion experienced in the bare soil of the flume. In addition, the saturated hydraulic conductivity of the soil in the laboratory was 12.8 cm/h, which was higher the field K_{sat} values of between 3.4 and 5.9 cm/h given in Table 4. The variability of the results in the field tests could be linked to the soil type, saturated hydraulic conductivity, initial soil moisture content, and the length of the swale analyzed. Greater side slope lengths allow more time of water infiltrating before saturation of the soil, which results in more volume of water infiltrated. Furthermore, when saturation occurs, there is a greater surface area infiltrating water at a constant rate (saturated hydraulic conductivity). Finally, the cases with almost 100% infiltration correspond to the site with the longest side slope (almost double the other sites) where gopher holes were observed.

2.e Initial Soil Moisture Content Effect on Infiltration

The initial soil moisture content during the spring experiments was higher than during fall. Additionally, the volume of water infiltrated during the spring experiments was lower than during the fall tests. The soil water deficit, which is the difference between the saturated and initial soil moisture content, and the percentage of volume infiltrated were measured. The saturated soil

moisture content was assumed to be the porosity of the soil. Figure 33 shows the relationship between the percentage of water infiltrated and the soil water deficit.

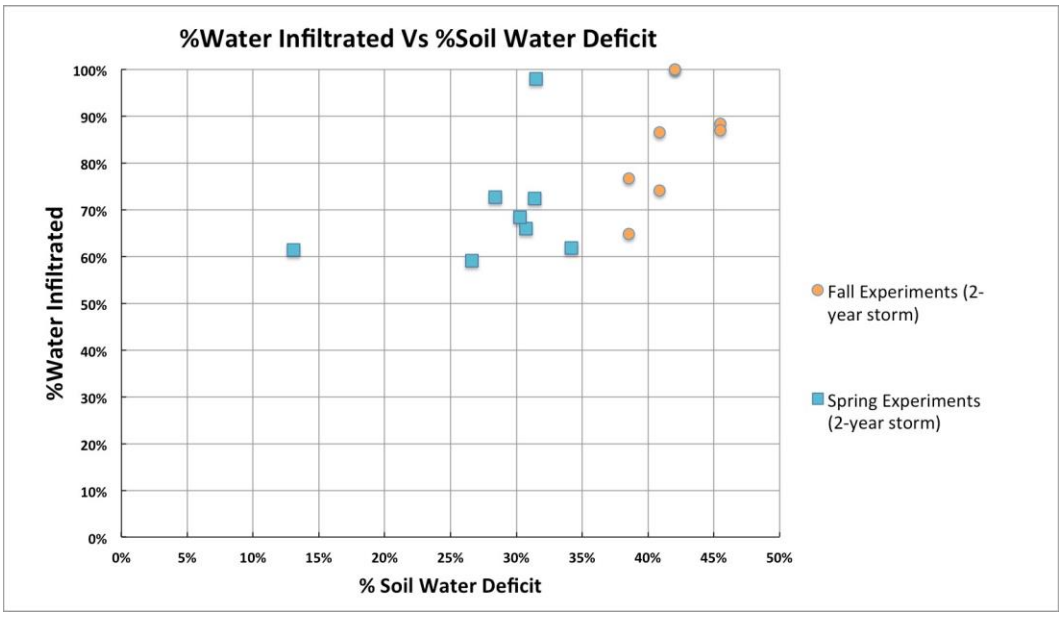

Figure 33 Percentage of water infiltrated versus soil water deficit. The two 100% infiltration events correspond to the Hwy 47 site, which had almost double the side slope length and where gopher holes were observed.

Soil water deficit did not make much difference until it reached 35%, then the soil water deficit and percentage of water infiltrated seem to follow a linear relationship. Above 35% of soil water deficit, for initially dryer soil conditions, the volume infiltrated is higher. Figure 34 shows a comparison between the infiltration performance and initial soil moisture content of the Fall and Spring 2-year event tests. Only two data points per highway were collected, in a total of four highways; it is not possible to provide statistically significant conclusions with these few data points. However, it appears that for differences in initial soil moisture content greater than 15%, the infiltration percentage can increase up to 25%.

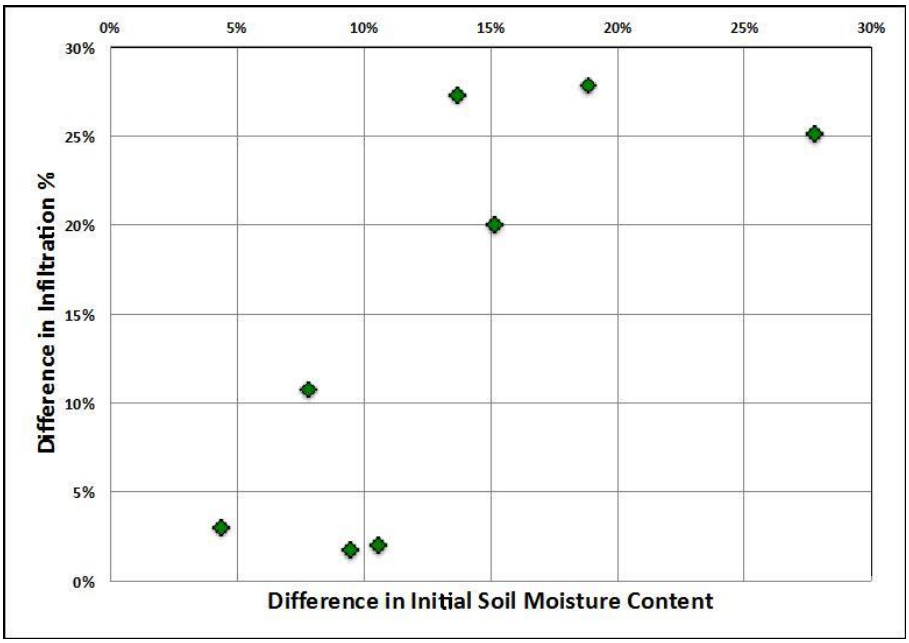

Figure 34 Difference in infiltration percentage versus difference in initial soil moisture content. Fall 2014 and Spring 2015 tests are compared for four different highways. Two tests per highway.

2.f Saturated Hydraulic Conductivity Effect on Infiltration

In the field experiments, the saturated hydraulic conductivity of the soil was an important factor for infiltration rates. Figure 35 displays the relationship between the percentage of water infiltrated and the dimensionless ratio of saturated hydraulic conductivity (K_{sat}) over rainfall intensity (i). The results confirm that, below a ratio of 0.3 to 0.4, the percentage of water infiltrated in the side slope of the swale increases with K_{sat}/i. Beyond that point, however, the percent infiltrated seems to be relatively constant. Since the K_{sat} values do not vary much, it is possible that this simply represents the influence of a higher intensity over shorter periods.

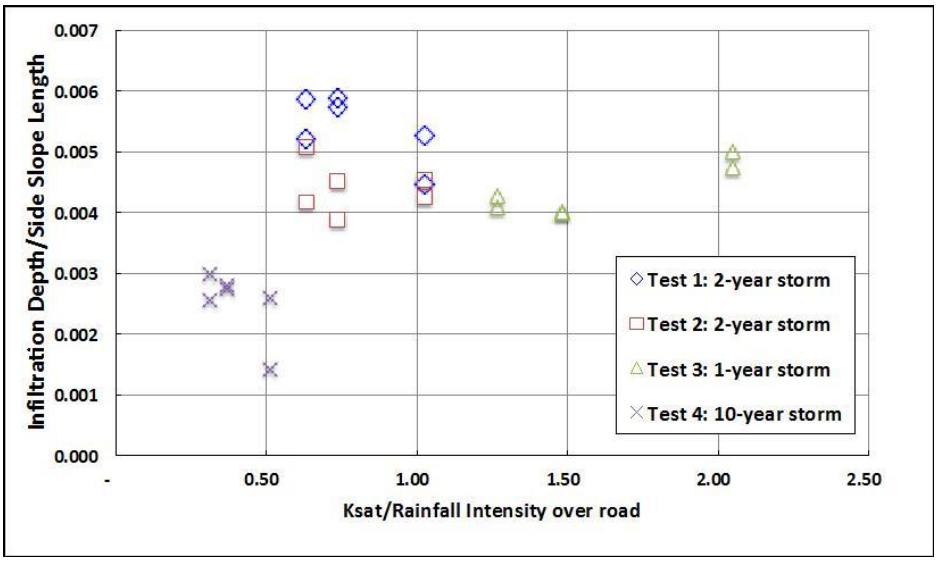

Figure 35 Percentage infiltration versus saturated hydraulic conductivity over rainfall intensity. Tests from highways: 13, 51, and 77. These highways had a side slope width of between 4.06 and 4.22 m and an assumed road and shoulder width of 10 m.

3. Summary

A total of thirty-two tests have been performed during three seasons in four different highways located in the Twin Cities metro area. The goal of this study was to analyze the effect of fractional coverage of water on infiltration rates. All the tests showed that water on the lateral slope of a swale flows as a concentrated flow in fingers, not as sheet flow, at the typical intensities for which infiltration practices are designed and utilized to improve surface water quality.

The minimum fraction wetted detected was 54% and maximum 88%, with an average of 72% and standard deviation of 10%. A linear relationship between intensity of precipitation and fraction wetted was observed, for the intensities tested. No signs of initial erosion were observed in any of the sites, except for the unique case of Hwy51 after the operations performed in the area. None of the intensities experienced soil erosion due to the water flow. The surface of the side slopes was close to flat, without evident micro-topographic features; this was supported by low random roughness (RR) estimations. When plotting percentage infiltration versus fraction wetted, a great variability was observed in the results, probably linked to the soil type, saturated hydraulic conductivity, initial soil moisture content, and the length of the swale analyzed.

Despite the initial compaction during construction, the porosity of consolidated drainage ditches soil was high due to the macroporous generated by vegetation roots, activity of macrofauna (e.g. earthworms), and construction procedures. The saturated hydraulic conductivities (K_{sat}) corresponded to hydrologic soil group A (Minnesota Stormwater Manual- Version2, MPCA), even though the soil textures indicated corresponded to hydrologic soils groups A, B and C. Therefore, the infiltration performance of these soils is better than the expected for these types of soil. The average percentage infiltration of all the tests was 67.6%, with a 20.9% standard deviation. In addition, the trend was to have more infiltration when the saturated hydraulic conductivity was higher and for a greater side slope length, as expected. The vegetation, type of

soil and length of the side slope would be important to consider for constructing roadside drainage ditches which will be efficient in stormwater treatment.

Finally, the soil during the spring experiments had higher initial soil moisture content, which means lower soil water deficit. The volume infiltrated during spring for the same intensity (1.1in-30min storm) was on average 12% lower than in fall due to the larger initial soil moisture content in the spring.

V. Infiltration Runoff Model (Task 4)

1. Introduction

A coupled overland flow-infiltration model that accounts for shallow concentrated flow has been developed. This numerical model can be used to estimate the infiltration performance of roadside drainage ditches (roadside swales) for given rainfall intensities. The Green-Ampt-Mein-Larson assumptions were implemented to calculate infiltration along with a kinematic wave model for overland flow that accounts for short-circuiting of flow. The model has been established in the MATLAB programming language and allows for a wide range of user inputs such as: rainfall intensity, initial moisture content of the soil, saturated hydraulic conductivity, wetting-front suction, and the geometry of the side slope. The model will be verified with the field experiments on side slope infiltration.

2. Review of Overland Flow Models

Most of the prior interest in modeling swales is on the channel portion, not the side slope. However, in roadside grassed swales the side slope is an important component when calculating the volume reduction. According to Barrett et al. (1998), as long as the road runoff is allowed to flow directly down the side slope into the swale, the side slope acts as a filter strip. Described below are vegetated or grassed filter strip (VFS or GFS) numerical models that calculate overland flow and infiltration based on the assumption that the slope receives uniform sheet flow. Additionally, these models assess sediment transport, a model aspect that is beyond the scope of this research.

Hayes et al. (1984) at the University of Kentucky developed the GRASSF model for filtration of suspended solids by grass filter strips. The model describes flow by the continuity equation and steady state infiltration; the flow rate decreased linearly from the upstream to downstream end of the filter. Wilson et al. (1984) modified and incorporated GRASSF into SEDIMOT II, a design oriented hydrology and sedimentology watershed model. The modification consisted of adding an algorithm to calculate the outflow hydrograph and considering change in the filter slope over space.

In 1999, Muñoz-Carpena *et al.* presented VFSMOD, a single event model for simulating the hydrology and sediment filtration in buffer strips. The hydrologic component was based on: a Petrov–Galerkin finite element kinematic wave overland flow submodel (Muñoz-Carpena *et al.*, 1993a,b) and a modified Green–Ampt infiltration submodel (Chu, 1978; Mein and Larson, 1971, 1973; Skaggs and Khaheel, 1982; Muñoz-Carpena *et al.*, 1993b). Good predictions were obtained with the model if shallow uniform sheet flow occurred within the filter. Other researchers (Abu-Zreig (2001), Dosskey *et al.* (2008), and White and Arnold (2009)) also adopted the VFSMOD

model. Muñoz-Carpena and Parsons (2004) later developed the VFSMOD-W model, an extension of VFSMOD in which the upstream inflow hydrograph and the sedigraph, plot of changing sediment concentrations with time, are generated for a specified design storm.

Abu-Zreig (2001) tested and validated VFSMOD. A total of 20 VFS, 2, 5, 10 and 15 m long, slopes 2.3 and 5%, and with various vegetation covers, were tested under simulated sediment and runoff conditions (1, 0.65 and 0.3 L/s). Application of the VFS model to experimental data was satisfactory under the condition that actual flow widths were used in the model instead of the total filter width. Assuming flow width equal to filter width caused a major failure in predicting infiltration volume for all experiments because flow in the filters was not distributed over the entire width of most filters.

Deletic (2001) created TRAVA, a mathematical model of sediment transport in runoff over grass. Three processes were modeled related to the hydrologic process: a) infiltration, b) surface retention, and c) overland flow. The Green-Ampt equations were solved using the fully implicit method; the previous infiltration depth was not taken into account to calculate infiltration rates. A calibration parameter, surface retention, was applied to model the accumulation of water in depressions. The kinematic wave equations for overland flow were solved using Preiss-Mann's four point implicit method. The momentum equation had two options: Darcy-Weisbach or Manning's equation. Only the sediment block of the model was verified with laboratory and field experiments (Deletic, 2005 and Deletic et al., 2006). The runoff block of TRAVA was calibrated to simulate the water runoff rates measured in the field, which had flow depths of 7 to 24 mm. The calibration parameters were saturated hydraulic conductivity, initial soil moisture content, and Manning's n.

Poletika *et al.* (2009) used the VFSMOD model (Muñoz-Carpena *et al.*, 1993b) to investigate the effect of drainage area ratio and flow concentration (uniform versus concentrated flow) on pesticide removal efficiency of a VFS. The flow concentration was investigated by changing the VFS width from full plot width to 10% of the plot width. In the field tests, even for the most extreme treatment (concentrated flow with high drainage area ratio), the VFS provided a small reduction (15%) in surface runoff flow (Figure 36). Without calibration, the model predicted a reduction in infiltration performance for the concentrated flow of 16%, regardless of the drainage area ratio.

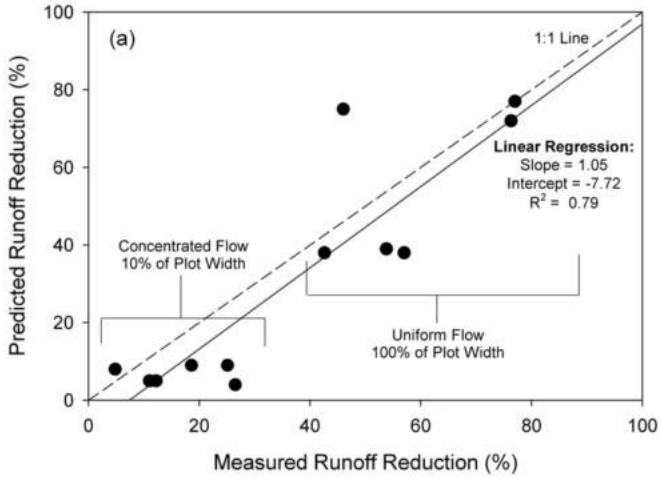

Figure 36 Linear regression between observed and VFS model predicted percent runoff volume reduction. The runoff reduction in the concentrated flow case (10% of the plot width) is underestimated by the model. Poletika *et al.*, (2009).

Akan (2014) simplified Muñoz-Carpena et al. (1993b) mathematical model and developed a set of charts for the quick hydrologic evaluation of vegetative filter strips. The simplifications were: 1) neglecting the rain falling directly over the filter strip or adding the volume of rainfall to the upstream inflow of water, and 2) approximation of the infiltration capacity equation assuming flow depth is much smaller than the characteristic soil suction head and depth of the wetted zone.

The previous models are focused on sediment transport, so the validation is usually centered in the outflow concentration of sediment. The models were created assuming sheet flow and, in some cases, a reduction of the width of the side slope was added to simulate concentrated flow (Abu-Zreig, 2001 and Poletika et al., 2009). In the latter cases, the simulations had either a poor correlation with the measured runoff for concentrated flows or were tested with higher flows (compared to the flows tested in this project). This project developed a calculator for roadside drainage ditches in Minnesota, and the tests performed correspond to 1-year (1.1in/60min), 2-year (1.1 in/30min) and 10-year (1.1 in/15min) storms, with flows of: 0.07, 0.14, and 0.28 L/s, respectively. In all the cases, shallow concentrated flow was observed and the water depths were around 5 mm.

3. Modeling Method

The model presented is a coupled infiltration-runoff model that can be used to calculate runoff from the side-slope and channel of a roadside grassed swale or drainage ditch. It includes the option of routing the water over only a fraction of the surface, instead of assuming sheet flow. The hydrologic components include the kinematic wave approximation and modified Green-Ampt-Mein-Larson infiltration modules, with the addition of depression storage on the side slope component. Finally, a range of rainfall events and initially wet/dry conditions can be simulated by changing the rainfall intensity and the initial moisture content of the soil.

3.a Hydrology

i.Overland flow

Lighthill and Whitham (1955) developed an approximation of the Saint-Venant's equations to model overland flow in 1-D, the kinematic wave approximation. The equation is based on the assumptions that the acceleration term and the pressure gradient term in the momentum equation are negligible, so that the energy slope is equal to the bottom slope. Singh (2001) concluded that the kinematic wave approximation is applicable to surface water routing, vadose zone hydrology, and many other hydrological processes. For shallow overland flow, neglecting the velocity and pressure head in the momentum equation is an adequate approximation. The kinematic wave equation is a first-order hyperbolic partial differential equation:

$$\frac{\partial A}{\partial t} + \frac{\partial Q}{\partial x} = i_e \, b \quad \text{(Continuity equation)} \tag{1}$$

where A is the wetted cross-section (A=*h***b*); h is the depth of flow; *b* is the width of the channel; *Q* is the discharge (*Q*=*q***b*); *q* is the discharge per unit width; i_e is the rain excess (i_e = *i*-*f*); *i* is the intensity of rainfall; *f* is the infiltration rate; *t* is the time; and *x* is the downslope distance.

When there is shallow concentrated flow, the width of the channel changes depending on the fraction of the area that is wetted (*fw*). That fraction wetted changes with time and space, until it reaches steady state and it becomes only a function of space (*fw(x)*). In this model we have assumed that the fraction wetted is steady, based on this assumption the width of the channel is:

$$b(x) = fw(x) * w \tag{2}$$

where *w* is the width of the study area (in both the field experiments and the laboratory experiments the width is 0.91 m (3 ft)) and *b(x)* the total width of the wetted surface calculated as the sum of the width of individual fingers of wetted surface.

If we substitute *A* = *b(x) h* and *Q* = *q b(x)* in equation (1):

$$\frac{\partial b(x)h}{\partial t} + \frac{\partial q * b(x)}{\partial x} = ie\,b(x) \tag{3}$$

Dividing by *b(x):*

$$\frac{\partial h}{\partial t} + \frac{1}{b(x)} \frac{\partial q * b(x)}{\partial x} = ie \tag{4}$$

Substituting Eq. (2) into Eq. (4):

$$\frac{\partial h}{\partial t} + \frac{1}{fw(x)} \frac{\partial q * fw(x)}{\partial x} = ie \tag{5}$$

In this model, Manning's equation, suitable for fully rough, turbulent flows, will be used to relate q and h. In addition, the kinematic wave assumption results in a energy gradeline slope for shallow flows that is approximately equal to the water surface slope. Then, incorporating a depression storage:

$$q = \frac{1}{n}\sqrt{S_o}(h - d_s)^{\frac{5}{3}} \quad (6)$$

where S_o is the slope of the plane, n is Manning's roughness coefficient, d_s is the depression storage, and metric units (m, s) are used for all the variables. In this case $\alpha = \frac{1}{n}\sqrt{S_o}$ and $m = 5/3$.

Initial condition for the side slope and channel model ($t = 0$):

$h = 0$, $0 \leq x \leq L$; where L is the length of the side-slope.

Boundary condition for the side slope model:

$q_{in} = q_0$ at $x = 0$; $t > 0$, $q_0 \geq 0$

Boundary conditions for the channel model:

$q_{in} = 0$ at $x = 0$;

For the kinematic wave approximation to be applicable, the flow Froude Number (Fr) must be less than 1.5 (Guo 1998, Bedient *et al.* in 2008), which is used as a constraint in the numerical program.

$$Fr = \frac{v}{\sqrt{gh}} < 1.5 \quad (7)$$

where v is the flow velocity and g the acceleration of gravity.

ii.Infiltration

In order to calculate the rain excess (i_e=i-f), the rainfall intensity (i) is an input of the model and an infiltration submodel is coupled with the overland flow model to estimate infiltration rate (f). The infiltration model is based on the Mein and Larson (1973) modification of the Green and Ampt (1911) method. The Green and Ampt method is a simplification of the Richards' equation assuming: sharp wetting front, uniform distribution of antecedent soil moisture, and homogenous soil profile. In order to model unsteady rainfall Chu (1978) adapted the Mein and Larson algorithm to make it applicable for unsteady rainfall.

$$F(t) - F(t - \Delta t) = \Delta F = \xi ln(\frac{F(t)+\xi}{F(t-\Delta t)+\xi}) + K_{sat}\Delta t = \xi ln(1 + \frac{\Delta F}{F(t-\Delta t)+\xi}) + K_{sat}\Delta t \quad (8)$$

where F is the infiltration depth; $\xi = \psi_f(\theta_s - \theta_i)$, ψ_f is the soil suction head, and θ_s, θ_i are the saturated and initial soil moisture content; K_{sat} is the saturated hydraulic conductivity.

Finally, Li *et al.* (1976) proposed a simple two-step method to estimate infiltration depth after surface saturation for a Green Ampt profile. The first step calculates ΔF using a truncated series expansion:

$$\Delta F_0 = \frac{1}{2}[Ksat\Delta t - 2F + \sqrt{K_{sat}\,\Delta t(K_{sat}\,\Delta t + 4F + 8\xi) + 4F^2}\,] \quad (9)$$

where ΔF_0 is the initial estimate of infiltration depth in Δt.

The second step uses a second-order Newton method to get ΔF, the infiltration depth within a time increment.

$$\Delta F = -F - \frac{(F+\Delta F_0)^2}{\xi} + \left(\frac{F+\xi+\Delta F_0}{\xi}\right)\sqrt{(F+\Delta F_0)^2 + 2\xi\left(\xi ln\left(1+\frac{\Delta F_0}{F+\xi}\right) + Ksat\Delta t - \Delta F_0\right)} \quad (10)$$

The intensity considered for each cell is:

$$i = q_{in}/\Delta x + i_{rainfall} \quad (11)$$

where q_{in} is the discharge per unit with entering the cell, Δx is the length of the cell, and $i_{rainfall}$ is the rainfall intensity.

If from eq. (11) $i = 0$, but there is ponded water (h>0), then

$$i = h/\Delta t \quad (12)$$

Finally, there are two options:

- If $\Delta P = i\,\Delta t < \Delta F$ then:

$$f = i \text{ and } F(t) = F(t-1) + \Delta P \quad (13)$$

- If $\Delta P = i\,\Delta t > \Delta F$ then:

$$f = Ksat\frac{\xi+F}{F} \text{ (Green Ampt equation) and } F(t) = F(t-1) + \Delta F \quad (14)$$

3.b Input Variables

The inputs of the model are the following:

i_r - Rainfall intensity over the road [L/T]
i - Rainfall intensity over the swale [L/T]
length - Length of the slope [L]
duration - Duration of study [T]
duration_storm - Duration of storm event [T]
psi - Effective wetting front suction [L]
deltatheta - saturated soil moisture content - initial soil moisture content
Ksat - Saturated hydraulic conductivity [L/T]
w_road – Width of the road perpendicular to traffic [L]
w_cell - Width of the study area [L]
fw(x) - Fraction wetted
S - Side slope
n - Manning's n value
ds - Depression storage depth (on side slope) [L]
rows - Number of sections down slope
T - Number of time steps

3.c Structure

This one-dimensional model has been established in the MATLAB programming language. In order to get a numerical solution, the model was discretized using an explicit scheme, represented in Figure 37, for both the overland flow and infiltration equations.

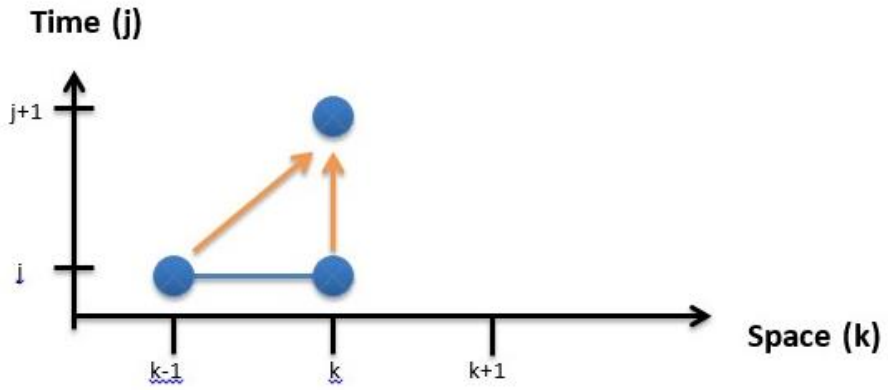

Figure 37 Explicit scheme representation. From known values at t=j, x=k-1 and x=k the model calculates the unknown values at t=j+1 and x=k.

The forward differences representation over time and space used to solve equation (4) are:

$$\frac{\partial h}{\partial t} = \frac{h_k^{j+1} - h_k^j}{\Delta t} \tag{15}$$

$$fw \frac{\partial q * fw}{\partial x} = \frac{q_k^j * \frac{fw_k + fw_{k+1}}{2} - q_{k-1}^j * \frac{fw_k + fw_{k-1}}{2}}{\Delta x \, fw_k} \tag{16}$$

Additionally, the effective intensity has been averaged between time steps:

$$ie = (ie_k^j + ie_k^{j+1})/2 \tag{17}$$

In summary, the linear equation in the explicit numerical scheme used to obtain the numerical solution of the first-order partial differential equation is:

$$\frac{h_k^{j+1} - h_k^j}{\Delta t} + \frac{q_k^j * \frac{fw_k + fw_{k+1}}{2} - q_{k-1}^j * \frac{fw_k + fw_{k-1}}{2}}{\Delta x \, fw_k} = (ie_k^j + ie_k^{j+1})/2 \tag{18}$$

Once we calculate water depth (h_k^{j+1}) then the discharge (q_k^{j+1}) is determined using eq. (7).

Explicit numerical algorithms require the Courant number, Cr, to have a value less than 1 in order

to prevent numerical oscillations.

$$C_r = C_k \frac{\Delta t}{\Delta x} < 1 \tag{19}$$

$$C_k = \alpha h^{\beta} \tag{20}$$

where C_k is the kinematic wave speed, $\alpha = am$ and $\beta = m\text{-}1$.

Model Flow Chart

The main loop increments over time and within each time step there is another loop incrementing over space. Depths and outflows are calculated for each cell and time step.

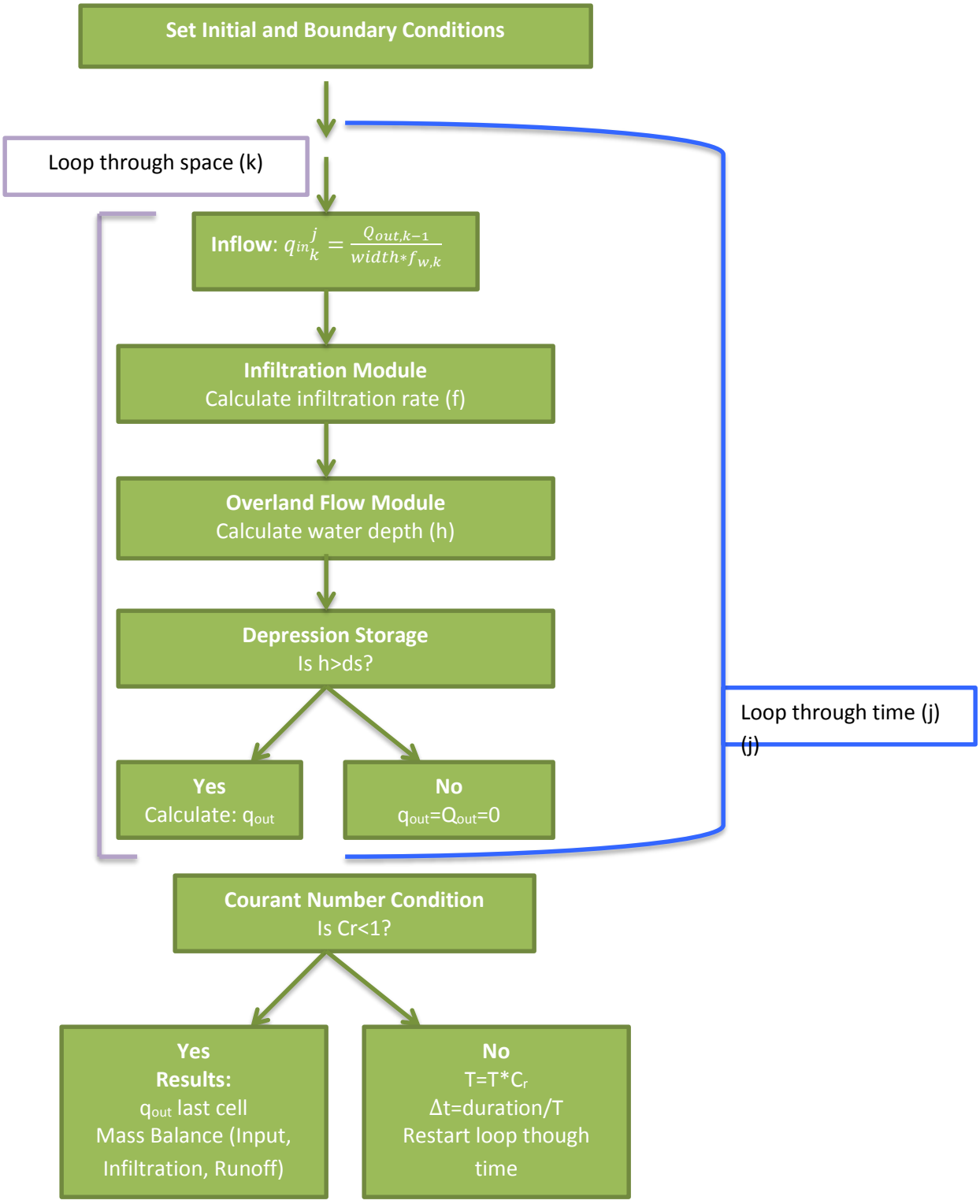

3.d Side slope

This overland flow-infiltration model has been used to calculate the amount of water infiltrated down the side slope of a roadside drainage ditch. The rainfall input is applied as: rainfall intensity over the side slope surface and discharge from the road. These simulations have added rainfall to

the laboratory and field experiments, where only the discharge from the road was included. The model has been divided into 2 sub-models (Figure 38):

i. **"Side slope with road runoff**: this sub-model calculates the runoff from the side slope applying a "fraction wetted" parameter, *fw*, that simulates the concentration of the road runoff into a fraction of the surface. This sub-model receives the water from the road as an upslope boundary condition, and applied rainfall onto the area, (*Area of side slope)*fw*.
ii. **Side slope without road runoff**: this sub-model calculates the discharge from the remaining part of the side slope that does not receive runoff from the road. This sub-model only receives direct rainfall, not road discharge = (*Area of side slope)* (1-fw).*

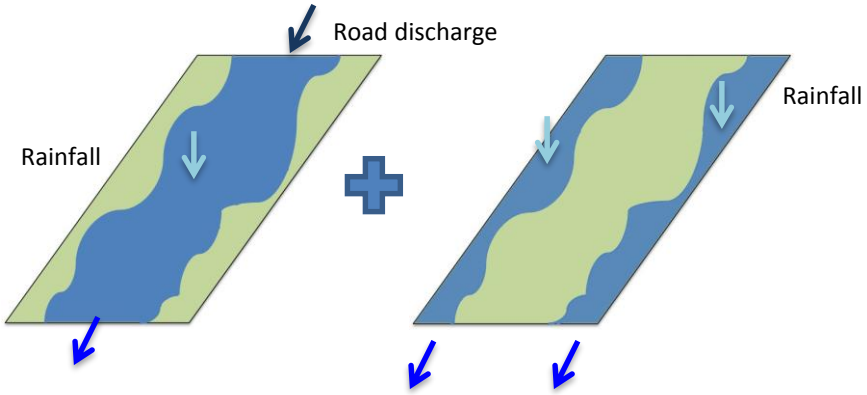

Figure 38 Schematic of **Left:** Side slope with road runoff. **Right:** Side slope without road runoff.

The result of coupling these two sub-models is a discharge over time from the side slope of the swale and a volume of water infiltrated.

3.e Channel

Based on the same overland flow and infiltration submodels, with the uniform flow kinematic wave assumptions explained in the previous section, a model of the channel has been developed with one additional feature: inclusion of the lateral discharge from the side slope entering the channel (Figure 39). The model represents a rectangular channel and accounts for rain falling over its entire surface and the additional input of water coming from the side slopes. The discharge from the channel represents the flow running off the entire system: side slope and channel. The groundwater level is assumed to be low in the channel section.

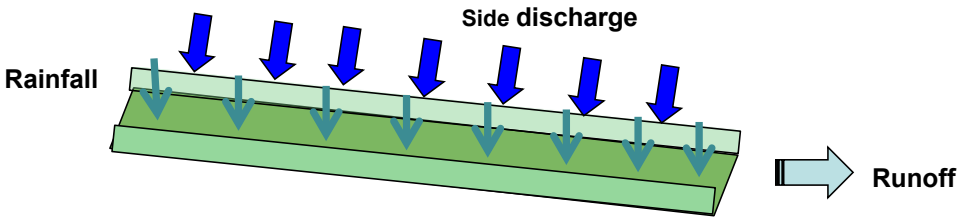

Figure 39 Schematic of the channel part of a drainage ditch.

3.f Coupled Model

The coupled model consists of a combination of the side slopes with and without road runoff, and the channel of the drainage ditch. The final volume infiltrated is the result of adding the volume infiltrated on the side slope and the channel. The model does not incorporate water retained in the surface of the road, neither interception by the vegetation. In addition, the shoulder of the road is assumed to be impervious, which is a conservative assumption. Furthermore, it is assumed that the rainfall over the road directly flows to the side slope, without a lag time. The effect of impact of raindrops in the overland flow process is not taken into account.

In order to understand the important processes in this partitioning, two K_{sat} values (0.51 and 5.1 cm/h, HSG C and A respectively) and three width ratios (W_{swale}/W_{road} = 0.2, 0.4, and 0.6) have been tested using five different rainfall intensities (from 8 - 0.5 in/h) (Table 6 and 7). . The width of the channel represented 25%, 12.5%, and 8.3% of the width of side slope. The results indicate that overall, utilizing the entire volume of water infiltrated in the system, 86% of the infiltration takes place in the side slope and 14% in the channel part of the drainage ditches. The percentage infiltration per unit width of the channel and side slope is comparable. However in a typical design the side slope length is generally greater than the channel, which explains the greater percentage of water, infiltrated in the side. The most important parameter to estimate the partitioning was the width of swale side slope. The MATLAB code is presented in the Appendix A.

Table 6 Results of infiltration-overland flow simulations of rainfall and runoff from road using the coupled model. The K_{sat} used was 5.1 cm/h and the rest of the parameters not included in the table were fixed. Both the side slopes and the channel had the same soil characteristics. The width of the channel used for the simulations was 0.5m and the width of the road was 10m.

Intensity (in/h)	W_{swale}/W_{road}	Input Volume L	Infiltrated Volume L	Volume Infiltrated (side slope) L	Volume Infiltrated (channel) L	Percentage infiltrated in the side slope
8	0.6	33528	5672	5162	510	91%
4	0.6	16764	5511	5015	496	91%
2	0.6	8382	4847	4411	436	91%
1	0.6	4191	3997	3637	360	91%
0.5	0.6	2096	2096	2033	63	97%
8	0.4	29464	3885	3380	505	87%
4	0.4	14732	3793	3300	493	87%
2	0.4	7366	3392	2917	475	86%
1	0.4	3683	2942	2530	412	86%
0.5	0.4	1842	1842	1787	55	97%
8	0.2	25400	1250	963	288	77%
4	0.2	12700	2115	1629	486	77%
2	0.2	6350	1934	1451	484	75%
1	0.2	3175	1746	1275	471	73%
0.5	0.2	1588	1520	1155	365	76%
					Average=	**85.5%**

Table 7 Results of infiltration-overland flow simulations of rainfall and runoff from road using the coupled model. The K_{sat} used was 0.51 cm/h and the rest of the parameters not included in the able were fixed. Both the side slopes and the channel had the same soil characteristics. The width of the channel used for the simulations was 0.5m and the width of the road was 10m.

Intensity (in/h)	W_{swale}/W_{road}	Input Volume L	Infiltrated Volume L	Volume Infiltrated (side slope) L	Volume Infiltrated (channel) L	Percentage infiltrated in the side slope
8	0.6	33528	1275	1173	102	92%
4	0.6	16764	1272	1170	102	92%
2	0.6	8382	1261	1160	101	92%
1	0.6	4191	1228	1130	98	92%
0.5	0.6	2096	1093	995	98	91%
8	0.4	29464	864	760	104	88%
4	0.4	14732	862	759	103	88%
2	0.4	7366	855	752	103	88%
1	0.4	3683	835	735	100	88%
0.5	0.4	1842	758	659	99	87%
8	0.2	25400	471	367	104	78%
4	0.2	12700	470	367	103	78%
2	0.2	6350	467	364	103	78%
1	0.2	3175	459	358	101	78%
0.5	0.2	1588	427	325	102	76%
					Average=	**85.7%**

4. Summary

A runoff-infiltration model that calculates the amount of water infiltrated along the side slope of a roadside drainage ditch has been coupled with a model of the ditch channel. The runoff discharge from the side slope is added to the channel together with direct rainfall. When coupled, a combined one dimensional runoff-infiltration model for both the side slope and channel of a roadside drainage ditch is obtained.

This numerical model can be used to estimate the infiltration performance of roadside drainage ditches (roadside swales) for given rainfall intensities. The Green-Ampt-Mein-Larson assumptions were implemented to calculate infiltration along with a kinematic wave model for overland flow that accounts for short-circuiting of flow. The model has been established in the MATLAB programming language and allows for a wide range of user inputs.

VI. Verification and Sensitivity Analysis of the Coupled Infiltration-Overland Flow Model (Task 5)

1. Introduction

The vegetated dry swale side-slope model will be used to simulate the field experiments, explained in detail in the Section IV of this report. The predicted infiltration loss on the side slope using the parameterized coupled infiltration-overland flow model will be compared with the actual infiltration loss determined from the monitored field tests. In this manner, the accuracy of the model can be estimated.

From the initial model, with 10 input parameters, sensitivity and uncertainty analyses will be developed and used to determine which parameters have the greatest impact on the model results for the Twin Cities metropolitan area. Based on the sensitivity analysis, the inputs of the model will be simplified for the Dry Swale Calculator.

2. Verification of the Coupled Infiltration-Overland Flow Model

The predicted infiltration loss on the side slope calculated with the coupled infiltration-overland flow model has been compared with the actual infiltration loss determined from the monitored field tests. The tests represent three different intensities, three seasons (fall, spring, and summer), four highways and two sites per highway. The parameters (Table 8) used were estimated and measured in the field; there was no calibration of any of the parameters. In this manner, the validity of the model as well as the associated soil hydraulic and surface geometry parameters has been evaluated. The field tests were meant to be used to validate the most important processes of the model. Although the rainfall over the side slope was not incorporated in the field tests, the model can simulate rainfall over the side slope and channel.

Table 8 Inputs used to simulate the field experiments at Hwy 51, 47, 13, and 77.

Input Parameters Field Experiments	1-year/ 2-year / 10-year storm
Rainfall intensity over road (i_r)	1.1 / 2.2 / 4.4 in/hr
Rainfall intensity over swale (i)	0 in/hr
Length of slope (L)	(See Table 4) m
Number of cells down slope	101
Duration of storm event	1 / 0.5 / 0.25 hr
Effective Wetting Front Suction (ψ)	(Different for each location) m
Soil Water Deficit ($\Delta\theta$)	(Different for each test)
Saturated Hydraulic Conductivity (K_{sat})	(See Table 4) cm/hr
Width of road in direction of slope (w_road)	10m
Width of swale (w_cell)	0.914m
Fraction wetted (fw)	(Different for each test)
Side slope (S)	(See Table 4)
Depression storage (d_s)	1mm
Manning's n (n)	0.25

First, the model was not able to capture the impact the gopher holes (Highway 47) in infiltration. Due to this exceptional characteristic, the Hwy 47 tests were not included in the validation process. Second, the sequence of the tests and saturated hydraulic conductivity estimations is important to understand the results obtained from the simulations. The first tests were performed in Fall 2014 (2-year storm). After winter, three tests were performed in the chronological order presented in Figure 40 during spring and summer 2015.

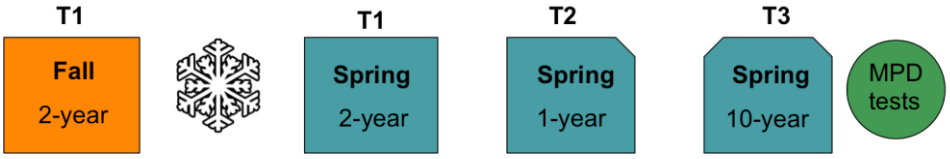

Figure 40 Sequence of field tests and MPD Infiltrometer measurements

The percentage infiltration measured in the 1 and 10-year storm tests at Highways 13, 51, and 77 have been compared the predictions from the model (Figure 41). For the twelve tests, the root mean square error (RMSE) was 6%, the mean square error (MSE) was 0.004, and the normalized MSE (normalized by the standard deviation of the observed data, 17%) was 12%. The normalized mean error was -2%. These statistical values indicate a good match between the infiltration losses estimated by the modeled and measured in the field. The saturated hydraulic conductivity, as well as the other 9 parameters was not calibrated.

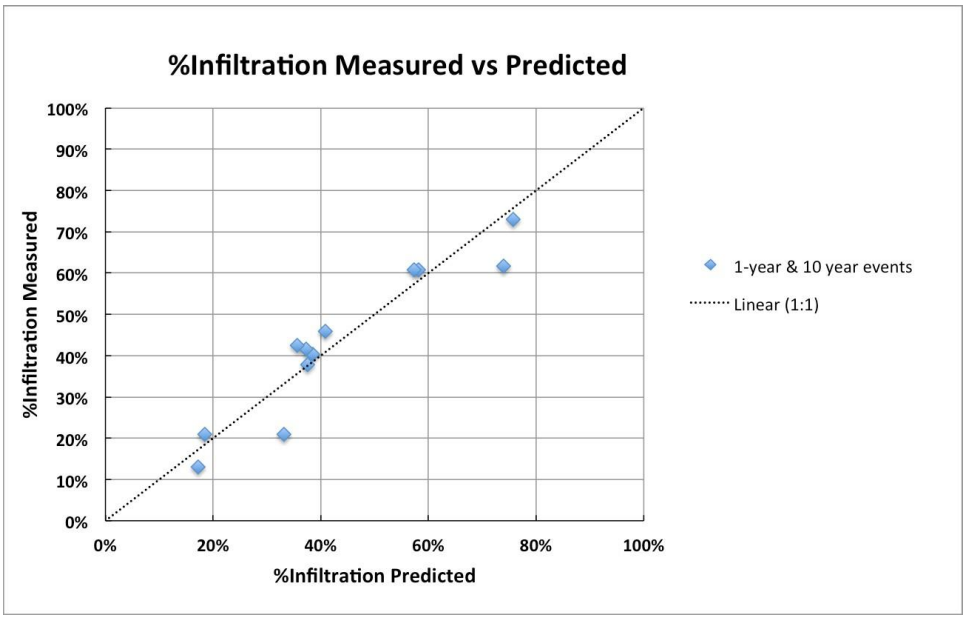

Figure 41 Percentage of infiltration measured versus predicted by the combined infiltration-overland flow model of the side slope of a swale for the 1 and 10-year storm events.

The hydrographs obtained from the model were compared with the runoff rates measured in the Hwy 13 tests for three different intensities (Figure 42). The hydrographs for the 1 and 10-year events represent well the field observations. The start time for those cases is overestimated, but

the shapes of the hydrographs were comparable to the observed. In the other hand, the model overestimates the runoff rates from the 2-year event test.

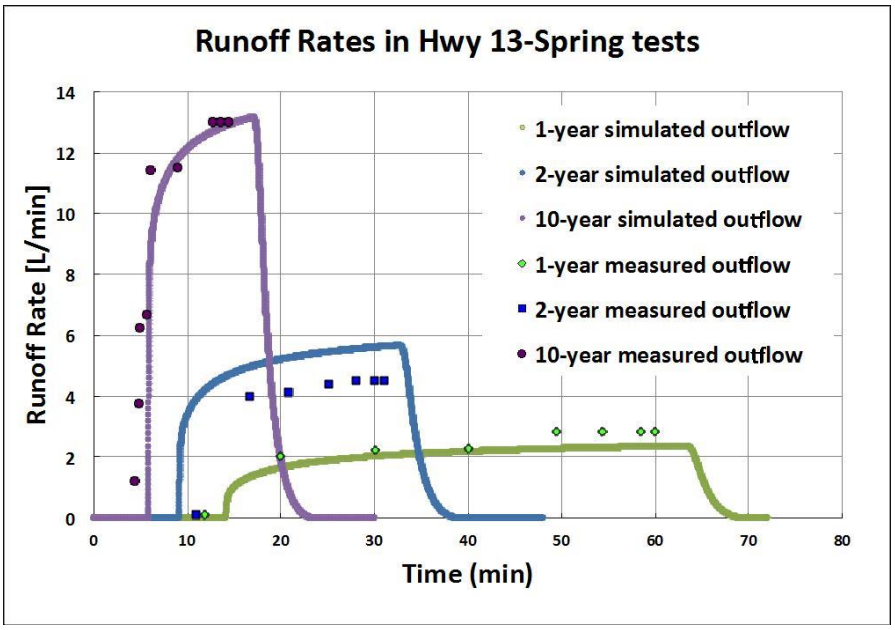

Figure 42 Hydrograph simulated by the model for the 1, 2, and 10-year storm events at Hwy 13 test1 and runoff rate points measured during the field tests.

Figure 43 presents the comparison between the measured and the predicted percentage infiltration for all the 2-year storm tests, which took place before the 1-year and 10-year storms. All the infiltration losses of the first tests are underpredicted. The saturated hydraulic conductivity used for the calculations was the same for all the tests. These results imply that there was a reduction in the saturated hydraulic conductivity in the consecutive tests; the first tests having a higher K_{sat} than the rest.

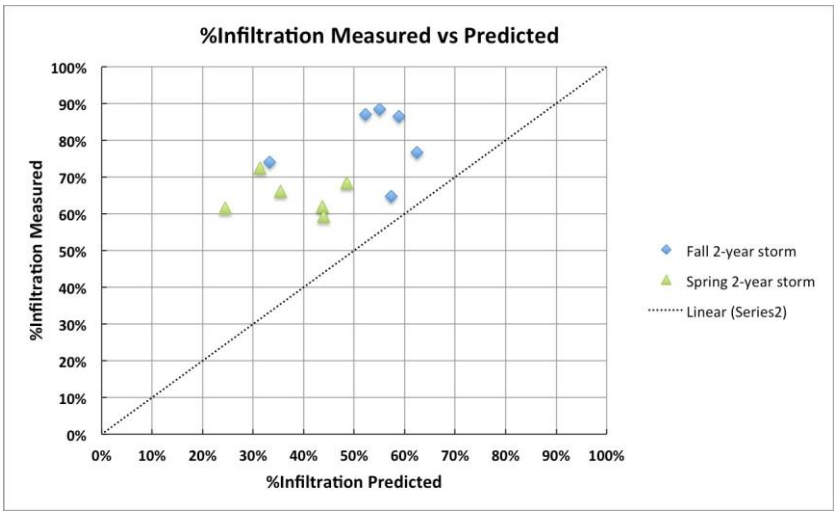

Figure 43 Percentage of infiltration measured versus predicted by the combined infiltration-overland flow model of the side slope of a swale for the 2-year events in fall and spring.

The coupled infiltration-runoff model was used to estimate the K_{sat} corresponding to the infiltrations rates observed in the first tests. The K_{sat} values were estimated to have diminished by a factor of 1.2 to 3; the estimated K_{sat} values during the first fall and spring tests were: 10.62 and 10.6 cm/h (Hwy 51), 6.89 and 9.18 cm/h (Hwy 77), and 9.11 and 7.04 cm/h (Hwy 13). The reduction of K_{sat} in the consecutive tests can be due to surface sealing (Moore (1981), Mohammed and Kohl (1987), Singer and Le Bissonais (1998), Gomez and Nearing (2005)). There are two types of rainfall-induced surface seals: structural seals (related to raindrop impact and sudden wetting), and sedimentary seals (result from settling of fine particles carried by runoff). Dense vegetation protects the surface of the swales from structural seals, since raindrop energy is mitigated before impacting the soil surface. However, during the field experiments, the vegetation was cut and during the first 30 minutes of flow, a process of sedimentary surface sealing, small particles filling in the pore space between the larger particles, could have occurred due to sediment transport and deposition. Additionally, the kaolinite particles suspended in the water could have precipitated and clogged some pores. The following tests would have started with an initially sealed surface, where the infiltration rates were lower than for the first experiment.

3. Uncertainty-Sensitivity Analysis of the Coupled Infiltration-Overland Flow Model

The uncertainty of runoff volume as a result of uncertainty of one of the independent parameters (such as K_{sat}, or fw) can be approximated by multiplying the sensitivity of runoff volume to the parameter times the uncertainty of the independent parameter:

$$U(\text{Runoff Volume}) = S_i\, U_i(\text{Parameter})$$

The *sensitivity analysis* (Figure 44) of the combined models consisted of calculating:

$S_i = \Delta(\text{Runoff Volume}) / \Delta(\text{Parameter}_i)$; where Δ indicates change of the term in parenthesis.

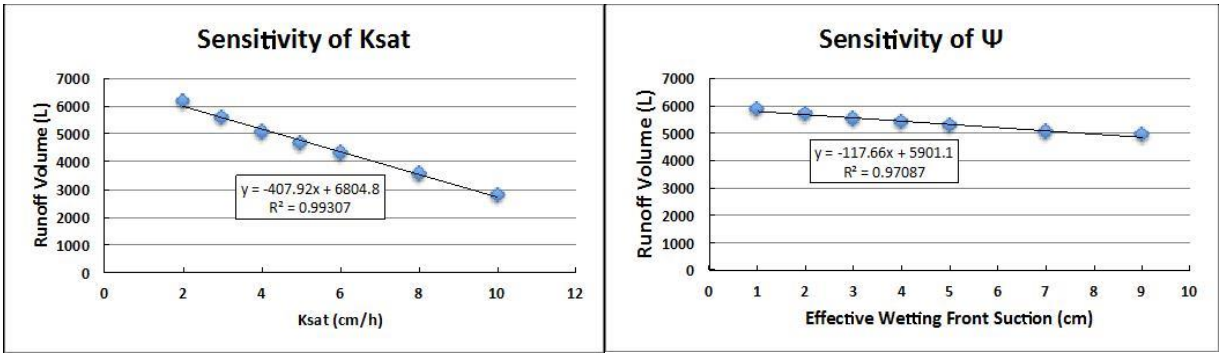

Figure 44 Left: Sensitivity analysis of saturated hydraulic conductivity (K_{sat}), S_{Ksat} = 407.92 L/cm. **Right:** Sensitivity analysis of effective wetting front suction (ψ), S_{ψ} =117.66 L/cm.

In order to perform the uncertainty analysis, a probability density function has to be assigned to each parameter. An analysis of a vegetative filter strips by Muñoz-Carpena *et al.* (2007) has been used as a model to assign probability distribution functions (pdfs) to the input parameters. To assign pdfs to the parameters not included in their analysis, field measurements from Task 3 have

been evaluated. The type of pdf for the uncertainty analysis and the source are given below for each independent variable:

- **K_{sat}**: Log-normal distribution (Muñoz-Carpena *et al.* 2007)
- **Ψ:** Uniform distribution (Muñoz-Carpena et al. 2007)
- **Δθ:** Uniform distribution (field measurements)
- **fw:** Normal distribution (field measurements)
- **n:** Triangular distribution (Muñoz-Carpena *et al.* 2007)
- **ds:** Triangular distribution (field measurements)
- **S:** Triangular distribution (field measurements)
- **B:** Uniform distribution (field measurements)

The uncertainties associated with each of the probability distributions functions are:

- Uniform distribution: $u = a / \sqrt{3}$, where a is the range of values observed.
- Triangular distribution: $u = a / \sqrt{6}$
- Normal distribution for fw: $u_{predicted\ value} = (t_{0.95} * \sigma)$, where σ is the standard deviation and $t_{0.95}$ the Student-t distribution for a 0.95 probability.
- Log-normal distribution for K_{sat}: $u_{mean} = (t_{0.975} * \sigma_{log\ param}) / \sqrt{N}$, where σ is the standard deviation of the log-values and N the total number of measured values at the site.

The uncertainty of the mean of the measured values was used for K_{sat} because 20 measurements were taken at each site, and the mean that represents infiltration was computed (Weiss and Gulliver 2015) Examples of probability distribution functions (pdfs) from field measurements are given in Figures 45 through 47.

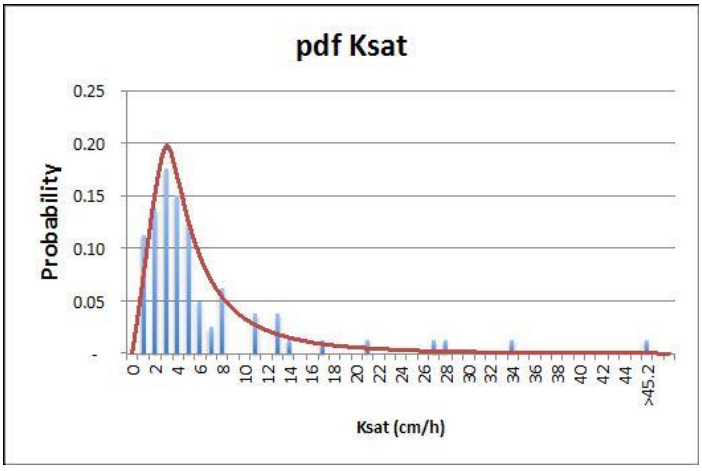

Figure 45 PDF of saturated hydraulic conductivity based on field estimations (log-normal distribution).

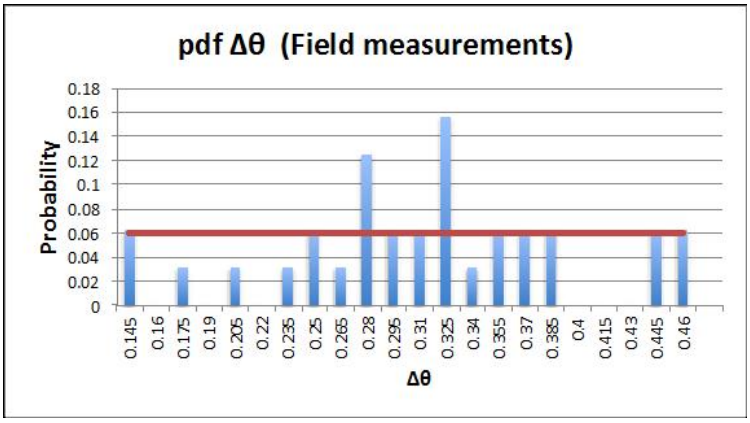

Figure 46 PDF of soil water deficit based on field estimations (uniform distribution).

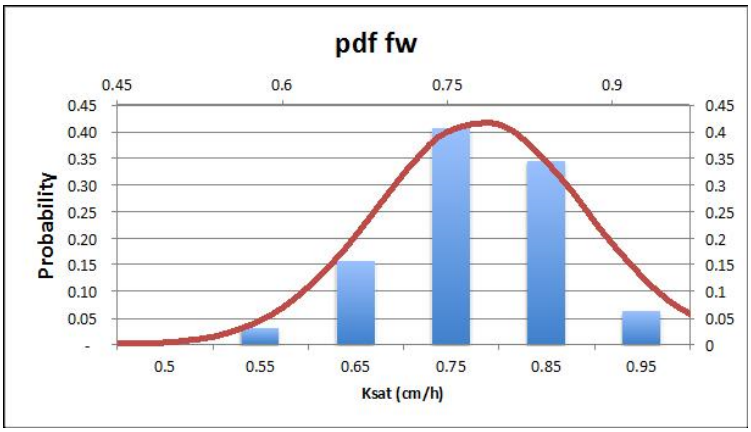

Figure 47 PDF of fraction wetted based on field estimations (normal distribution).

The uncertainty for each of the independent parameters is as follows:

- **K_{sat}**: 1.64 cm/h in a log-normal distribution
- **Ψ:** 2.60 cm in a uniform distribution
- **Δθ:** 0.05 fraction moisture content in a uniform distribution
- **fw:** 0.13 fraction wetted in a normal distribution
- **n:** 0.04 in a triangular distribution
- **ds:** 0.08 mm in a triangular distribution
- **S:** 0.026 in a triangular distribution
- **B:** 0.14 m in a uniform distribution

The result of multiplying the sensitivity and uncertainty parameters has units of volume (L). In order to make the results dimensionless, the volume has been divided by the total input of water to the swales used in all the sensitivity computations (8102.6 L). The total volume comes from

applying 2.2 in/h over a 10 m width road, 4 m width side slope, and 0.5 m width channel of length of 10 m.

The results of the sensitivity analysis are given below and in Figure 48. The results are most sensitive to anticipated variations in K_{sat}. They are also somewhat sensitive to anticipated variations in soil suction pressure (Ψ) and the difference between initial and final soil moisture ($\Delta\theta$). These later two, however, are variables of weather, which changes continually at each site. Moisture content changes with time depending upon precipitation patterns, and soil suction pressure changes with soil moisture content. Thus, each site will see a variation of each parameter changing over time, and a representative value may be the best at describing performance of a given site over time.

Results: *Sensitivity (S) * Uncertainty (U)*

- Higher impact:
  S * *U* (K_{sat}) = 669.47 Liters (8.26%);
  S * *U* (Ψ) = 305.68 Liters (3.77%);
  S * *U* ($\Delta\theta$) = 110.34 Liters (1.36%).

- Lower impact:
  S * *U* (fw) = 41.36 Liters (0.51%);
  S * *U* (B) = 34.55 Liters (0.43%);
  S * *U* (n) = 24.26 Liters (0.3%);
  S * *U* (ds) =3.13 Liters (0.04%);
  S * *U* (S) = 2.18 Liters (0.03%).

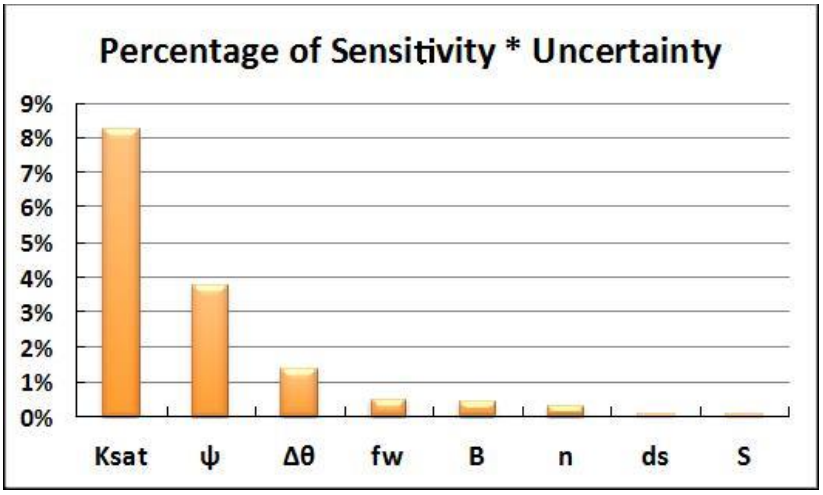

Figure 48 Percentage of sensitivity by uncertainty for 8 parameters of the coupled model.

The saturated hydraulic conductivity (K_{sat}) is the most significant parameter, followed by the effective wetting front suction and soil water deficit, with 54% and 84% less importance. The channel width, Manning's n, fraction wetted surface, depression storage and slope are not as critical of parameters to calculate infiltration performance. These variables have less than 1/16 the impact on runoff and infiltration than K_{sat}. This lower impact justifies assigning average values to those independent parameters in the simplified model.

The saturated hydraulic conductivity does not significantly change with season (Ahmed *et al.*, 2015), however effective wetting front suction changes with soil moisture content and week-to-week the soil moisture content fluctuates (dry and wet conditions). The computations of percent infiltrated, however, will be based upon the hydrology of many seasons. In each of these seasons there will be wetter and dryer periods of variable duration. For this reason, the two parameters (Ψ, $\Delta\theta$) have been fixed to average values. As the kinematic wave model assumes that the slope is equal to the bottom slope with a "normal depth", the length of the channel does not affect the percentage of water infiltrated (Figure 49).

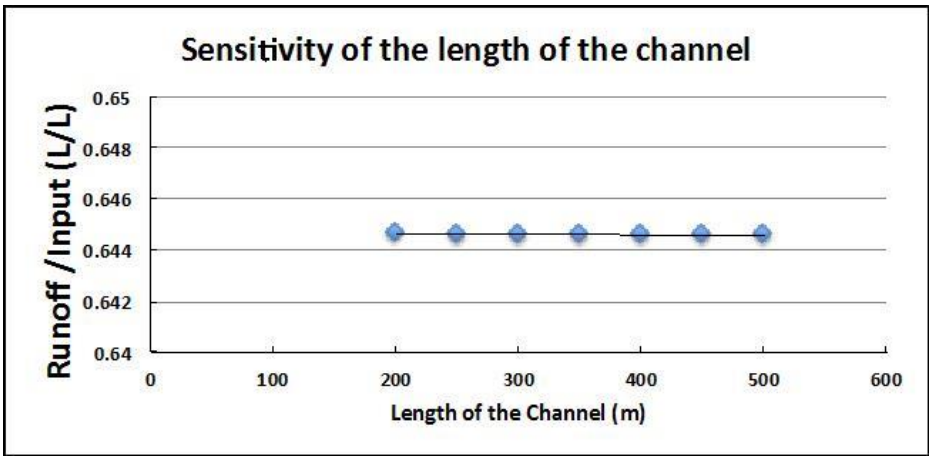

Figure 49 Sensitivity of the runoff over input water with increase of the length of the channel.

Thus, the variable inputs used in the simplified model will be:

- K_{sat}, W_{road} and W_{swale}
- i and duration of the storm

The fixed inputs will be:

- The average of field measurements:
  - Ψ = 5cm; $\Delta\theta$ = 0.3; fw = 0.7 (side-slope); ds = 0; S = 1/5 (side), and B = 0.5m.
- Assumption: The flow in the channel is not concentrated in rills.
  - fw = 1 (channel)
- Typical channel slope values are between 4% and 0.5% (MN Stormwater Manual)
  - S = 2% (channel)
- Manning's n is a function of the vegetation density, surface roughness and depth of flow.
  - n = 0.25 (Minton, 2005)

4. Summary

The coupled overland flow-infiltration model for the side slope has been validated with the field experiments from Task 3 (Section IV). The field tests did not include the channel section of the drainage ditch; consequently there is not enough data to validate this part of the model. However, the model showed that only 14% of the infiltration occurred in the channel section, with the

remaining 84% occurring on the side slope of the swale. It has been hypothesized that the first experiments in the series of tests experienced a reduction in the saturated hydraulic conductivity, possibly due to surface sealing or clogging of the porous by the kaolinite added to the water. Using the K_{sat} estimated in the field after the infiltration experiments were completed, without parameter calibration, the model well-represents the second and third tests of the series (RMSE=6% and the normalized MSE= 12%).

From the sensitivity and uncertainty analyses it has been found that the saturated hydraulic conductivity (K_{sat}) is the most significant parameter, followed by the soil suction and soil water deficit. The saturated hydraulic conductivity does not significantly change with season (Ahmed et al., 2015). However effective wetting front suction changes with soil moisture content and week-to-week the soil moisture content fluctuates (dry and wet conditions). As the simplified model is designed to compute infiltration over many years of precipitation with soil conditions that are changing over time, the two parameters (Ψ, $\Delta\theta$) have been fixed to average values. The channel width, Manning's n, fraction wetted surface, depression storage and slope have less than 1/16 the impact of K_{sat} in calculating infiltration performance, and so they will be fixed to average values.

The final inputs of the model, after the simplifications would be the saturated hydraulic conductivity, width of the swale, width of the road, intensity, and duration of the rainfall event.

VII. Simplification of the Coupled Runoff Model into the Minnesota Dry Swale Calculator (Task 6)

1. Objective

The objective of this task is to answer the question: *What percentage of the annual rainfall (in MN) does a vegetated roadside drainage ditch infiltrate?* The annual infiltration performance of drainage ditches was estimated for multiple case scenarios with the coupled model. The results have been used to generate power-law curves to place into a simplified calculator in an Excel spreadsheet, where the only inputs are: $K_{sat,}$ W_{swale}, $W_{road,}$ shown in Figure 50, and the location's rainfall volume percentile as a function of rainfall depth. The input width of the swale corresponds to the length of the side slope, without including the width of the channel.

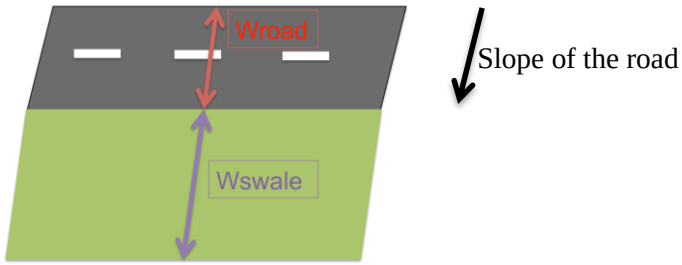

Figure 50 Sketch of the width of the road (Wroad) and width of the swale/drainage ditch (Wswale).

2. Annual Performance of Swales

In order to estimate annual performance we first need to know the annual precipitation. Issue Paper B (Emmons & Olivier Resources, 2005) includes frequency-volume graphs for several locations in Minnesota (Figure 51). The rainfall frequency specifies the number of daily rain events, expressed as a percent of all events that are less than a certain depth. The rainfall volume curve represents the percent exceedance in terms of annual volume. For example, storms of 1 in or less represent 63% of the total volume of annual precipitation. The runoff/infiltration model input for precipitation is intensity [L/T]), and the volume percentile graphs represent depth [L].

- ***Assumption***: The duration of precipitation events is 1 hour. This means that a 5 in depth would be introduced in the model as a 5 in/h event that lasts 1 hour.

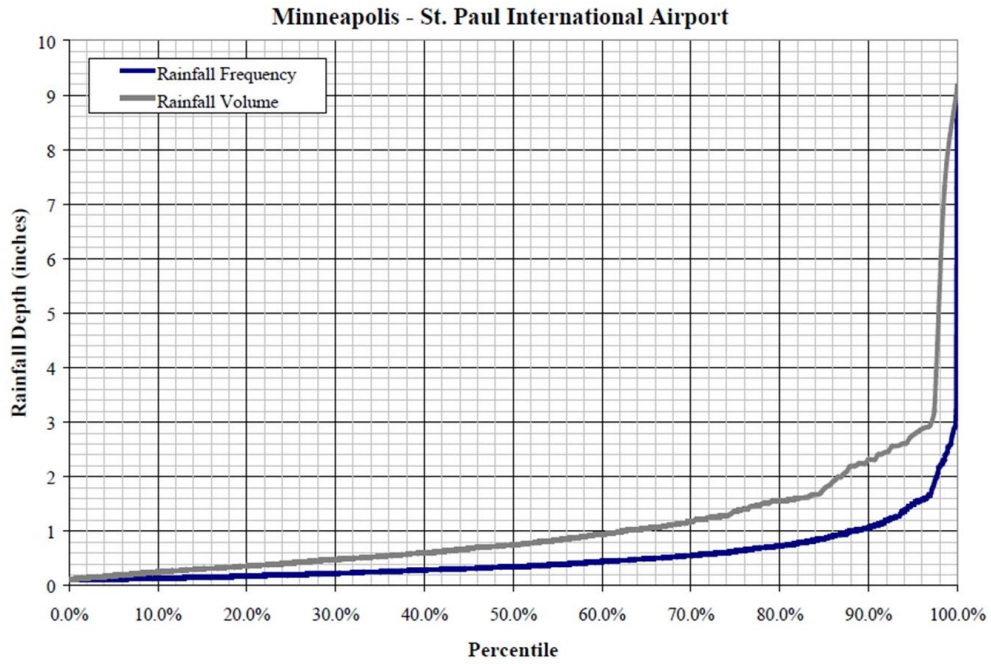

Figure 51 Percentile Rainfall Volume (PRV) and Frequency graph for the Minneapolis – St. Paul International Airport Station. Issue Paper "B" (Emmons & Olivier Resources, 2005).

A set of curves (Figure 52 and Appendix B) has been developed that relate precipitation depth with percentage infiltration, with a variable K_{sat} and a fixed width of swale over width of the road (W_{swale}/W_{road}).

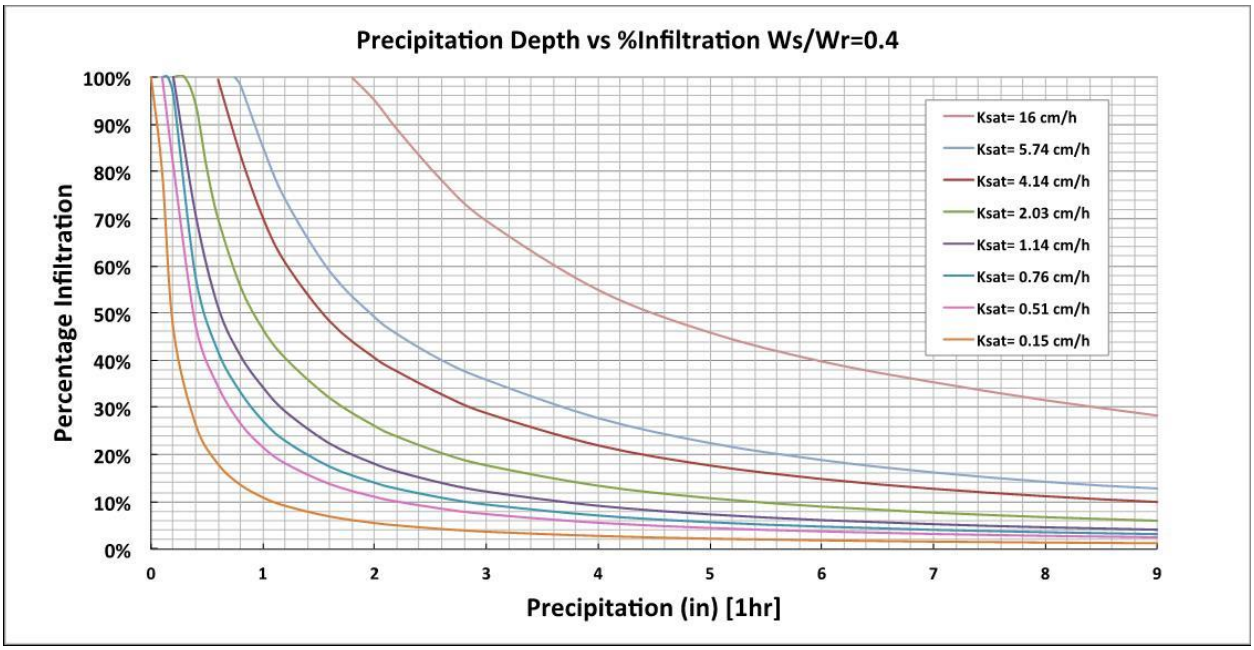

Figure 52 Precipitation depths versus percentage infiltration for a ratio of width of the swale side over width of the road of 0.4. The eight curves represent different saturated hydraulic conductivities. Both the side slope and the channel were included in the calculations.

The smallest six saturated hydraulic conductivities (Table 9) correspond to design infiltration rates for A, B, C, and D soil groups (Minnesota Stormwater Manual- Version 2, MPCA). The hydrologic soil group B has two different values corresponding to two unified soil classifications. The hydrologic soil group A has two different K_{sat} values corresponding to two different soil textures and unified soil classifications. The K_{sat} value of 5.74 cm/h corresponds to the maximum mean (0.68 times the geometric mean and 0.32 times the arithmetic mean (Weiss and Gulliver, 2015)) saturated hydraulic conductivity estimated in the field (Hwy 77) during the field experiments of this project (Task 3). Finally, the maximum geometric mean of K_{sat} observed during field tests at Hwy 51 in Madison, WI (Ahmed *et al.* 2015) was 16 cm/h.

Table 9 Saturated hydraulic conductivity values (in in/h and cm/h) and their corresponding hydrologic soil group. *Soil texture and unified soil classification for HSG A and B. GW: well-graded gravels; GP: gap-graded gravels; GM: silty gravels; SW: well-graded gravels; SP: gap-graded sands; SM: silty sands; MH: micaceous silts. (Minnesota Stormwater Manual- Version 2, MPCA).

K_{sat} [in/h]	K_{sat} [cm/h]	Hydrologic Soil Group	Soil Texture*	Unified Soil Classification*
6.30	16	A		
2.26	5.74	A		
1.63	4.14	A	Gravel, sandy gravel, silty gravel	GW,GP, GM, SW
0.8	2.03	A	Sand, loamy sand, sandy loam	SP
0.45	1.14	B		SM
0.3	0.76	B	Loam, silt loam	MH
0.2	0.51	C		
0.06	0.15	D		

The fraction of total annual precipitation that will be infiltrated in a particular swale can be calculated using the information given in the precipitation graphs (example Figure 51) and the appropriate infiltration performance graph (example Figure 52). The calculation of the infiltrated percentage of annual precipitation is obtained by taking the appropriate table (based on the information shown in the performance curves); the appropriate table is selected based on the site W_{swale}/W_{road}, and mean K_{sat} for the site. Next, determining the infiltrated percentage for the complete range of daily precipitation amounts, multiplying those precipitation amounts by the probability of occurrence of the precipitation amount, and summing those values. An example calculation of this procedure is given in Table 10, giving the percentage of the annual rainfall (in the Minneapolis –St. Paul station) infiltrated into a vegetated roadside drainage ditch (with a K_{sat} = 2.03 cm/h and W_{swale}/W_{road} = 0.4). The result is 60.6% of the annual rainfall.

Table 10 Example of swale annual infiltration performance for the parameters: W_{swale}/W_{road}=0.4 and K_{sat}=2.03cm/h, at Minneapolis-St. Paul. Percentile Rainfall Volume (PRV) and Probability Distribution Function (PDF).

Rainfall Depth (in)	PRV (Annual Rainfall)	PDF (Annual Rainfall)	Infiltration (%)	Annual Performance
9	100.0%		6.0%	
8	99.0%	1.0%	6.8%	0.1%
7	98.3%	0.7%	7.7%	0.1%
6	98.0%	0.3%	9.0%	0.03%
5	97.8%	0.2%	10.8%	0.02%
4	97.6%	0.2%	13.4%	0.02%
3	97.0%	0.6%	17.7%	0.1%
2.6	94.0%	3.0%	20.4%	0.6%
2.2	88.0%	6.0%	23.9%	1.3%
2	87.0%	1.0%	26.1%	0.2%
1.6	80.0%	7.0%	32.0%	2.0%
1.2	70.0%	10.0%	40.5%	3.6%
1	63.0%	7.0%	46.6%	3.0%
0.8	52.0%	11.0%	55.6%	5.6%
0.6	40.0%	12.0%	70.0%	7.5%
0.4	22.0%	18.0%	94.1%	14.8%
0.2	6.0%	16.0%	100.0%	15.5%
0.1	0.0%	6.0%	100.0%	6.0%
				Σ=60.6

The model has been used to develop a series of figures (Figure 53 and 54) of annual infiltration performances based on historical rainfall data versus saturated hydraulic conductivity corresponding to different rainfall stations: Minneapolis - St. Paul International Airport and Grand Marais.

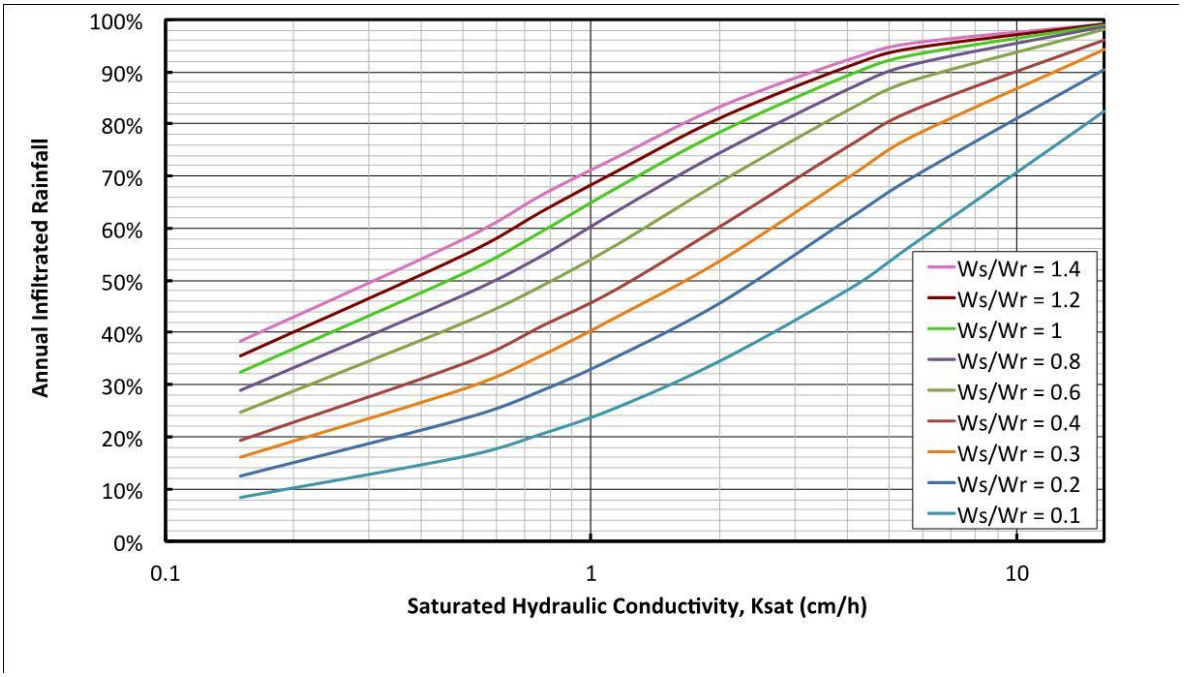

Figure 53 Annual infiltration performances versus saturated hydraulic conductivity (Ksat) based on the Minneapolis - St. Paul International airport rainfall station.

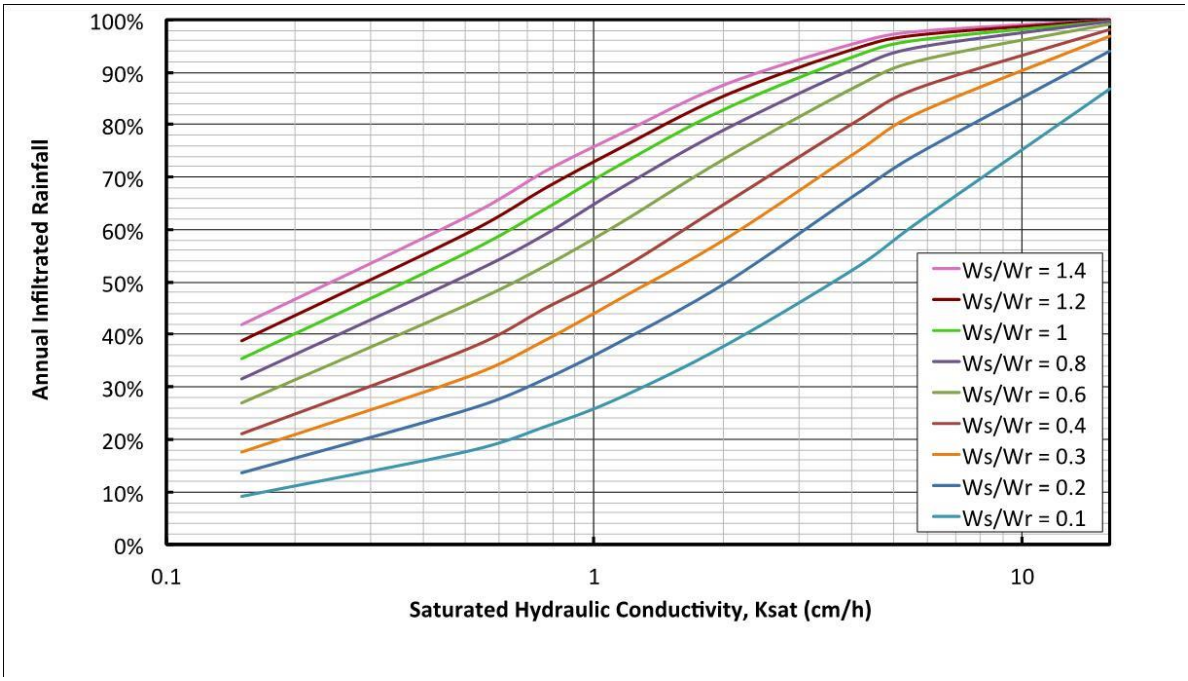

Figure 54 Annual infiltration performances versus saturated hydraulic conductivity (Ksat) based on the Grand Marais rainfall station.

The annual infiltration performance is overall higher in Grand Marais because of the percentage of low intensity events representing a greater percentage of the total annual rainfall than in Minneapolis – St. Paul Airport area.

5. Swale Calculator User's Manual

The Swale Calculator exists in an Excel spreadsheet where the user inputs the width of the swale side-slope, width of the road, K_{sat}, and location. The result is the percentage of the annual rainfall infiltrated by the swale/drainage ditch.

5.a Components

The Excel spreadsheet has four sheet tabs:

0. *Instructions*
1. *Calculator*
2. *Additional Information*
3. *Computations*

0. Instructions

Swale Calculator User's Manual

(i) Calculator

There are three steps to calculate the annual infiltration performance of a drainage ditch or swale:

Step 1 Location

Cell *C7 (upper left side):* Choose from the drop down options the *location of the swale.* By selecting a location, the curve representing Percentile Rainfall Volume (PRV) associated with a particular rain depth will be displayed (based on Issue Paper "B" (Emmons & Olivier Resources, 2005)). *User-Defined* option: The user can add a new PRV curve (G10-27, center column) if a different location is needed. The Probability Distribution Function (PDF) is automatically generated based on the data selected.

Step 2 Parameters

The user inputs:

- Cell *F34 (first row of the table)*: **Saturated hydraulic conductivity (K_{sat})** in cm/h. The maximum value of K_{sat} that the user can input is 16 cm/h.
- Cell *F35 (second row)* and *F36 (third row):* **Width of the road** (m or ft) and **width of the swale** (m or ft). Both widths should be in the same units. The Wswale/Wroad (*F37*, fourth row) is dimensionless (m/m or ft/ft). The range of values of W_{swale}/W_{road} that the user can input is: [0.1- 0.8].

Results

The annual infiltration performance is displayed in cell F47 (*last row of the table*). The table to the right presents performances of the swale for six values of W_{swale}/W_{road}. The graph displayed shows: Annual Infiltrated Rainfall versus K_{sat} (Saturated Hydraulic Conductivity) (Figure 55).

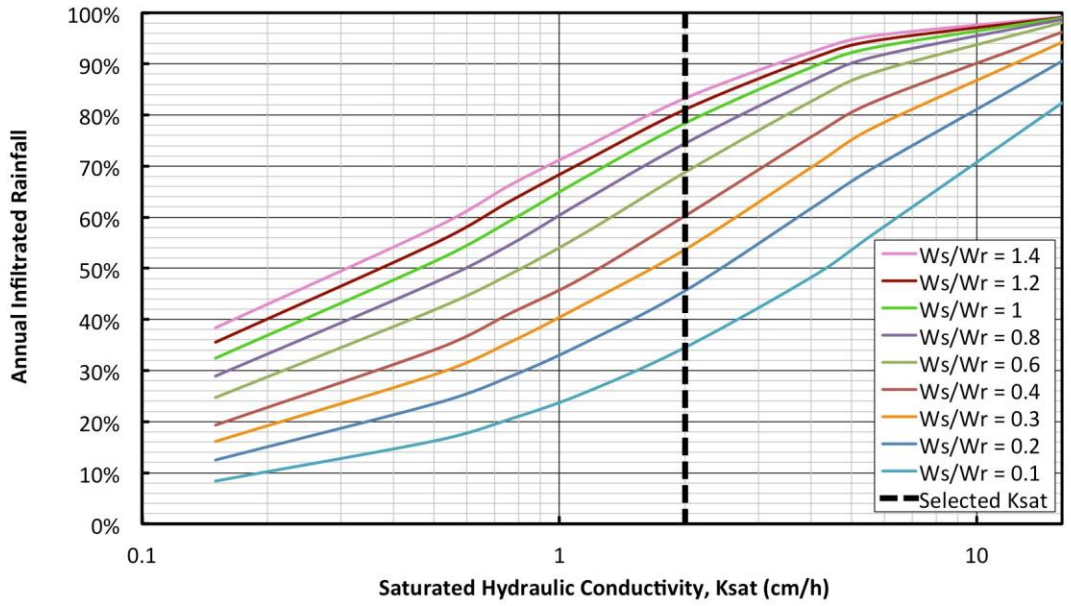

Figure 55 Example of graph plotted in the Results of the calculator. These results represent the annual performance of a drainage ditch in the Minneapolis-St. Paul Airport area with a K_{sat}=2 cm/h.

(ii) Additional Information

This sheet tab offers the user information related to:

- Percentage infiltration for each rainfall depth (%).
- Infiltrated depth (in) = Precipitation depth * percentage infiltration for a rainfall depth.
- Annual Performance for each depth (%) = Percentage Infiltration * probability distribution function.
- Summary table for eight different saturated hydraulic conductivities and six ratios of width of the swale over width of the road.

(iii) Computations

In this tab the tables with the rainfall volume percentage for eight locations in Minnesota are displayed, in addition to the interpolations needed for the calculator.

5.b Limitations

The most important parameter of the swale calculator is the saturated hydraulic conductivity (K_{sat}). As such, a satisfactory estimation of this parameter in the field is necessary to obtain a suitable estimation of the annual infiltration performance of a swale. An in-depth procedure to make the field infiltration measurements can be found in Ahmed *et al.*, (2014). The minimum number of Ksat estimations in the field should be twenty for a swale with less than 350 m (Ahmed *et al.*, 2015).

For a pre-construction estimation of the saturated hydraulic conductivity of a swale or drainage ditch, a nearby reference site should be analyzed. The soil and vegetation of the new swale should

be consistent with the reference site. Ahmed *et al.*, (2015) presents some reference sites and K_{sat} estimations.

Finally, the calculator assumes that there is no erosion in the side slope of the drainage ditch. Having an eroded surface would decrease the infiltration performance.

VIII. Conclusions and Recommendations

This research develops and demonstrates the means by which the appropriate pollution prevention credits for swales can be captured. Based on previous studies, infiltration performance of swales is linked to infiltration capacity of the soil, initial soil moisture content, ratio of impervious drainage area-swale area, length and width of the vegetated area, slope, type of flow down the side slope of the swale (spread or concentrated flow), and total depth and intensity of precipitation. The analysis of the results from laboratory and field experiments, together with a coupled infiltration runoff model have provided evidence to determine how these parameters affect the percentage of water infiltrated in the side slope and channel of a drainage ditch or swale. From the field laboratory experiments it was observed that water on the lateral slope of a swale flows as a concentrated flow, not as sheet flow, at the typical intensities for which infiltration practices are designed and utilized to improve surface water quality.

In the laboratory tests with initially smooth surfaces, the scour volume has a linear relationship with the Random Roughness (RR). For greater RRs perpendicular to the flow, greater scour volumes were observed in the flow direction; the more scour volume, the more percentage of runoff was seen in the experiments. This means that if the side slope of drainage ditches experience erosion, their infiltration performance would be reduced. Although all surfaces experienced erosion, the initially rilled surfaces had less infiltration. This can be due to the shorter runoff start time for initially eroded surfaces.

A total of 32 field tests were performed during three seasons in four different highways located in the Twin Cities metro area. The minimum fraction wetted detected was 54% and maximum 88%, with an average of 72% and standard deviation of 10%. A linear relationship between intensity of precipitation and fraction wetted was observed for the intensities tested. No signs of initial erosion were observed in any of the sites, except for the unique case of Hwy 51 after the construction operations performed in the area. None of the intensities experienced soil erosion due to the water flow. The surface of the side slopes was relatively flat, without evident micro-topographic features; this was supported by low random roughness (RR) measurements. When plotting percentage infiltration versus fraction wetted, substantial variability was observed in the results, probably linked to the soil type, saturated hydraulic conductivity, initial soil moisture content, and length of the swale analyzed.

Despite the initial compaction during construction, the porosity of consolidated drainage ditch soil was high due to the macropores generated by vegetation roots, activity of macrofauna, and construction procedures. The saturated hydraulic conductivities (K_{sat}) corresponded to hydrologic soil group A (Minnesota Stormwater Manual- Version2, MPCA) for all sites, even though their designation based upon soil texture would be in groups A, B and C. The average percentage infiltration of all of the tests was 67.6%, with a 20.9% standard deviation. In addition, the trend

was to have more infiltration when the saturated hydraulic conductivity was higher and for a longer swale side slope. The vegetation, type of soil and width of the side slope (perpendicular to traffic direction) would be an important consideration for constructing roadside drainage ditches with high efficiency in stormwater treatment.

A coupled overland flow-infiltration model for the side slope was developed and validated with the field experiments. Using the K_{sat} estimated in the field, without parameter calibration, the model represents well the observed infiltration percentages (RMSE=6% and the normalized MSE= 12%). The field tests did not include the channel section of the drainage ditch; consequently there is not enough data to validate this part of the model. However, computations indicated that an average of only 16% of the infiltration occurred in the channel section, while an average of 84% occurred on the side slope.

From the sensitivity and uncertainty analyses it has been shown that the saturated hydraulic conductivity (K_{sat}) is the most significant parameter, followed by the soil suction and soil water deficit. The saturated hydraulic conductivity does not significantly change with season (Ahmed et al., 2015). However, effective wetting front suction changes with soil moisture content, and week-to-week the soil moisture content fluctuates (dry and wet conditions). As the simplified model is designed to compute infiltration over many years of precipitation with soil conditions that are changing over time, the two parameters (Ψ, $\Delta\theta$) have been fixed to average values. The channel width, Manning's n, fraction wetted surface, depression storage and slope have less than 1/16 the impact of K_{sat} in calculating infiltration performance, and so they will be fixed to average values.

The sensitivity and uncertainty analyses allowed simplification of the computational model. Characteristic curves were developed using the coupled infiltration-overland flow model and used in a spreadsheet calculator of the annual infiltration performance of a vegetated drainage ditch. The final inputs of the model, after the simplifications, are the saturated hydraulic conductivity of the soil, width of the swale, width of the road, and the location's rainfall volume percentile as a function of rainfall depth. Provided that there is a satisfactory estimation of the saturated hydraulic conductivity in the field, and the side slope does not show signs of erosion, the calculator can be used to provide a good estimation of the water captured by the channel and side slope of a swale or drainage ditch.

References

Abida H. and Sabourin, J. F. (2006). "Grass swale-perforated pipe systems for stormwater management." *Journal of Irrigation and Drainage Engineering*, 132(1): 55–63.

Abrahams, A. D., Parsons, A. J., and Hirsch, P. J. (1992). "Field and laboratory studies of resistance to interrill overland flow on semi-arid hillslopes, southern Arizona." Overland flow, A. J. Parsons and A. D. Abrahams, ed., *UCL Press, Univ. College London*, London, 1–23.

Abu-Zreig, M., Rudra, R. P., and Whiteley, H. R. (2001). "Validation of a vegetated filter strip model (VFSMOD)." *Hydrological Processes*, 15(5): 729–742. doi:10.1002/hyp.101

Ackerman, D., and Stein, E. D. (2008). "Evaluating the Effectiveness of Best Management Practices Using Dynamic Modeling." *Journal of Environmental Engineering*, 134(8): 628–639.

Ahearn, D., and Tveten, R. (2008). "Legacy LID: Stormwater Treatment in Unimproved Embankments Along Highway Shoulders in Western Washington", *International Low Impact Development Conference*, November 16-19, 2008, Seattle, WA.

Ahmed, F., Gulliver, J. S., and Nieber, J. L. (2015). "Field Infiltration Measurements in Grassed Roadside Drainage Ditches: Spatial and Temporal Variability." *Journal of Hydrology*, 530(11): 604-611.

Ahmed, F., Natarajan, P., Gulliver, J. S., Weiss, P. T. and Nieber, J. L. (2014a). "Assessing and Improving Pollution Prevention by Swales. Final Report 2014-30", Research Services and library, Office of Transportation System Management, Minnesota Department of Transportation, St. Paul, MN.

Ahmed, F., Nestingen, R., Nieber, J. L., Gulliver, J. S., and Hozalski, R. M. (2014b). "A Modified Philip–Dunne Infiltrometer for Measuring the Field-Saturated Hydraulic Conductivity of Surface Soil." *Vadose Zone Journal*. Vol. 13(10). *doi:10.2136/vzj2014.01.0012*

Akan, A. O. (2014). "Hydrologic Modeling of Urban Vegetative Filter Strips." *Journal of Hydrologic Engineering*, *19* (1): 188–195. doi:10.1061/(ASCE)HE.1943-5584.0000761.

Alestra, S. and Battiato, S. (2008). Fuzzy Image Processing. Implementazione di plug-in per l'ambiente ImageJ. Universita di Catania, Departimento di Matematica e Informatica. Internet, url: http://svg.dmi.unict.it/iplab/imagej/Plugins/Fuzzy%20Image%20Processing/downloads/Fuzzy%20Image%20Processing%20-%20Implementazione%20di%20plug-in%20per%20l'ambiente%20ImageJ.pdf (accessed April 6, 2016).

Allmaras, R. R., Burwell, R. E., Larson, W. E., and Holt, R. F. (1966) "Total porosity and random roughness of the interrow zone as influenced by tillage." *USDA Conservation Research Report* 7, USDA, Washington, DC.

Alvarez-Mozos, J., Campo, M. A., Giménez, R., Casalí, J. Leibar, U. (2011) "Implications of scale, slope, tillage operation and direction in the estimation of surface depression storage." *Soil and Tillage Research*, 111: 142–153.

Appels, W. M., Bogaart, P. W., and van der Zee, S.E.T.M. (2011). "Influence of spatial variations of microtopography and infiltration on surface runoff and field scale hydrological connectivity." *Advances in Water Resources*, 34(2): 303–313.

ASTM D2216-10 (2010), Standard Test Methods for Laboratory Determination of Water (Moisture) Content of Soil and Rock by Mass, ASTM International, West Conshohocken, PA.

ASTM D2937-10 (2010), Standard Test Method for Density of Soil in Place by the Drive-Cylinder Method, *ASTM International*, West Conshohocken, PA.

ASTM D422-63 (2007)e2, Standard Test Method for Particle-Size Analysis of Soils, ASTM International, West Conshohocken, PA.

ASTM D6913 (2009). Standard test methods for particle size distribution (Gradation) of soils using sieve analysis, D18.03. ASTM International, West Conshohocken, PA.

Barrett, M. E. (2008). "Comparison of BMP performance using the International BMP Database", *Journal of Irrigation and Drainage Engineering*, 134(5): 556-561.

Barrett, M. E., Keblin, M. V., Walsh, P. M., Malina, J. F., and R. B. Charbeneau, (1998b). "Evaluation of the performance of permanent runoff controls: summary and conclusions", Center for Transportation Research, University of Texas at Austin, TX.

Barrett, M. E., Walsh, P. M., Malina, J. F., and R. B. Charbeneau, (1998a). "Performance of vegetative controls for treating highway runoff", *Journal of Environmental Engineering*, 124(11): 1121-1128.

Bedient, P. B, Huber, W. C., and Vieux B. E. (2008), *Hydrology and Floodplain Analysis*, 4th Edition, Prentice-Hall Publishing Co., Upper Saddle River, NJ.

CALTRANS (2003). "Final Report: Roadside Vegetated Treatment Sites (RVTS) Study." CTSW-RT-03-028, Caltrans Division of Environmental Analysis, Sacramento, CA.

Chi, Y., Yang, J., Bogart, D., and Chu, X. (2012). "Fractal Analysis of Surface Microtopography and its application in understanding hydrologic problems." *American Society of Agricultural and Biological Engineers*, 55(5): 1781–1792.

Chu S. T. (1978). "Infiltration during unsteady rain." *Water Resources Research* 14(3): 461–466.

Darboux, F., Davy, P., Gascuelodoux, C., and Huang, C. (2001). "Evolution of soil surface roughness and flowpath connectivity in overland flow experiments", *Catena*, 46 (2-3): 125–139.

Davis, A. P., Stagge, J. H., Jamil, E., and Kim, H. (2012). "Hydraulic performance of grass swales for managing highway runoff." *Water Research*, 46(20): 6775–86.

Deletic, A. (2001). "Modelling of water and sediment transport over grassed areas." *Journal of Hydrology*, *248*(1-4): 168–182. doi:10.1016/S0022-1694(01)00403-6

Deletic, A. (2005). "Sediment transport in urban runoff over grassed areas." *Journal of Hydrology*, 301, 108–122. doi:10.1016/j.jhydrol.2004.06.023

Deletic, A., and Fletcher, T. D. (2006). "Performance of grass filters used for stormwater treatment—a field and modelling study." *Journal of Hydrology*, 317(3-4): 261–275. doi:10.1016/j.jhydrol.2005.05.021

Emmons & Olivier Resources (2005) Issue Paper "B", Precipitation Frequency Analysis and Use. Prepared for the Minnesota Stormwater Manual Sub-Committee, Emmons & Olivier Resources, Oakdale, MN.

Erickson, A. J., Weiss, P.T. and Gulliver, J. S. (2013). *Optimizing Stormwater Treatment Practices: A Handbook of Assessment and Maintenance*, Springer, New York, NY.

Fassman, E. A., and Liao, M. (2009). "Monitoring of a Series of Swales within a Stormwater Treatment Train." In Proceedings of the *32nd Hydrology and Water Resources Symposium*, Newcastle, Australia, 30 Nov–3 Dec 2009.

Ferguson, B. K. (1998). *Introduction to stormwater: concepts, purpose, design*. John Wiley & Sons, Inc., New York, NY.

Frei, S., and Fleckenstein, J. H. (2014). "Representing effects of micro-topography on runoff generation and sub-surface flow patterns by using superficial rill / depression storage height variations." *Environmental Modelling & Software*, 52: 5–18.

GIMP, GNU Image Manipulation Program. Internet, url: http://www.gimp.org (accessed December 10, 2015).

Gomez, J. A. and Nearing, M. A. (2005) "Runoff and sediment losses from rough and smooth soil surfaces in a laboratory experiment." *CATENA,* 59(3): 253-266.

Green, W. H. and Ampt, G. (1911). "Studies of soil physics, part I – the flow of air and water through soils." *Journal of Agricultural Science* 4: 1-24.

Hayes, J. C., Barfield, B. J., and Barnhisel, R. I. (1984). "Performance of grass filters under aboratory and field Conditions", *Transactions of the American Society of Agricultural Engineers,* 27(5): 1321–1331.

Hunt, W. F., Hathaway, J. M., Winston, R. J., and Jadlocki, S. J. (2010). "Runoff Volume Reduction by a Level Spreader–Vegetated Filter Strip System in Suburban Charlotte, N.C." *Journal of Hydrologic Engineering*, 15(6): 499–503.

Hwang, C., and Weng, C. (2015). "Effects of rainfall patterns on highway runoff pollution and its control." *Water and Environment Journal*, 29: 214–220.

Kachchu Mohamed M.A., Lucke, T., and Boogard, F. (2013). "Using swales to pre-treat stormwater runoff and prolong the effective life of permeable pavement systems." Proceedings of the *8th International Conference NOVATECH*, June 2013, Lyon, France.

Kirkby, M. J. (2014). "Do not only connect: a model of infiltration-excess overland flow based on simulation." *Earth Surface Processes and Landforms*, 39(7): 952–963.

Knight, E. M. P., Hunt, W. F., and Winston, R. J. (2013). "Side-by-side evaluation of four level spreader-vegetated filter strips and a swale in eastern North Carolina." *Journal of Soil and Water Conservation*, 68(1): 60–72.

Lancaster, C. D. (2005). "A Low Impact Development Method for Mitigating Highway Stormwater Runoff - Using Natural Roadside Environments for Metals Retention and Infiltration." Masters Thesis, Washington State University, Department of Civil and Environmental Engineering, Pullman, WA.

Lane, S. N. (2005). "Roughness - Time for a re-evaluation? *Earth Surface Processes and Landforms*, 30(2): 251–253.

Le Bissonnais, Y., Lecomte, V., and Cerdan, O. (2004) "Grass strip effects on runoff and soil loss." *Agronomie*, EDP Sciences, 24 (3): 129-136.

Legout, C., Darboux, F., Nédélec, Y., Hauet, A., Esteves, M., Renaux, B.,and Cordier, S. (2012). "High spatial resolution mapping of surface velocities and depths for shallow overland flow." *Earth Surface Processes and Landforms*, 37(9): 984–993. *doi:10.1002/esp.3220*

Li, H. (2015). "Green Infrastructure for Highway Stormwater Management : Field Investigation for Future Design, Maintenance, and Management Needs." *Journal of Infrastructure Systems.* 10.1061/(ASCE)IS.1943-555X.0000248 , 05015001

Li, R. M., Stevens, M. A., and Simons, D.B. (1976). "Solutions to Green-Ampt Infiltration Equation." *Journal of Irrigation and Drainage. Division of ASCE 102(IR2): 239-248.*

Lighthill, M. J. and Whitham, G. B. (1955). "On kinematic waves. I. Flood movement in long rivers." *Proceedings of the Royal Society of* London. *Series A, Mathematical and Physical Sciences.* 229 (1178): 317–345.

Lucke, T., Mohamed, M. A. K.. Tindale, N. (2014) "Pollutant Removal and Hydraulic Reduction Performance of Field Grassed Swales during Runoff Simulation Experiments." *Water*, 6: 1887-1904.

Marr, J. and Heitkamp, B. (2015) Minnesota Steel Culvert Pipe Service-Life Map. Final Report 2015-31, Research Services and library, Office of Transportation System Management, Minnesota Department of Transportation, June 2015, St. Paul, MN.

MATLAB and Statistics Toolbox Release 2014a, *The MathWorks, Inc*., Natick, MA.

Mein, R. G. and Larson, C. L. (1971). "Modelling the infiltration component of the rainfall-runoff process", *Bulletin 43,* University of Minnesota, MN, Water Resources Research Center, Minneapolis, MN.

Minnesota Department of Transportation (2000) Standard Specifications for Construction, 2000 Edition, 2565 -2581, St. Paul, MN.

Minnesota Department of Transportation (2016) Standard Specifications for Construction, 2016 Edition, 2571.3, St. Paul, MN.

Minton, G. R. (2005) *Stormwater Treatment Biological, Chemical, and Engineering Principals*. Sheridan Books, Inc., Seattle, WA.

Mohammed, D., and Kohl, R. A. (1987). "Infiltration response to kinetic energy." *Transactions of the American Society of Agricultural Engineers,* 30:108–111.

Moore, I. D. (1981) "Infiltration Equations Modified for Surface Effects." *Transactions of the American Society of Agricultural Engineers*. 24: 1546-1553.

MPCA (2013). *Minnesota Minimal Impact Design Standards.* Minnesota Pollution Control Agency, St. Paul, MN.

MPCA (2015) Minnesota Stormwater Manual- Version 2. Minnesota Pollution Control Agency, St. Paul, MN.

Muñoz-Carpena, R. and Parsons, J. E. (2004). "A design procedure for vegetative filter strips using VFSMOD-W." *Transactions of the American Society of Agricultural Engineers*, 47(6): 1933-1941.

Muñoz-Carpena, R., Miller, C. T., and Parsons, J. E. (1993a). "A quadratic Petrov-Galerkin solution for kinematic wave overland flow." *Water Resources Research*. doi:10.1029/93WR00610

Muñoz-Carpena, R., Parsons, J. E. and Gilliam, J. W. (1993b). "Numerical approach to the overland flow process in vegetative filter strips." *Transactions of the American Society of Agricultural Engineers*. 36(3): 761- 770.

Muñoz-Carpena, R., Parsons, J. E., and Gilliam, J. W. (1999). "Modeling overland flow and sediment transport in vegetative filter strips: Model development and application." *Journal of Hydrology* 214:111–129.

Muñoz-Carpena, R., Zajac, Z., and Kuo, Y. M. (2007), "Global sensitivity and uncertainty analysis of the water quality model VFSMOD-W" *Transactions of the American Society of Agricultural and Biological Engineers*, 50 (5): 1719–1732

Onstad C. A. (1984). "Depressional storage on tilled surfaces." *Transactions of the American Society of Agricultural Engineers*, 27(3): 729–732.

Poletika, N., Coody, P. N., Fox, G., Sabbagh, G. J., Dolder, S. C., and White, J. (2009). "Chlorpyrifos and atrazine removal from runoff by vegetated filter strips: experiments and predictive modeling." *Journal of Environmental Quality*, *38*(3): 1042–1052.

Prewitt, J. M. S. and Mendelsohn, M. L. (1966). "The analysis of cell images", *Annals of the New York Academy of Sciences 128: 1035-1053*

Rasband W. S. (1997–2014) ImageJ, U.S. National Institutes of Health, Bethesda, MD. Internet, url: *imagej.nih.gov/ij/* (accessed January 15, 2016).

Singer, M. J., and Le Bissonnais, Y. (1998). "Importance of surface sealing in the erosion of some soils from a Mediterranean climate." *Geomorphology*, 24(1): 79–85.

Singh, V. P. (2001). "Kinematic wave modelling in water resources: a historical perspective." *Journal of Hydrological Processes* 15 (4): 671–706.

Skaggs, R. W., and Khaleel, R. (1982). "Chapter 4: Infiltration", in *American Society of Agricultural Engineers Monograph Hydrologic Modeling of Small Watersheds, C.T. Haan Ed.,* St. Joseph, MI.

Stagge, J. H., Davis, A. P., Jamil, E., and Kim, H. (2012). "Performance of grass swales for improving water quality from highway runoff." *Water Research*, 46(20): 6731–42.

Stomph, T. J., De Ridder, N., Steenhuis, T. S., and Van De Giesen, N. C. (2002). "Scale effects of hortonian overland flow and rainfall-runoff dynamics: Laboratory validation of a process-based model." *Earth Surface Processes and Landforms*, 27(7): 847–855. doi:10.1002/esp.356

Thompson, S. E., Katul, G. G., and Porporato, A. (2010). "Role of microtopography in rainfall-runoff partitioning: An analysis using idealized geometry." *Water Resources Research*, 46(7). W07520.

U.S. Department of Agriculture (2014). Natural Resources Conservation Service Soil. Internet, url: http://www.nrcs.usda.gov/wps/portal/nrcs/detail/soils/survey/?cid=nrcs142p2_054167 (accessed December 5, 2015).

U.S. Department of Commerce NOAA Atlas 14 (2013). Precipitation-Frequency Atlas of the United States, Volume 8, Version 2.0 Midwestern States, Silver Spring, MD.

USDA NRCS (1986) "Urban Hydrology for Small Watersheds, Technical Release 55 (TR-55)", 210-VI-TR-55, 2nd Ed., Conservation Engineering Division, Washington, DC.

USDA NRCS (2009). *Part 630 Hydrology National Engineering Handbook*, Natural Resources Conversation Services, U.S. Department of Agriculture, Washington, DC.

Vermang, J., Norton, L. D., Huang, C., Cornelis, W. M., da Silva, A.M., and Gabriels, D. (2015). "Characterization of Soil Surface Roughness Effects on Runoff and Soil Erosion Rates under Simulated Rainfall." *Soil Science Society of America Journal*, 78(3): 903-916.

Warrick, A. W., Lazarovitch, N., Furman, A., and Zerihun, D. 2007. "Explicit infiltration function for furrows." *Journal of Irrigation and Drainage Eng*ineering, 133: 307–313.

Weiss, P. T. and Gulliver, J. S. (2015). "Effective Saturated Hydraulic Conductivity of an Infiltration-Based Stormwater Control Measure." *Journal of Sustainable Water Built Environment*, 10.1061/JSWBAY.0000801, 04015005.

Weiss, P. T., Gulliver, J. S., and Erickson, A. J. (2010). "The Performance of Grassed Swales as Infiltration and Pollution Prevention Practices. A Literature Review." Internet, url: http://stormwater.safl.umn.edu/sites/g/files/pua941/f/media/weiss-gulliver-erickson_2010_-_performance_of_grassed_swales_as_infiltration_and_pollutation_prevention_practices.pdf (accessed February 15, 2016).

Wilson, B. N., Barfield, B. J., and Moore, I. D. (1984). "A hydrology and sedimentology watershed model. Part I: Modeling techniques." *Transactions of the American Society of Agricultural Engineers*, *27*(5): 1370–1377.

Yang, J. and Chu, X. (2013). "Effects of DEM Resolution on Surface Depression Properties and Hydrologic Connectivity." *Journal of Hydrologic Engineering*, 18(9):1157–1169.

Yousef, Y.A., Hvitvedjacobsen, T., Wanielista, M.P., and Harper, H.H. (1987). "Removal of contaminants in highway runoff flowing through swales", *Science of the Total Environment,* 59: 391-399.

Yu, S. L, Kuo, J. T., Fassman, E. A., and Pa, H. (2001). "Field test of grassed- swale performance in removing runoff pollution", *Journal of Water Resources Planning and Management*, 127(3): 168–171.

Appendix A: Literature Review - Micro-topography

Influence of Micro-Topography on Overland Flow and Infiltration (Task 1)

Formation of bed geometry, combining micro-topographic formations and surface sealing and crusting, is a dynamic process that has been associated with roughness parameters, rainfall intensity and the initial soil moisture content. Micro-topography and surface sealing are related; consequently these two processes should not be analyzed independently, but as a combined process.

Micro-channels, depressions, and mounds all constitute the micro-topography of a surface and represent roughness. Roughness can be completely random or be a defined structure with a dominant direction; authors do not always mention which kind of roughness they are evaluating when studying how it affects overland flow and infiltration. In general, cross-slope roughness has a greater impact on runoff dynamics than downslope direction roughness (Thompson *et al.* 2010; Kirkby *et al.*, 2014). The overall thrust of the literature is that most surfaces with surface depressions tend to enhance infiltration and decrease runoff, although rilled surfaces (channels in the slope direction) exhibit an increase of runoff. Rainfall intensities also affect the influence of depressions in runoff-infiltration partitioning and precipitation events can generate the formation of micro-channels in initially smooth surfaces. Additionally, flow depth is usually a determining factor for the spatial distribution of runoff in a rough surface, as a result of blockage (Abrahams *et al.*, 1992 and Lane, 2005).

Determining empirical relationships between roughness variables and flow characteristics simplifies the representation of the latter, avoiding cumbersome measurements of the flow or surface crust. There are roughness parameters that have been successfully used to interpret hydrological processes; e.g. fractal D (Chi *et al.*, 2012); however other factors like variogram analysis cannot be used alone to deduce the dynamics of runoff generation (Darboux *et al.*, 2001).

The focus of literature regarding functional and structural hydrologic connectivity has been depression storage; while micro-channels or fingering organization have not been widely studied in terms of connectivity. The effect of depressions on runoff generation is more complex than the approach where runoff only starts when depression storage capacity is full. The distribution, size, rainfall intensity, micro-topography and spatial variation in infiltration are factors that should be analyzed to better represent a puddle to puddle flow. When calculating connectivity, infiltration should be included in the analysis, because it reduces the water available to become runoff; particularly, varying spatial distribution of infiltration properties has been postulated to affect connectivity (Appels *et al.*, 2011). One future research need is the effect of varying infiltration properties on the functional and structural hydrologic connectivity. Furthermore, the effect that overland flow patterns have on infiltration processes has not been satisfactorily verified.

Cracks can generate microchannels on the soil surface with higher infiltration capacity, but water flows and concentrates in a narrow surface. On the other hand, crusts are prone to develop in the bottom of the depressions, which reduces their infiltration capacity; however water has a greater residence time and low velocity in those depressions. Consequently, infiltration capacity should not be used as the only factor to estimate infiltration volumes; retention time is also an important factor. Drainage network and micro-topography should be taken into consideration.

Roughness parameters can be applied to map spatial patterns neglecting the evolution of the surface during the process (fully developed surface) or to establish empirical relationships to predict the formation of new bed geometries (dynamic surface). More research is required to determine the conditions under which initial soil roughness of an erodible surface can be used to estimate runoff and infiltration volumes. Once the surface is fully developed, only the main micro-topographic features (channels, mounds and depressions) are needed to adequately represent runoff processes. The final developed surface can be predicted from an initial surface using roughness factors (Darboux *et al.*, 2001 and Vermang *et al.*, 2015).

Overland flow models often use roughness factors in order to establish direct relationships between micro-topographic features and hydrologic processes. Prior to full development of the surface, detailed sediment transport models need to be used to predict the dynamic processes occurring on an erodible hillslope due to the rainfall and overland flow. Once a surface is fully developed, implementing a planar model with a lower grid resolution and superimposed spatially distributed rill or depression storage (Frei and Fleckenstein, 2014) is an efficient solution to represent the effect of micro-topographic features on hydrologic processes.

However, the research in micro-topography impacts on sloped surface flow and infiltration requires information that is not usually available for drainage ditch side slopes. In addition, measured parameters such as relative roughness do not adequately describe surface morphology such that flow relationships can be developed. A standard measure that can be used to determine the important morphological features needs to be researched and developed.

Appendix B: MATLAB Code of the Dry Swale Calculator

Components:

1. **Infiltration Sub-model** (function)
2. **Overland Flow Model: Side-slope** (function)
3. **Overland Flow Model: Channel** (function)
4. **Combined Model: Side-slope + Channel** (script)

1. Infiltration Sub-model *(function:* Green_Ampt_rate_ML)

```
function [ f, SurfaceSat ] = Green_Ampt_rate_ML(
psi,deltheta,Ks,ie,dt,F,SurfaceSat )

%psi effective wetting front suction
%deltheta Soil water deficit
%Ks Saturated hydraulic conductivity
%ie intensity over cell
%dt time step
%F cumulative infiltration depth
%SurfaceSat (1=ponded water, 0=no ponded water)

X=psi*deltheta;
dP=ie*dt;

if SurfaceSat==1
   dF_go=0.5*(Ks*dt-2*F+sqrt(Ks*dt*(Ks*dt+4*F+8*X)+4*(F^2)));
   dF_g=-F-(((F+dF_go)^2)/X)+((F+X+dF_go)/X)*sqrt(((F+dF_go)^2)...
            +2*X*(X*log(1+((dF_go/(F+X))))+Ks*dt-dF_go));
    if dP<dF_g
       f=ie;
       F=F+dP;
    else
       F=F+dF_g;
       f=Ks*(X+F)/F;
    end
else
    if ie<Ks
       F_s=10^20;
    else
       F_s=(Ks*X)/(ie-Ks);
    end

    if F_s>F+dP
       F=F+dP;
       f=ie;
    else
        SurfaceSat=1;
        dF_go=0.5*(Ks*dt-2*F+sqrt(Ks*dt*(Ks*dt+4*F+8*X)+4*(F^2)));
        dF_g=-F-(((F+dF_go)^2)/X)+((F+X+dF_go)/X)*sqrt(((F+dF_go)^2)...
            +2*X*(X*log(1+((dF_go/(F+X))))+Ks*dt-dF_go));
         if dP<dF_g
             f=ie;
             F=F+dP;
         else
```

```
            F=F+dF_g;
            f=Ks*(X+F)/F;
        end
    end
end
```

2. Overland Flow Model: Side-slope *(function: Runoff_side)*

```
function [Total_Inflow,Runoff,Infiltration, Qslope]=Runoff_side(i,ir,fw,Ks,
length, w_side, duration, duration_storm, T, ds, psi, deltheta,n)

%% Inputs
%i Rainfall intensity over swale (in/hr)
%ir Rainfall intensity over road (in/hr)
%fw Fraction wetted (it can be a constant or a matrix of values)
%Ks Saturated hydraulic conductivity (cm/h)
%length Length of slope (m)
%w_side Width of the side-slope study area (m)
%duration Duration of study (h)
%duration_storm Duration of storm event (h)
%T Number of time steps
%ds depression storage (mm)
%psi effective wetting front suction (cm)
%deltheta Soil water deficit
%n Manning's n value (SI s/m^(1/3))

rows=50; % Number of sections down slope
w_road=10; %Length of road in direction of swale slope(perp. to traffic) (m)
S=1/5; % Side slope

w_cell=w_side; % Width of study area (m)
fw=fw*ones(rows,1); % Fraction wetted (Option 1:constant)
%or fw= xlsread('Name of Excel file')(Option 2: matrix size [rows,1])
%   (1-fw)=ones(rows,1)- fw;

%%Kinematic wave Variables (SI units)
m=5/3;
Beta=m-1;
a=(S^0.5)/n;
alpha=a*m;

%% Unit conversions
ir=ir*2.54/360; % Converts to mm/s
i=i*2.54/360; % Converts to mm/s
length=length*1000; % Converts to mm
w_road=w_road*1000; % Converts to mm
w_cell=w_cell*1000; % Converts to mm
dx=length/rows;
duration=duration*3600; % Converts to s
duration_storm=duration_storm*3600; % Converts to s
dt=duration/T;
T_s=round(duration_storm/dt);
psi=psi*10; % Converts to mm
Ks=Ks/360; % Converts to mm/s
```

```
n=n*10;
X=psi*deltheta;

%% Calculations
max_Cou=1;

while max_Cou>=1
    % Setting up variables
    qin=zeros(T,rows);
    Volinf=zeros(rows,1);
    qout=zeros(T,rows);
    Qout=zeros(T,rows);
    ie=zeros(T,rows);
    f=zeros(T,rows);
    F=zeros(rows,1);
    h=zeros(T,rows);
    Cou=zeros(T,rows);
    infil=0;
    standing=0;
    qslope=zeros(T,1);
    Int_e=zeros(T,rows);
    start=0;
    SurfaceSat=zeros(rows,1);
    runoff=0;
    Runoff_rate=0;
    Input_road=0;

    % Unsteady Input of water
    ir_v=zeros(T,1);
    i_v=zeros(T,1);
    for j=2:T_s+1
        ir_v(j)=ir;
        i_v(j)=i;
    end

    %Initial condition: h=0 q=0
    for j=1:(T-1) % Loop through time
       for k=1:rows % Loop through space
           if k==1 %First cell
              qin(j+1,k)=ir_v(j)*w_road/fw(k); % Inflow from road
              Input_road=Input_road+qin(j+1,k)*w_cell*fw(1)*dt; %mm3 of
                                                          water input from road
           else
              qin(j+1,k)=Qout(j+1,k-1)/(w_cell*fw(k)); % Inflow from cell
                                                            above
           end
           ie(j+1,k)=qin(j+1,k)/dx+i_v(j); % Effective intensity

           %%Infiltration Submodel Green-Ampt-Mein-Larson
           if ie(j+1,k)==0
               if h(j,k)>0 %Ponded water
                   ie(j+1,k)=h(j,k)/dt;
               end
           end
           [f(j+1,k),
```

```
        SurfaceSat(k)]=Green_Ampt_rate_ML(psi,deltheta,Ks,ie(j+1,k)
        ,dt,F(k),SurfaceSat(k));
   F(k)=F(k)+f(j+1,k)*dt; %infiltration depth

    %Explicit numerical solution for h
      if k==1 %first cell
          Int_e(j+1,k)=qin(j+1,k)/dx-f(j+1,k)+i_v(j);
          h(j+1,k)=h(j,k)-
               (dt/dx)*(qout(j,k)*((0.5*(fw(1)+fw(2))/fw(1))))+(0.5*(
               Int_e(j,k)+Int_e(j+1,k)))*dt;
          if h(j+1,k)>ds
              qout(j+1,k)=a*(h(j+1,k)-ds)^m;
          end
      else %Rest of the cells
         Int_e(j+1,k)=-f(j+1,k)+i_v(j);
      end

      if k>1 %Rest of the cells
        if j==1 %First time step
           h(j+1,k)=dt*0.5*(Int_e(j,k)+Int_e(j+1,k));
           if h(j+1,k)>ds
              qout(j+1,k)=a*(h(j+1,k)-ds)^m;
           end
        else %Rest of time steps
            if k<rows
                h(j+1,k)=dt*0.5*(Int_e(j,k)+Int_e(j+1,k))+h(j,k)-
                     ((qout(j,k)*(0.5*(fw(k)+fw(k+1))))-(qout(j,k-
                     1)*(0.5*(fw(k)+fw(k-
                     1)))))*(dt/(dx*(0.5*(fw(k)+fw(k-1)))));
            else
                h(j+1,k)=dt*0.5*(Int_e(j,k)+Int_e(j+1,k))+h(j,k)-
                    ((qout(j,k)*fw(k))-(qout(j,k-1)*(fw(k-
                    1))))*(dt/(dx*((fw(k)))));
            end
           if h(j+1,k)>ds
              qout(j+1,k)=a*(h(j+1,k)-ds)^m;
           end
        end

      end
      if h(j+1,k)<0
         h(j+1,k)=0;
         qout(j+1,k)=0;
      end

      if qout(j+1,k)>0
         Qout(j+1,k)=qout(j+1,k)*w_cell*fw(k);
      end
      if h(j+1,k)>0
         Cou(j+1,k)=alpha*((h(j+1,k))^Beta)*dt/dx;
      end
      if j==T-1
         Volinf(k)=F(k)*dx*w_cell*fw(k);
      end
end
qslope(j+1)=qout(j+1,rows);
```

```
        Qslope(j+1)=qslope(j+1)*w_cell*fw(rows);
        runoff=runoff+(qslope(j+1)*w_cell*fw(rows)*dt);
        if start==0 && qslope(j+1)>(i*dx/10)
           start=(dt*j)/60; %Start of runoff from last cell
        end
    end

    Runoff_rate=qslope(T_s)*w_cell*fw(rows)*1E-6*60; %rate L/min
    max_Cou=max(max(Cou));
    if max_Cou>1
        T=round(T*max_Cou);
        dt=duration/T;
        T_s=round(duration_storm/dt);
    end
end

%% Results
rain=i*dx*w_cell*sum(fw)*duration_storm;
infil=sum(Volinf);
standing=h(T,:)*fw*dx*w_cell;
Volume_Runoff=(runoff)*1E-6;
Total_Inflow=(Input_road+rain)*1E-6;
Runoff=Volume_Runoff;
Infiltration=(infil+standing)*1E-6;
```

3. Overland Flow Model: Channel *(function: Runoff_channel)*

```
function [Runoff,Infiltration,rain,ratio_ch_side]=Runoff_channel(i, Ks,
Q_side, Channel_length, w_side, duration, duration_storm, T, ds, psi,
deltheta,n,B)

%% User Inputs
%i Rainfall intensity over swale (in/hr)
%Ks Saturated hydraulic conductivity (cm/h)
%Q_side Discharge from side-slope (mm3/s)
%Channel_length length of the channel
%w_side width of side slope modeled
%duration Duration of study (h)
%duration_storm Duration of storm event (h)
%T Number of time steps
%ds depression storage (mm)
%psi effective wetting front suction (cm)
%deltheta Soil water deficit
%n Manning's n value (SI s/m^(1/3))
%B width of the rectangular channel

length=Channel_length; % Length of channel (m)
ratio_ch_side=length/w_side; %Length channel/Width side
rows=50; % Number of sections down slope channel
fw=1*ones(rows,1); % Fraction wetted (1=whole surface channel wetted)
S=0.02; % Slope channel

%%Kinematic wave Variables (SI units)
m=5/3;
```

```
Beta=m-1;
a=(S^0.5)/n;
alpha=a*m;
w_cell=B;

%% Unit conversions
i=i*2.54/360; % Converts to mm/s
length=length*1000; % Converts to mm
w_cell=w_cell*1000; % Converts to mm
dx=length/rows;
duration=duration*3600; % Converts to s
duration_storm=duration_storm*3600; % Converts to s
dt=duration/T;
T_s=round(duration_storm/dt);
psi=psi*10; % Converts to mm
Ks=Ks/360; % Converts to mm/s
n=n*10;
X=psi*deltheta;
%% Calculations for flow down slope during storm
max_Cou=1;

while max_Cou>=1
    % Setting up variables
    qin=zeros(T,rows);
    Volinf=zeros(rows,1);
    qout=zeros(T,rows);
    Qout=zeros(T,rows);
    ie=zeros(T,rows);
    f=zeros(T,rows);
    F=zeros(rows,1);
    h=zeros(T,rows);
    Cou=zeros(T,rows);
    infil=0;
    standing=0;
    qslope=zeros(T,1);
    Int_e=zeros(T,rows);
    start=0;
    SurfaceSat=zeros(rows,1);
    runoff=0;
    Runoff_rate=0;
    q_side=zeros(T,1);

    q_side=Q_side*(ratio_ch_side)/(w_cell*length);

    % Unsteady Input of water
    i_v=zeros(T,1);
    for j=1:T_s
        i_v(j)=i; %L/T
    end
    i_v=i_v+q_side;

    %Initial condition: h=0 q=0

    for j=1:(T-1) % Loop through time
       for k=1:rows % Loop through space
```

```
if k>1
   qin(j+1,k)=Qout(j+1,k-1)/(w_cell*fw(k)); % Inflow from cell
                                                above
end
ie(j+1,k)=qin(j+1,k)/dx+i_v(j); % Effective intensity

%%Infiltration Submodel Green-Ampt-Mein-Larson
if ie(j+1,k)==0
    if h(j,k)>0 %Ponded water
        ie(j+1,k)=h(j,k)/dt;
    end
end
[f(j+1,k),
       SurfaceSat(k)]=Green_Ampt_rate_ML(psi,deltheta,Ks,ie(j+1,k
       ),dt,F(k),SurfaceSat(k));
F(k)=F(k)+f(j+1,k)*dt; %infiltration depth

 %Explicit numerical solution for h
 Int_e(j+1,k)=-f(j+1,k)+i_v(j);
   if k==1 %first cell
       h(j+1,k)=h(j,k)-
            (dt/dx)*(qout(j,k)*((0.5*(fw(1)+fw(2))/fw(1))))+(0.5*(
            Int_e(j,k)+Int_e(j+1,k)))*dt;
       if h(j+1,k)>ds
           qout(j+1,k)=a*(h(j+1,k)-ds)^m;
       end
   end

   if k>1 %Rest of the cells
     if j==1 %First time step
        h(j+1,k)=dt*0.5*(Int_e(j,k)+Int_e(j+1,k));
        if h(j+1,k)>ds
           qout(j+1,k)=a*(h(j+1,k)-ds)^m;
        end
     else %Rest of time steps
         if k<rows
             h(j+1,k)=dt*0.5*(Int_e(j,k)+Int_e(j+1,k))+h(j,k)-
                ((qout(j,k)*(0.5*(fw(k)+fw(k+1))))-(qout(j,k-
                1)*(0.5*(fw(k)+fw(k-1)))))*(dt/(dx*((fw(k))))));
         else
             h(j+1,k)=dt*0.5*(Int_e(j,k)+Int_e(j+1,k))+h(j,k)-
                   ((qout(j,k)*fw(k))-(qout(j,k-1)*(fw(k-
                   1))))*(dt/(dx*((fw(k))))));
         end
        if h(j+1,k)>ds
           qout(j+1,k)=a*(h(j+1,k)-ds)^m;
       end
     end

   end
   if h(j+1,k)<0
      h(j+1,k)=0;
      qout(j+1,k)=0;
   end
```

```
            if qout(j+1,k)>0
               Qout(j+1,k)=qout(j+1,k)*w_cell*fw(k);
            end
            if h(j+1,k)>0
               Cou(j+1,k)=alpha*((h(j+1,k))^Beta)*dt/dx;
            end
            if j==T-1
               Volinf(k)=F(k)*dx*w_cell*fw(k);
            end
        end
        qslope(j+1)=qout(j+1,rows);
        runoff=runoff+(qslope(j+1)*w_cell*fw(rows)*dt);
        if start==0 && qslope(j+1)>(i*dx/10)
           start=(dt*j)/60; %Start of runoff from last cell
        end
    end

    Runoff_rate=qslope(T_s)*w_cell*fw(rows)*1E-6*60; %rate L/min
    max_Cou=max(max(Cou));
    if max_Cou>1
        T=round(T*max_Cou);
        dt=duration/T;
        T_s=round(duration_storm/dt);
    end
end

%% Results
rain=i*w_cell*length*duration_storm*1E-6;
side=sum(q_side*w_cell*length*dt)*1E-6;
infil=sum(Volinf)*1E-6;
standing=h(T,:)*fw*dx*w_cell*1E-6;
runoff_final=runoff*1E-6;
Volume_Runoff=runoff_final+standing;
Runoff=Volume_Runoff;
Infiltration=(infil);

%% Plot discharge (q)
fig1 = figure;
tt=(dt/3600):(dt/3600):(duration/3600);
figure(fig1)
plot(tt,qslope*1E-6);
title('Specific Discharge into Swale Channel Over Time');
xlabel('Time (hr)');
ylabel('Specific Discharge (m^{2}/s)');
axis auto
```

4. Combined Model: Side-slope + Channel *(Script: Runoff_linked)*

```
%% Inputs
i=2.2; %in/hr
Ks=1.45; %cm/h
psi=5; % effective wetting front suction (cm)
deltheta=0.3; % Soil water deficit
n=.25;% Manning's n value (SI s/m^(1/3))
```

```
length=4; %m length of side slope
Channel_length=10; %m length of the channel
B=0.5; %width of the rectangular channel [m]
duration_storm=1; %duration of the storm event[h]
duration=1.6; %duration of the study[h]
ds=1; %depression storage of the side slope[mm]
ds_ch=1; %depression storage of the channel [mm]
T=10000; %Number of time steps
w_side=0.914; % Width of the side-slope study area (m)
fw=0.7; %fraction wetted (if fw over the side-slope is a constant)

%% Calculations Side-Slope
ir=i;
[Total_Inflow_1,Runoff_1,Infiltration_1, Qslope1]=Runoff_side(i,ir, fw, Ks,
length, w_side, duration,duration_storm, T, ds, psi, deltheta,n);

ir=0;
if fw<1
    [Total_Inflow_2,Runoff_2,Infiltration_2, Qslope2]=Runoff_side(i,ir, (1-
fw), Ks, length, w_side, duration, duration_storm, T, ds, psi, deltheta,n);
else
    Total_Inflow_2=0;
    Runoff_2=0;
    Infiltration_2=0;
     Qslope2=0;
end
Q_side=transpose(Qslope1)+transpose(Qslope2);
Total_Inflow=Total_Inflow_1+Total_Inflow_2;
Total_Runoff=Runoff_1+Runoff_2;
Infiltration=Infiltration_1+Infiltration_2;
Percentage_Infiltration(1)=100*Infiltration/Total_Inflow;

%% Calculations Channel
ds=ds_ch; %depression storage of the channel [mm]
[Runoff_3,Infiltration_3,rain_3,ratio_ch_side]=Runoff_channel(i, Ks, Q_side,
Channel_length, w_side, duration,duration_storm, T, ds, psi, deltheta,n, B);

%% Side slope + Channel
TOTAL_INFLOW=Total_Inflow*ratio_ch_side+rain_3;
INFILTRATION=Infiltration*ratio_ch_side+Infiltration_3;
RUNOFF=Runoff_3;
Total_PERCENTAGE_INFILT=100*(INFILTRATION/TOTAL_INFLOW);
Side_Slope_inf_perc=100*(Infiltration*ratio_ch_side/INFILTRATION);
Channel_inf_perc=100-Side_Slope_inf_perc;

%% Results
fprintf('Total Inflow Swale = %.1f L\n',TOTAL_INFLOW);
fprintf('Total Infiltration = %.1f L\n',INFILTRATION);
fprintf('Total Runoff = %.1f L\n',RUNOFF);
fprintf('Mass Balance Error = %.4f%%\n',100*(((TOTAL_INFLOW)-
(INFILTRATION+RUNOFF))/TOTAL_INFLOW));
fprintf('Percentage Infiltration %.1f%%\n',Total_PERCENTAGE_INFILT);
fprintf('Percentage Infiltration Side = %.2f%%\n',Side_Slope_inf_perc);
fprintf('Percentage Infiltration Channel = %.2f%%\n',Channel_inf_perc);
```

Appendix C: Calculator Infiltration Graphs

Precipitation depths versus percentage infiltration (side slope and channel) for different ratios of width of the swale side over width of the road, based on the Minneapolis – St. Paul Airport station:

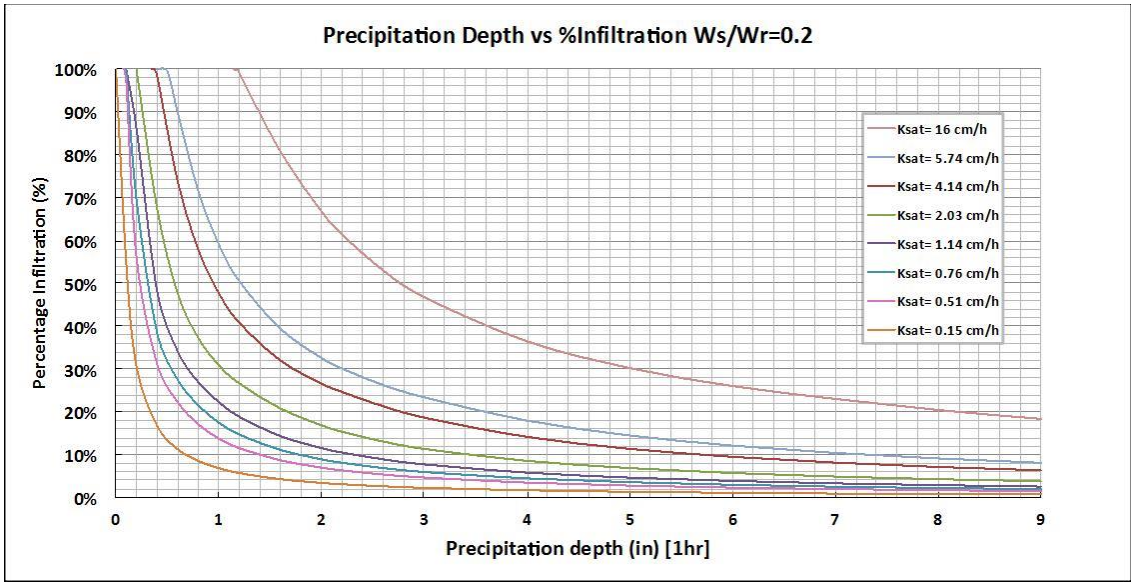

Figure 56 Precipitation depths versus percentage infiltration for a ratio of width of the swale side slope over width of the road of 0.2. The eight curves represent different saturated hydraulic conductivities.

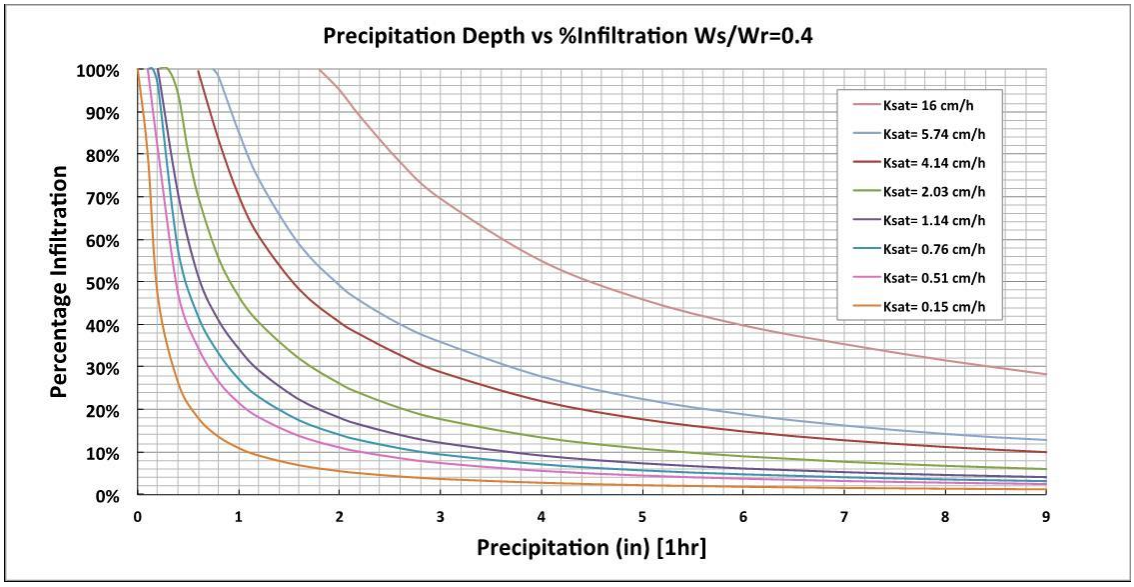

Figure 57 Precipitation depths versus percentage infiltration for a ratio of width of the swale side slope over width of the road of 0.4. The eight curves represent different saturated hydraulic conductivities.

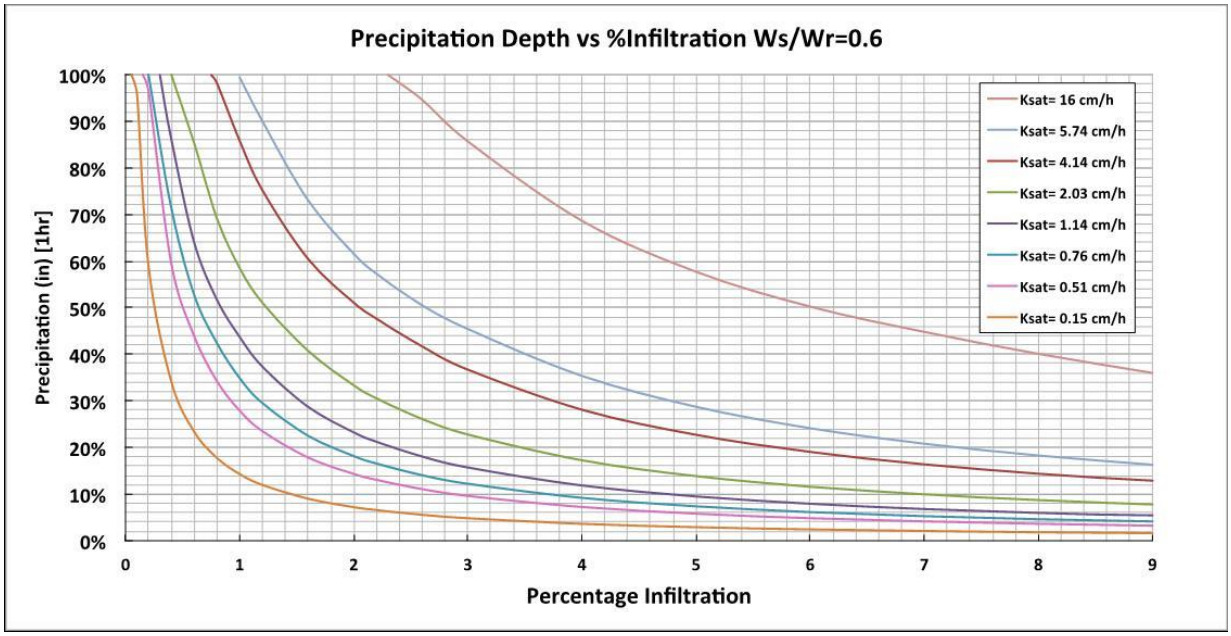

Figure 58 Precipitation depths versus percentage infiltration for a ratio of width of the swale side slope over width of the road of 0.6. The eight curves represent different saturated hydraulic conductivities.

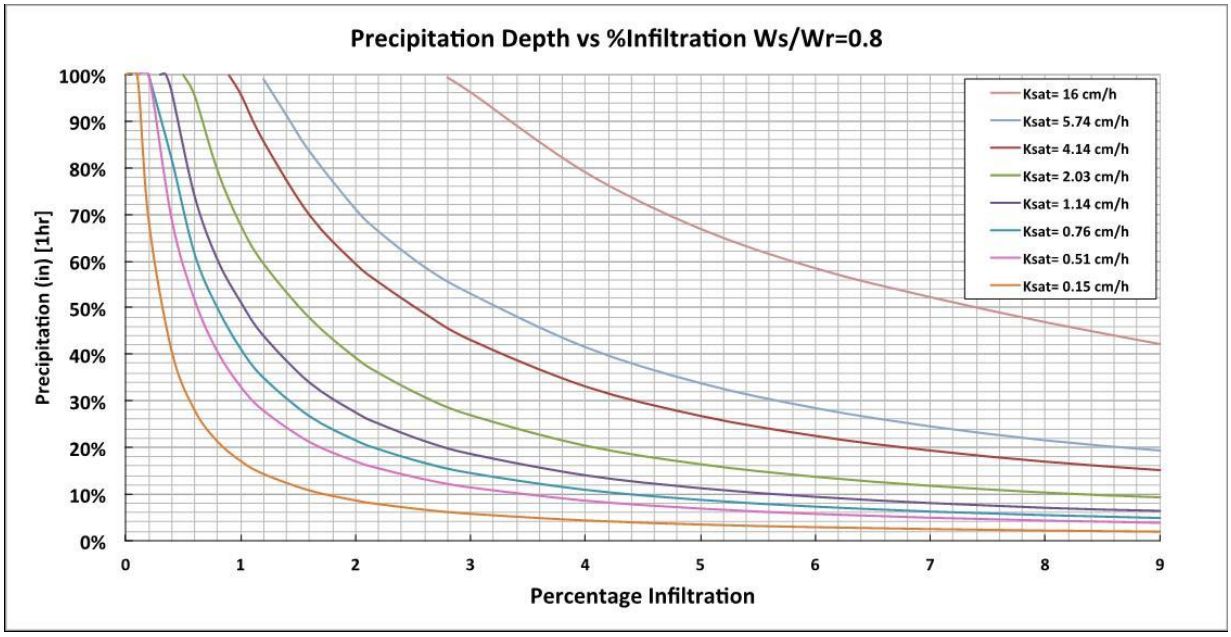

Figure 59 Precipitation depths versus percentage infiltration for a ratio of width of the swale side slope over width of the road of 0.8. The eight curves represent different saturated hydraulic conductivities.